NANOROD ARRAY-SURFACE ENHANCED RAMAN SPECTROSCOPY (NA-SERS) FOR THE HIGHLY SENSITIVE AND SPECIFIC DETECTION OF *MYCOPLASMA PNEUMONIAE* IN A COMPLEX BIOCHEMICAL BACKGROUND

by

KELLEY CAROLEANNE HENDERSON

(Under the Direction of Duncan C. Krause)

ABSTRACT

Mycoplasma pneumoniae is a novel, cell-wall-less bacterial pathogen of the human respiratory tract that accounts for up to 20% of community-acquired pneumonia. Detection and diagnosis of mycoplasma infections is limited by several factors, including poor success at culture from clinical samples. At present the most effective means for detection and genotyping is quantitative polymerase chain reaction (qPCR), which can exhibit excellent sensitivity and specificity but requires separate tests for detection and genotyping, lacks standardization between available tests, and has limited practicality for widespread, point-of-care use. We have developed and previously described a silver nanorod array-surface enhanced Raman spectroscopy (NA-SERS) biosensing platform capable of detecting *M. pneumoniae* in simulated and true clinical throat swab samples with statistically significant specificity and sensitivity, and the ability to distinguish between reference strains of the two main genotypes of *M. pneumoniae*. Here we ascertained that differences in sample preparation influence the integrity of mycoplasma cells for NA-SERS analysis, which in turn impacts the resulting spectral signature. Furthermore we established the lower limit of detection by NA-SERS for *M. pneumoniae* intact-cell sample

preparations. Using partial-least squares discriminatory analysis (PLS-DA) of sample spectra, we found that NA-SERS consistently detected intact *M. pneumoniae* to 0.66 genome equivalents (cells/µl) with 90% cross-validated statistical accuracy. By comparison, qPCR of samples in parallel yielded a lower limit of detection of 2.5 cells/µl. In addition, we used PLS-DA to demonstrate that NA-SERS was able to detect 30 *M. pneumoniae* clinical isolates from globally diverse origins and *M. pneumoniae* reference strain controls, and could distinguish all *M. pneumoniae* clinical isolates and reference strains from a panel of 12 other human commensal and pathogenic *Mollicutes* species with 100% cross-validated statistical accuracy. Lastly, PLS-DA correctly classified by genotype all 30 clinical isolates with 96% cross-validated accuracy for type 1 strains, 98% cross-validated accuracy for type 2 strains, and 90% cross-validated accuracy for type 2V strains.

INDEX WORDS: Mycoplasma, Nanotechnology, Surface-enhanced Raman Spectroscopy (SERS), Silver nanorod array, Chemometric analysis, Biosensing

NANOROD ARRAY-SURFACE ENHANCED RAMAN SPECTROSCOPY (NA-SERS) FOR THE HIGHLY SENSITIVIE AND SPECIFIC DETECTION OF *MYCOPLASMA PNEUMONIAE* IN A COMPLEX BIOCHEMICAL BACKGROUND

by

KELLEY CAROLEANNE HENDERSON

B.S., Kennesaw State University, 2008

A Dissertation Submitted to the Graduate Faculty of The University of Georgia in Partial Fulfillment of the Requirements for the Degree

DOCTOR OF PHILOSOPHY

ATHENS, GEORGIA

2014

NANOROD ARRAY-SURFACE ENHANCED RAMAN SPECTROSCOPY (NA-SERS) FOR THE HIGHLY SENSITIVE AND SPECIFIC DETECTION OF *MYCOPLASMA PNEUMONIAE* IN A COMPLEX BIOCHEMICAL BACKGROUND

by

KELLEY CAROLEANNE HENDERSON

Major Professor:	Duncan C. Krause
Committee:	Richard A. Dluhy Robert J. Maier Frederick D. Quinn

Electronic Version Approved:

Julie Coffield
Interim Dean of the Graduate School
The University of Georgia
August 2014

DEDICATION

This dissertation is dedicated to my husband who is my best friend and has stood by me and encouraged me throughout my graduate career, my parents who have given me the opportunity to pursue an education from the best institutions and offered their endless support and invaluable advice at every step along the way, and my siblings who have kept me on my toes and always pushed me to be my best. Without my Faith and the love and support of my family, I would not be who I am or where I am today.

ACKNOWLEDGEMENTS

I would like to thank first and foremost my major professor, Duncan Krause, for his support and guidance over the course of my graduate career, I could not ask for a better mentor or role model for my professional development. His counsel, patience, and wisdom have been invaluable to me over the past five years, and have helped me to grow both as a scientist and as a person. It is also with immense gratitude that I acknowledge Jonas Winchell for his mentorship and encouragement throughout my studies, and the Pneumonia Response and Surveillance Laboratory at the CDC in Atlanta, Georgia, for all their help with making my research project possible. Additionally I would like to thank my committee members Rich Dluhy, Fred Quinn, and Rob Maier for their advice and guidance throughout my graduate school tenure, I am a significantly better scientist thanks to them. Lastly, I would like to thank from the bottom of my heart all my lab-mates at UGA both past and present, the Dluhy lab in the chemistry department at UGA, and the UAB Diagnostic Mycoplasma Laboratory for their help and contributions to making my work possible.

TABLE OF CONTENTS

Page

ACKNOWLEDGEMENTS v

LIST OF TABLES viii

LIST OF FIGURES x

CHAPTER

1 INTRODUCTION 1

2 REVIEW OF THE LITERATURE 6

Introduction to the Key Physiology of *M. pneumoniae* 6

The Terminal Organelle, Cytadhesion, and Gliding Motility 9

Clinical Relevance and Pathology of *M. pneumoniae* 18

Clinical Manifestation and Epidemiology of *M. pneumoniae* Infection 27

Current Methods for Detecting and Genotyping *M. pneumoniae* Infection 32

Evolution of NA-SERS for Biosensing Purposes 34

3 COMPARISON OF THE ENDPOINTS FOR DETECTION OF *MYCOPLASMA PNEUMONIAE* BY NANOROD ARRAY-SURFACE ENHANCED RAMAN SPECTROSCOPY AND QPCR 65

Abstract 66

Introduction 67

Materials and Methods 70

Results and Discussion 74

Conclusions....80

Acknowledgements....81

Manuscript Data....82

Supplementary Information....89

4 SPECIFICITY AND STRAIN-TYPING CAPABILITIES OF NANOROD ARRAY-SURFACE ENHANCED RAMAN SPECTROSCOPY FOR *MYCOPLASMA PNEUMONIAE* DETECTION AND GENOTYPING....99

Abstract....100

Introduction....101

Methods....104

Results and Discussion....109

Conclusions....119

Acknowledgements....120

Manuscript Data....121

5 CONCLUSIONS....139

REFERENCES....144

LIST OF TABLES

Page

Table 3.1: Representative Raman bands appearing in the NA-SERS spectra of intact- and lysed-cell *M. pneumoniae* samples 84

Table 3.2: Initial culture information for *M. pneumoniae* intact-cell NA-SERS datasets 85

Table 3.3: NA-SERS lower endpoint of detection (EOD) for *M. pneumoniae* datasets 86

Table 3.4: Initial culture information for qPCR analysis 87

Table 3.5: Lower EOD of *M. pneumoniae* by qPCR analysis 88

Supplementary Table 3.6: PLS-DA modeling statistics for NA-SRS detection of intact-cell *M. pneumoniae* dataset (a) 93

Supplementary Table 3.7: PLS-DA modeling statistics for NA-SRS detection of intact-cell *M. pneumoniae* dataset (b) 94

Supplementary Table 3.8: PLS-DA modeling statistics for NA-SRS detection of intact-cell *M. pneumoniae* dataset (c) 95

Supplementary Table 3.9: Crossing threshold values for qPCR EOD dataset (a) 96

Supplementary Table 3.10: Crossing threshold values for qPCR EOD dataset (b) 97

Supplementary Table 3.11: Crossing threshold values for qPCR EOD dataset (c) 98

Table 4.1: Strain/isolate information for all *M. pneumoniae* specificity cultures 121

Table 4.2: Quality control and sample information for *Mollicutes* species and *M. pneumoniae* control culture 126

Table 4.3: Cross-validated PLS-DA individual modeling statistics representing the prediction performance for NA-SERS genotyping of type 1 and type 2 *M. pneumoniae* clinical isolates 133

Table 4.4: Cross-validated PLS-DA individual modeling statistics representing the prediction performance for NA-SERS genotyping of type 2V *M. pneumoniae* clinical isolates 134

LIST OF FIGURES

Page

Figure 2.1: Phylogeny of mycoplasmas....43

Figure 2.2: Microscopic imaging of *M. pneumoniae*....45

Figure 2.3: Schematic of *M. pneumoniae* terminal organelle....47

Figure 2.4: Structure of sialylated oligosaccharide compound most effective for inhibition of *M. pneumoniae* binding and gliding motility....49

Figure 2.5: Transmission electron micrograph (TEM) of *M. pneumoniae*-infected hamster tracheal ring....51

Figure 2.6: Schematic of P1 adhesin protein....53

Figure 2.7: Epidemiological data for incidence of *M. pneumoniae* infection....55

Figure 2.8: Type-switching periodicity of *M. pneumoniae* infection....57

Figure 2.9: Differences in biofilm formation between *M. pneumoniae* strain types....59

Figure 2.10: Schematic of SERS and NA-SERS substrate composition....61

Figure 2.11: Image of PDMS multi-well array and TEM of NA-SERS subsrate....63

Figure 3.1: Scanning electron micrograph (SEM) image of lysed- and intact-cell *M. pneumoniae* sample preparations and their respective SERS spectra....82

Supplementary Figure 3.2: Scanning electron micrograph (SEM) image of intact *M. pneumoniae* cells grown on glass coverslips....89

Supplementary Fig. 3.3: Example of PLS-DA modeling scheme used to determine the NA-SERS endpoint of detection for intact-cell *M. pneumoniae* samples....91

Figure 4.1: Comparison of averaged, baseline-corrected, and normalized SERS spectra for the nanorod substrate, growth medium control, and *M. pneumoniae* reference strain controls and clinical isolates 122

Figure 4.2: PLS-DA of 32 *M. pneumoniae* clinical isolates, including reference strain controls M129 and FH 124

Figure 4.3: PLS-DA distinguishing *M. pneumoniae* strains from other human commensal and pathogenic *Mollicutes* species 127

Figure 4.4: PLS-DA for NA-SERS genotyping of type 1 and 2 *M. pneumoniae* strains 129

Figure 4.5: PLS-DA for NA-SERS genotyping of type 2V *M. pneumoniae* clinical isolates 131

Figure 4.6: Comparison of averaged, baseline-corrected, and normalized SERS spectra for type 1, type 2, and type 2V genotypes 135

Figure 4.7: Principle component analysis of *M. pneumoniae* strain typing and other human commensal and pathogenic *Mollicutes* species 137

CHAPTER 1

INTRODUCTION

The cell wall-less prokaryote *Mycoplasma pneumoniae* is a major cause of respiratory disease in humans, accounting for 20% to 40% of all community acquired pneumonia (CAP), and in addition is the leading cause of CAP in older children and young adults [1-5]. For adults alone the annual economic burden of CAP is > $17 billion, and the incidence of infection in the very young and the elderly is on the rise [4,6]. Macrolide resistance is a growing concern, particularly in children [5], and extra-pulmonary sequelae occur in up to 25% of infections. Finally, evidence continues to indicate a contributing role for *M. pneumoniae* infection in the onset, exacerbation, and recurrence of asthma [5].

An area of growing interest is the role of *M. pneumoniae* genotype in pathogenesis and disease epidemiology. Genetic diversity is relatively limited among *M. pneumoniae* strains and can be categorized into two major groups (type 1 or type 2) based on variation within sequence of the *P1* (MPN141) gene, with variant strains of the two becoming increasingly more common [7]. The P1 protein is an important virulence factor and plays a significant role in the immunogenic response to *M. pneumoniae* infection [8-10]. P1 must complex with several other proteins in order to localize to the tip of the terminal organelle, where it mediates receptor binding for attachment to the respiratory epithelium, an essential step in successful colonization of the airways [9,11]. Variation in the *P1* gene sequence is used to distinguish between type 1 and type 2 strains of *M. pneumoniae*, but little is known about phenotypic differences arising

from this genetic variation. Perhaps notable in regard to strain variation is the periodicity of type-switching between the two major genotypes that occurs in regular patterns every 4-7 years [12].

M. pneumoniae infection is transmitted through aerosolized respiratory secretions and spreads slowly but efficiently through close living quarters, with incubation periods up to three weeks [13,14]. Symptoms tend to be non-descript, often with complex and variable clinical presentations, which makes definitive diagnosis challenging [1,4,15]. As a result, diagnosis is often presumptive and relies heavily on the combination of physical findings and the elimination of other possible causes [3,5,14]. The success rate for laboratory culture is poor, even for experienced labs, while serologic testing, historically considered the foundation for diagnosis of *M. pneumoniae* infection, has limited sensitivity and specificity, a high tendency for false-negatives, and must often be paired with another diagnostic method [1,3,5,10,14]. Of the currently existing methods, the most reliable means for detection is quantitative polymerase chain reaction (qPCR). At present, the only FDA approved qPCR-based test is the FilmArray® Respiratory Panel (BioFire Diagnostics Inc., Salt Lake City, Utah), providing nested, multiplex qPCR with high resolution melt analysis on nasopharyngeal swabs for 21 different viral and bacterial respiratory pathogens, and capable of detecting *M. pneumoniae* as low as 30 colony-forming units (CFU)/ml [16]. The current standard for *M. pneumoniae* genotyping is PCR-restriction fragment length polymorphism but can also be done by nested PCR and sequencing, or by qPCR and high resolution melt curve analysis [15,17-19]. These methods for detection and genotyping exhibit high sensitivity and specificity for all known strain variants, can allow for detection in the early stages of infection, and can be performed in hospitals and reference laboratories [1,3,5]. However, the requirement of separate tests for detection and genotyping, as well as the cost, complexity, and expertise required, limits the practicality for widespread, point-

of-care use [1,3-5,14]. These limitations create a critical barrier to the accurate and timely diagnosis of *M. pneumoniae* infection, and a rapid, simple, diagnostic platform capable of simultaneous detection and genotyping would greatly improve the control of *M. pneumoniae* disease.

Vibrational spectroscopy has an inherent biochemical specificity that led to its consideration as a next-generation platform for the rapid detection, characterization, and identification of infectious agents [20-23]. Raman spectroscopy in particular has several advantages for application to biological samples, including narrow bandwidths, good spatial resolution, and the ability to analyze aqueous samples due to the absence of interference by water molecules [20,21,24]. Furthermore, Raman spectra provide detailed structural information on the chemical composition of a sample and can serve as a characteristic molecular fingerprint for pathogen identification [23,24]. Despite these advantages, standard Raman spectra are inherently limited by weak signals for detection. As a result, the application of traditional Raman spectroscopy for biosensing applications was impractical and inefficient [13,21,24] until the discovery that sample adsorption onto nanoscopically roughened metallic surfaces results in significant enhancements in Raman signal and spectral intensity [23-25]. This enhancement, by factors up to 10^{14}-fold, is attributed to the increased electromagnetic field for molecules in close proximity to the metallic surface [20,21]. Surface-enhanced Raman spectroscopy (SERS) retains the advantages of standard Raman spectroscopy, in addition to markedly improved sensitivity, allowing for considerable success at whole organism molecular fingerprinting [20,24,26,27].

Inconsistency and lack of reproducibility in the preparation of SERS-active substrates has hindered its widespread use for biosensing applications [20,21,24]. However, highly ordered silver nanorod array (NA) substrates fabricated using oblique angle deposition (OAD) yield

consistent SERS enhancement factors of around 10^8, with less than 15% variation between substrate batches [21]. The reproducibility of NA-SERS substrates can be improved further when patterned into a multiwell format with polydimethylsiloxane (PDMS) [20]. The highly reproducible detection capabilities of NA-SERS have been well demonstrated for multiple infectious agents, including RSV, rotavirus, influenza, HIV, adenovirus, SARS coronavirus, and *M. pneumoniae* [13,22,28-30].

Hennigan et al. previously described an NA-SERS-based assay capable of detecting *M. pneumoniae* in both simulated and true clinical throat swab samples, with statistically significant sensitivity and specificity [13]. Their initial evaluation of the NA-SERS biosensing platform capabilities indicate the potential for application as a next-generation diagnostic tool for the clinical detection of *M. pneumoniae*, but a more comprehensive analysis is needed prior to proceeding with clinical validation [13]. In addition, the initial study analyzed samples prepared in water, and we hypothesize that as a result the content of the analyte on the substrate consisted predominately of lysed cells, cytoplasmic content, and membrane debris.

The objectives of this dissertation project were:

I. To further explore the impact of differences in sample preparation on the SERS spectra of *M. pneumoniae*, to define the lower endpoint of detection for *M. pneumoniae* intact-cell preparations by NA-SERS, and to evaluate in parallel the endpoint of detection by qPCR;

II. To evaluate the specificity of NA-SERS for *M. pneumoniae* detection with a panel of 30 *M. pneumoniae* isolates collected from representative global outbreaks and spanning clinically relevant genotypes, as well as against a panel of 12 other human commensal and pathogenic *Mollicutes* species; and

III. To determine the strain typing capabilities of NA-SERS for the panel of 30 *M. pneumoniae* clinical isolates and known reference strain controls of the major *M. pneumoniae* genotypes.

CHAPTER 2

REVIEW OF THE LITERATURE

Introduction to the Key Physiology of *Mycoplasma pneumoniae*

Mycoplasmas are small, cell wall-less prokaryotes that have minimal genomes and lack the major biosynthetic pathways, classical transcription factors, chemotactic and other common two-component systems, and prototypical cell division apparatus of walled bacteria [31,32]. As such, they are extremely fastidious organisms requiring an obligate parasitic lifestyle in order to obtain exogenous essential metabolites for growth in nature, and highly supplemented media for culturing *in vitro* [32]. Mycoplasmas are characterized by small genomes that consist of a single, circular chromosome with a low G+C content [32,33]. The lack of a cell wall confers a high degree of pleomorphism amongst mycoplasma cell shapes and as such they do not fall into traditional cocci or bacilli classification categories [33]. Additionally, the lack of a cell wall makes mycoplasma cells subject to dessication, and sterols are required in artificial growth medium as they are necessary components of the triple-layered cell membrane that bounds the cell and provides some stability from osmotic stress [33].

Phylogeny of mycoplasmas. Mycoplasmas belong to the class *Mollicutes*, which originates from the Latin words meaning soft ("*mollis*") and skin ("*cutis*"), due to their lack of a cell wall [33]. This class comprises four orders, five families, eight genera, and approximately 200 known species that have been found to be present in humans, vertebrates, arthropods, and plants [33]. 16S rRNA sequencing indicates that mycoplasmas are most closely related to members of the gram-positive eubacterial subgroup including bacilli, lactobacilli, and

streptococci, though *Mollicutes* do not possess the ability to synthesize peptidoglycan cell walls [33]. 16S rRNA sequence phylogeny of mycoplasmas is shown in **Figure 2.1**. Furthermore, in mycoplasma spp. the universal stop codon UGA codes for tryptophan, making genetic manipulation in these organisms difficult [34]. In humans some mycoplasma species exist as commensal organisms whereas others are known human pathogens, including the respiratory agent *Mycoplasma pneumoniae*, which will herein be the focus of this literature review.

***M. pneumoniae* cell biology.** *M. pneumoniae* cells are typically 1 to 2 μm in length and 0.1 to 0.2 μm in width. Typical *M. pneumoniae* colonies rarely exceed 100 μm in size and can be examined under a stereomicroscope whereas individual cells are most commonly viewed using electron microscopy (**Figure 2.2**) [33]. The *M. pneumoniae* genome is 816,394 base pairs in size containing approximately 694 genes, five times smaller than the *E. coli* genome [32,33]. Due to the biosynthetic limitations imparted by such a small genome, *M. pneumoniae* does not synthesize purines or pyrimidines *de novo* but instead scavenges for nucleic acid precursors and many other essential cell nutrients from its host [35]. *M. pneumoniae* is able to utilize glucose, fructose, or glycerol as a carbon source and relies solely on glycolysis for metabolism, as it makes all ten glycolytic enzymes but lacks the full complement of enzymes required for the citric acid cycle and electron transport chain [36]. *M. pneumoniae* generates ATP by converting glucose to lactic acid via substrate phosphorylation by phosphoglycerate kinase (pgk) and pyruvate kinase (pk) [33]. A unique feature of *M. pneumoniae* metabolism from that of other mycoplasmas is its ability to reduce tetrazolium both aerobically and anaerobically [33]. Furthermore, *M. pneumoniae* may produce capsular material external to the cell membrane, and it has recently been shown that *M. pneumoniae* produces biofilms of varying thickness depending on strain type, which will be discussed in more detail later in this review [33,37].

Metabolism of *M. pneumoniae.* Due to the limitations in metabolism described above, *M. pneumoniae* relies on glycerol and phospholipid transporters to import nutrients from the surrounding host habitat. In fact, unexplored transporters and lipoproteins make up approximately 17% of *M. pneumoniae's* total protein complement, and *M. pneumoniae* encodes a total of 53 membrane-spanning transporters and 67 lipoproteins [38]. Furthermore, since *M. pneumoniae* lacks the citric acid cycle and β-oxidation pathway, it is unable to use the fatty acid component of phospholipids [39]. To overcome these metabolic limitations, *M. pneumoniae* imports glucose and fructose via phosphotransferase systems and glycerol via the essential glycerol facilitator, GlpF [40,41]. Glucose and fructose are phosphorylated prior to entering glycolysis whereas glycerol is first converted to dihydroxyacetone phosphate before proceeding into glycolysis [41]. *M. pneumoniae* does not make any phospholipases, but it is assumed these enymes are present in the host pulmonary surfactant where they produce glycerophosphodiesters, mainly glycerophosphocholine [38]. In humans, the most abundant choline-containing phospholipid is lecithin, and phopsholipids and derived metabolites such as glycerol are thought to be major sources of carbon and energy for *M. pneumoniae* on lung epithelia [33]. Additionally, the enzyme that catalyzes the oxidation of glycerol-3-phosphate in *M. pneumoniae* and related mycoplasma spp. is a unique glycerol-3-phosphate oxidase, as it produces hydrogen peroxide (H_2O_2) as opposed to using NAD as an electron acceptor as is seen in most organisms. H_2O_2 is a known virulence factor *in vitro*, and so there is a direct link between glycerol metabolism and virulence in *M. pneumoniae* infection [38]. Interestingly, while *M. pneumoniae* contains this unique enzyme capable of oxidizing glycerol 3-phosphate to generate H_2O_2 molecules, it is unable to utilize it for energy when cultured in the presence of glycerol 3-phosphate as the sole carbon source [38]. This begs the question what is the exact role of this

enzyme for *M. pneumoniae in vivo*, raising the possibility that it exists to generate H_2O_2 and cause mild injury to host cells in order to facilitate nutrient acquisition for itself.

The Terminal Organelle, Cytadhesion, and Gliding Motility

One of the most defining features of *M. pneumoniae* cells is a polar, differentiated, membrane bound cell protrusion known as the terminal organelle, that mediates gliding motility and cytadherence to host respiratory epithelium [42,43]. The genomes of *M. pneumoniae* and other mycoplasma spp. contain no homologues to known bacterial motility genes in other prokaryotes, making the terminal organelle and mode of motility in these organisms unique to their genus [32]. The terminal organelle is defined by an electron dense core that is a component of the Triton-X-100-insoluble fraction [11,44,45]. This fraction has been examined via mass spectrometry and using antibody probes [44,45]. The electron dense core appears as two parallel, flattened rods via conventional electron microscopy, with electron cryotomography revealing a complex, multi-subunit composition to this structure [46,47]. *M. pneumoniae* binds and glides on glass surfaces *in vitro* with the terminal organelle at the leading end, and gliding motility and attachment *in vivo* are essential for colonization and subsequent infection to occur [33,48]. Gliding motility is believed to facilitate access to host cell surface receptors and lateral spread within the host environment [42,49]. The exact mechanism of gliding in this organism remains unknown, but evidence points to a potential catch-pull-and-release process by the terminal organelle that results in a "treadmill-approach" mediated by the surface proteins located in the tip of the attachment organelle [50].

Protein localization to the terminal organelle. It has been found that numerous integral membrane proteins localize to the terminal organelle and play key roles in motility,

cytadherence, and immunogenicity [42,51-56]. The electron dense core is composed of multiple high molecular weight (HMW) proteins that are aligned longitudinally to form a terminal button at the distal end and radiating into perpendicular spokes at the base [42,57,58]. The cytoskeletal components of the core interact with the integral membrane proteins of the adhesin complex to provide structural stability vital to terminal organelle development and function [59,60]. Much of the work on terminal organelle component localization has been done using fluorescent protein fusions and time-course studies of wild type *M. pneumoniae* strains in comparison to terminal organelle protein mutants and their complemented counterparts. Briefly, cytoskeletal protein HMW1 and adhesin complex proteins P1, B, C, and P30 localize to the distal end of the terminal organelle and are required for gliding and cytadherence [54,55,58,61]. Cytadherence-associated proteins of undefined function P41 and P65 also localize to this structure [54,55]. HMW2 is essential for formation of the electron dense core of the terminal organelle [53]. See **Figure 2.3** for a schematic of the terminal organelle and approximate locations of known key terminal organelle proteins.

While many terminal organelle proteins remain uncharacterized and have little known about them, studies have examined the structure, binding partners, and processing of the major cytadherence and cytoskeletal proteins that make up the terminal organelle [54,55,62]. The major focus of this research has been on cytadherence or motility mutants to identify primary defects and the secondary, downstream effects associated therewith to elucidate the role and interactions of each [58]. The following paragraphs will summarize what is known about the structure, function, and protein-protein interactions for the major terminal organelle proteins.

P1. The major adhesin protein required for motility and cytadherence is P1 [8,9,61]. In order for P1 to function properly, upon translation it must be inserted into the cytoplasmic

membrane, trafficked to the terminal organelle, folded into the correct conformation, and interact with all appropriate protein partners of the adhesin complex [61]. The *P1* gene is the second of a polycistronic transcriptional unit containing three open reading frames (ORFs) [61]. P1 is encoded for by the gene MPN141, which is 4,881 nucleotides in length and encodes a protein of 1,627 amino acids with a calculated molecular weight of 176,288 Daltons [63]. Properties of the N-terminal sequence suggest that P1 is likely synthesized as a precursor with subsequent cleavage of a leader peptide ~59 amino acids in length to generate the mature 170-kDa protein upon reaching the appropriate subcellular compartment [43,63]. Mature P1 can be divided into three domains that are linked by flexible hinges preferentially digested by trypsin [58,61]. Domain I is located at the N-terminus of the protein, is a highly conserved region among known orthologs, and contains surface-exposed regions recognized by adherence-inhibiting antibodies [8,9,56,64,65]. Domain II is located near the C-terminus and contains the single transmembrane segment of the protein and also contains surface-exposed regions recognized by adherence-inhibiting antibodies [8,9,56,64,65]. Domain III is the smallest domain, is located in the cytoplasm, and may interact with the cytoskeletal rod structure within the cell [56,66,67]. P1 is the major adhesin and major immunogenic protein in *M. pneumoniae* pathogenesis and will be discussed in greater detail later in this review.

B and C. The gene for these two accessory proteins, MPN142, is the third gene within the P1 transcriptional unit, and is separated by only five nucleotides from the ORF encoding P1 [68]. The gene product of MPN142 is initially synthesized as a single polypeptide chain approximately 130-kDa in size that is cleaved to yield B (90-kDa) and C (40-kDa). The proximity of their respective genes suggests that the P1, B, and C are likely transcriptionally and translationally linked to one another [61]. Additionally, cross-linking studies show a close

association and likely adhesin complex between P1, B/C, and P30 [61,69]. Further evidence for the formation of a protein complex between P1, B, and C is the requirement of P1 for the stability of B and C, as B/C are quickly degraded in the absence of P1 [61].

P30. Another crucial and interesting member of the adhesin complex, P30, is a 30-kDa transmembrane protein encoded for by gene MPN453 [70,71]. P30 is known to localize to the distal end of the terminal organelle, and is also required for cytadhesion and gliding motility [58]. The extracellular C-terminal domain of the protein contains repeating proline-rich motifs that are required for P30 function [62,71]. While mutants lacking P30 are unable to cytadhere or glide at wild-type levels, the localization of P1/B/C to the pole of the terminal organelle is unaffected in the absence of P30 [72]. Conversely, the loss of P1/B/C does not affect P30 stability or localization [58]. Localization of P30 to a nascent terminal organelle alone, however, is not sufficient to provide gliding competence [73]. The exact role P30 plays in attachment remains unknown, though evidence of the significance of this terminal organelle protein for cytadhesion and gliding motility is convincing [74,75].

P65. Terminal organelle protein P65 is encoded by the MPN309 gene and is part of a transcriptional unit along with the genes for HMW2, P28, P41, and P24 [55,73,76]. Structurally P65 is characterized by a prominent acidic and proline-rich (APR) domain located at the N-terminus near a coiled-coil region of the protein [77,78]. P65 can be found at the surface of the terminal organelle despite lacking an obvious signal sequence, and co-localizes with P30 although its exact function remains unknown [73]. Experiments using P65 mutants showed that truncations of P65 had an impact on cytadherence (though it is not required for cytadherence), gliding motility, the surface dynamics and steady-state levels of P30, as well as downstream polar effects on HMW2, P28, P41, and P24 [55,58]. Interestingly, despite the deficits in P65

these mutants were able to develop P30-YFP foci as seen in wild-type *M. pneumoniae* but showed abnormal behavior during cell gliding [55]. P65 requires the presence of a stable terminal organelle core, as indicated by its instability in the absence of HMW3. Mutants that lack HMW1 and HMW2 also show reduced steady-state P65 levels [67,79].

HMW 1, HMW2, and HMW3. For a stable core to exist, both HMW1 and HMW2 must be present [80,81]. HMW1 is encoded for by the gene MPN447, and is a known cell surface protein that localizes along the filamentous extensions of the mycoplasma cell with a C-terminus that is thought to help in stabilizing HMW2 [60,82]. The amino acid sequence of HMW1 suggests that the protein contains three domains [80]. Domain I at the N-terminus is proposed to consist mainly of β-strands and contains an enriched in aromatic and glycine residues (EAGR) box, domain II is an acidic, proline-rich (APR) region, and domain III is located at the C-terminal domain and contains two predicted coiled-coil regions and is postulated to be involved in targeting for proteolytic degradation [80,83,84]. In addition to contributing to the stability of HMW2, the C-terminus of HMW1 is essential for function in the localization of P1 and core stabilization [58,82]. HMW2 is encoded for by the gene MPN310 yielding a large protein 1,818 amino acid residues in size, and has the greatest degree of similarity to proteins characterized by their potential to form coiled-coil structures such as those seen in the tail region of myosin type II heavy chain [76]. HMW2 is predicted to have 10 of these dimeric or trimeric coiled-coil domains interspersed with leucine zipper motifs [76]. Coiled-coil structures are common in cytoskeletal proteins with filamentous domains, and so this type of predicted structure and the high periodicity of hydrophobic-hydrophillic regions in HMW2 suggest it is a major structural element of the terminal organelle [53,76]. The effects on the stability of P1, P65, and P30 for HMW1, and on P1, P65, P30, HMW1, and HMW3 for HMW2, indicate that these proteins are

required early in terminal organelle development [43,53,58,76]. Another key component in core stabilization is HMW3. HMW3 is encoded by the gene MPN 452 and predominately consists of tandem APR domains located near the N-terminus of the protein [59,85]. It appears to localize with the cytoplasmic side of the membrane with no exposure to the cell exterior and no direct role in attachment [42]. Polymers of this protein are found surrounding the core and in the terminal button in a linear pattern, where it possibly serves to help stabilize the terminal organelle core [86]. HMW3 co-localizes with P30, and in the absence of HMW3, P30 is stable but fails to localize to the terminal organelle [79]. A non-reciprocal requirement for stability is observed for HMW1, HMW2, and HMW3, wherein HMW3 is unstable if HMW1 and HMW2 levels are reduced [61]. In wild type cells where HMW1, HMW2, and HMW3 are all present, the terminal organelle core takes on a characteristic spindle shape [11,58,80].

P41 and P24. These two cytadhernece-associated proteins of undefined function play key roles in terminal organelle development and gliding motility [54]. ORF MPN311 encodes for P41 and shortly downstream of that is the gene for P24, MPN312 [87]. Unlike most of the terminal organelle proteins described thus far, P41 and P24 localize to the base of the terminal organelle [88]. Furthermore, P41 localizes to the base of developing organelles prior to cessation of gliding, indicating that it is also incorporated early in the developmental process [58,73]. Interestingly, mutants lacking P41 exhibited terminal organelles that detach from the *M. pneumoniae* cell body entirely [54]. A 2007 study by Hasselbring and Krause showed that P41 is responsible for anchoring the terminal organelle to the cell body, and is required for *M. pneumoniae* to achieve a wild-type gliding velocity [54]. It is envisioned that P41 links the bowl structure at the base of the terminal organelle with the filamentous cytoskeletal network present throughout the cell body, and in the absence of this linkage the terminal organelle is unable to

transmit force or modulate drag resulting in a decrease in gliding velocity [44,45,54,58]. In the absence of P24, cells are unable to form new terminal organelles at wild type rates [54]. It remains unclear whether P24 interacts directly with P41 or rather with a P41-dependent protein instead [54].

Terminal organelle formation and development. Research is ongoing into the timeline of events and exact biochemistry behind the development and formation of nascent terminals, but for now most of the details remain unclear. The Hasselbring et al. 2006 study, however, shed some light onto the process showing that gliding ceased upon formation of a new terminal organelle adjacent to an existing one at a cell pole, and also that protein P41 appeared to precede P30 and P65 in the development of the new terminal organelle [58,73]. In addition, data indicated that incorporation of P30, P41, and P65 into nascent terminal organelles was a result of new protein synthesis, as opposed to originating from an existing organelle as early electron microscopy images had suggested [57,73]. P1 is trafficked to the terminal organelle later in the developmental process, where it must form a protein complex with P30, B, and C prior to becoming fully active and functional [58,73]. Terminal organelle development and assembly is very closely tied with cell division in *M. pneumoniae*, which will be discussed next.

Cell division and the terminal organelle. *M. pneumoniae* has evolved a specialized reproductive cycle, reproducing by binary fission that is temporally linked with duplication of its attachment organelle, and gliding is required for normal cell division to occur [42]. Without gliding, daughter cells are unable to separate, which is non-lethal but results in cell aggregates as seen in non-motile strains [42]. Initial light microscopy studies indicated that cell division appeared to begin with the formation of a second terminal organelle adjacent to the existing one [89]. Data correlating DNA content with location and number of total terminal organelles is

consistent with this model [66]. It has since been shown that nascent terminal organelles originate *de novo* rather than from a semi-conservative duplication from the original terminal organelle [57,73]. Terminal organelle duplication and separation precedes cell division, and multiple new terminal organelles often form before cell division is observed [73]. Furthermore, separation appears to be a function of resumption of gliding, specifically by the existing terminal organelle, rather than due to the migration of the new terminal organelle to the opposite pole of the cell as was previously thought [73]. In their experiments and under culture conditions, terminal organelle duplication and cytokinesis did not appear to be tightly regulated. That being said, the exact sequence of events and link between cell division, migration of attachment organelles to opposite poles, and daughter cell separation *in vivo* remains unknown [33,73].

Mechanism of gliding motility in *M. pneumoniae*. The mechanism of gliding in *M. pneumoniae* is not well understood. However, there is abundant evidence that cytadherence is required for gliding to occur, which has been the focus of most *M. pneumoniae* motility research [58,90-92]. Inhibition studies have found that *M. pneumoniae* binds to sulfated glycolipids and sialylated oligosaccharides [91,93-95]. It has also been shown that during gliding, the proteins located in the tip of the terminal organelle structure catch, pull, and release sialylated oligosaccharides fixed on a solid surface [50]. Further evidence in support of sialic acid-mediated attachment is the observed deficit in *M. pneumoniae* hemadsorption to respiratory epithelial cells and fibroblasts treated with neuraminidase [96]. Miyata et al. demonstrated that recognition of sialylated oligosaccharides proceeds in a lock and key fashion, and that binding is cooperative with Hill constants ranging from 2-3 depending on the specific oligosaccharide in question [50]. Furthermore, the same study indicated that *M. pneumoniae* might generate a drag force after the gliding stroke [94]. Miyata et al. found that the most effective sialylated

oligosaccharide recognized by *M. pneumoniae* was Neu5Ac-α-2,3-lactosamine (**Figure 2.4**), which is also well known as the target for binding by avian influenza virus [50,97]. Furthermore, this is consistent with the observed route of *M. pneumoniae* infection in which *M. pneumoniae* binds to the lower part of the human trachea during the early stages of colonization, as Neu5Ac-α-2,3-lactosamine is known to be abundant in that region of the respiratory tract [98]. Their results suggest that P1 acts as a foot in gliding over sialylated oligosaccharides to help the organism localize along the respiratory tract, as opposed to motility occurring in response to a chemoattractant, which is a hypothesis supported by the fact that the *M. pneumoniae* has no known chemoattractant genes [32,94].

Regulation of gliding motility in *M. pneumoniae.* Very little is known about the functional mechanism for gliding motility and the exact roles of the cytoskeletal and terminal organelle proteins described above, but a recent study by Page and Krause showed evidence of a potential regulatory circuit for gliding in *M. pneumoniae* driven by reversible phosphorylation [31]. The only annotated ser/thr protein kinase in *M. pneumoniae* is PrkC and its cognate phosphatase PrpC [99]. A similar system is known to exist in *Bacillus subtillus* wherein PrkC and PrpC homologues help regulate sporulation and cell wall development through reversible phosphorylation [100-102]. In *M. pneumoniae*, PrkC mutant cells glide at half the frequency of wild type, whereas PrpC mutant cells glide at twice the frequency of wild type cells [31]. Additionally, Pro Q diamond staining indicates that HMW1, HMW2, P1, and predicted cell surface protein MPN474 are phosphorylated [31,103]. Of these, it is known that HMW1 and HMW2 are phosphorylated in an ATP-dependant manner, and an association between phosphorylation of HMW1, HMW2, and P1 and gliding phenotype has been observed in various PrkC and PrpC mutant strains [31,104,105]. Evidence from the Page and Krause study suggests

that PrkC and PrpC work in opposition to up- and down- regulate gliding in *M. pneumoniae*, and reversible protein phosphorylation is likely a regulatory circuit for gliding motility rather than what drives the actual motor [31].

Clinical Relevance and Pathology of *Mycoplasma pneumoniae*

Mycoplasma pneumoniae is a major cause of respiratory disease in humans, accounting for approximately 20% to 40% of all community-acquired pneumonia (CAP) cases, and is the leading cause of CAP infection in older children and young adults [1-5]. In adults alone the annual economic burden of CAP exceeds $17 billion, and the incidence of infection in the very young and elderly is on the rise [4,6]. Furthermore, extra-pulmonary sequelae occur in up to 25% of cases, and chronic *M. pneumoniae* infection may play a contributing role in the onset, exacerbation, and recurrence of asthma [5].

History of *M. pneumoniae.* *M. pneumoniae* was initially discovered when isolated in tissue culture from the sputum of a patient with primary atypical pneumonia in 1944 by Eaton et al., and was known as the Eaton agent until 1963, when Chanock et al. successfully cultured the organism on cell free medium and proposed the current taxonomic nomenclature, *Mycoplasma pneumoniae* [106-108]. Several other mycoplasma species, notably *Mycoplasma orale* and *Mycoplasma salivarium*, exist as commensal flora in the oropharangeal region in humans but rarely cause disease outside of immunocompromised persons [33]. Mycoplasmas are primarily mucosal pathogens of typically the respiratory or urogenital tracts and live in very close association with the epithelial cells of these regions [109]. *M. pneumoniae* is exclusively a human pathogen with no known reservoir of infection outside of the human host [33]. Evidence accumulated since the 1960's from animal models, *in vitro* cell cultures, and organ culture

systems, indicates that attachment to the host epithelium is the crucial and prerequisite step in initiating *M. pneumoniae* infection (**Figure 2.5**) [33,110].

Cytadherence. *M. pneumoniae* is known to attach to and infect the extracellular surfaces of respiratory epithelium [52,111]. Though evidence of fusion with host cells and intracellular localization, survival, and replication in artificial cell culture systems exists for some mycoplasma spp., including *Mycoplasma pneumoniae,* whether or not *M. pneumoniae* invades host cells during the course of infection *in vivo* remains unknown [33,112]. That being said, the ability to have an intracellular existence would facilitate the establishment of latent or chronic infections, immune evasion, and eventual extrapulmonary spread as is common with *M. pneumoniae* pathogenesis [113].

The terminal organelle of *M. pneumoniae* facilitates a very tight association between the pathogen and the host cells [33,42,51,61,65,93]. This close association between *M. pneumoniae* and the respiratory epithelial cells prevents the host's mucociliary defense mechanism from effectively clearing the organism, which in turns allows *M. pneumoniae* to replicate and produce a variety of cytotoxic effects [33,110]. The host cell ligand for mediating this attachment has yet to be conclusively identified, but as discussed in an earlier section of this review is likely a sialylated oligosaccharide or sulfated glycolipid [33,50,93]. Furthermore, it has also been observed that *M. pneumoniae* cell surface proteins elongation factor Tu and pyruvate dehydrogenase E1 β are capable of binding to fibronectin, a common eukaryotic cell surface, basement membrane, and extracellular matrix protein [114]. However, it has been shown that the key protein mediating attachment to host respiratory epithelium is P1 [11,64].

Evidence for P1's role in attachment is abundant [5,8,9,11,52,56,64,65]. In summary, loss of P1 through mutation or trypsin treatment results in avirulence and a significant decrease in

adhesion capabilities [52]. Restoration of P1 function via spontaneous reversion leads to a return of infectivity and cytadhering phenotype [115]. Furthermore, additional proof stems from studies showing that monoclonal antibodies against P1 block adherence in a hamster tracheal ring model of infection whereas antibodies to other terminal organelle proteins do not block infection or prevent attachment capabilities [65]. However, P1 expression alone is not sufficient for attachment, and B/C and P30 proteins are required for normal function, implying a conformational or protein:protein interaction requirement between P1 and a complex of these proteins to establish successful colonization and subsequent infection [61,62].

P1 is also a major immunogen during *M. pneumoniae* infection [9]. As such, P1-mediated cytadherence is considered the major virulence factor for *M. pneumoniae* infection [5,33,49,109]. A study conducted by Gerstenecker and Jacobs in 1989 showed that three regions of P1 seemed to be involved in adherence based on topological mapping of five adherence-inhibiting monoclonal antibodies (mAbs), and the antibody binding was further characterized using a variety of linear octapeptides [8]. The identified binding sites were at the N-terminus from amino acids 1-14 and 231-238, a domain designated D1 located approximately in the middle of the molecule from amino acids 851-858 and 921-928, and a D2 domain near the C-terminus of the protein from residues 1303-1310, 1391-1398, and 1407-1414 (**Figure 2.6**) [8]. Of the five mAbs used in their experiments, P1.26 and P1.62 reacted with two primary amino acid sequences [8]. Both bound to the D1 region, with P1.62 showing additional binding to the N-terminus sequences and P1.26 with a second epitope sequence in the D2 region [8]. The dual binding observed by the two antibodies suggests that in the native proteins the adhesin epitopes consist of two sequences located in two different parts of the molecule, requiring a conformational binding site of the antibody to the native protein [8]. From their data Gerstenecker and Jacobs speculated

that the native attachment structure is possibly composed of several surface-exposed loops [8]. Jacobs et al. conducted another study using linear overlapping octapeptides representing approximately 1/5 of the total amino acid sequence to P1 in enzyme-linked immunosorbent assays to identify key immunodominant epitopes for antibody binding to P1 protein [9]. The experiments in this study revealed at least two defined epitopes recognized by anti-P1 antibodies originating from patients infected by *M. pneumoniae* [9]. Both identified binding sites were linear and neither corresponded with computer predictions regarding hydrophilicity or chain flexibility, however, peptide 810-817 (recognized by IgM) is predicted to be a surface-exposed region in the native protein [9]. IgG from infected patients in this study bound to the synthetic peptides between amino acids 970-1139, whereas binding by IgM fell between amino acids 810-817 and 1124-1131 [9]. Furthermore, P1 may exhibit antigenic mimicry in the adhesin binding sites, as evidenced by a lack of response in convalescent sera to octapeptides of previously identified adhesin epitope regions [9,116]. The P1 adhesin mAbs used in that study showed cross-reactivity with intracellular antigens of eukaryotic cell lines, specifically glyceraldehyde 3-phosphate dehydrogenase (GAPDH) and 2-phospho-D-glycerate hydrolase [116].

Additionally, prestimulation of guinea pigs with purified P1 did not protect against subsequent experimental *M. pneumoniae* infection challenge [117]. Moreso, the development of autoimmune antibodies during *M. pneumoniae* infection is well known and described in the literature [113,116,118-120]. For example, Lind et al. showed that greater than half of patients suffering from *M. pneumoniae* infection with positive complement fixation titers were also positive for auto antibodies to the mitotic spindle of eukaryotic cells and for cold agglutination [118]. *M. pneumoniae* structures reacting with the host as autoantigens could potentially explain the pathogen's role in chronic inflammatory disorders arising from long-term damage to the

respiratory epithelium, such as asthma, for example [116,118]. Essentially, the failure of convalescent sera to recognize the adhesin epitopes could allow *M. pneumoniae* to escape detection by the host immune response and the blocking action of adherence-inhibiting antibodies during primary and subsequent infections [116,117,121]. As cytadherence is the mediating step in *M. pneumoniae* infection, this molecular mimicry at the adhesin binding sites could explain the prolonged isolation of *M. pneumoniae* from the respiratory tract of infected patients, as well as the deficiency of a protective immune response to subsequent infection [116].

Cytotoxicity and inflammation. Upon attachment to host epithelial cells a variety of cytotoxic and inflammatory effects can occur, and internalization of *M. pneumoniae* cells is not a prerequisite for disease manifestation [33]. In animal models of *M. pneumoniae* infection it has been demonstrated that an initial pneumonia lasts three to four weeks total, similar to what is observed in humans and characterized by histological lung inflammation and elevated cytokine and chemokine levels [122,123]. It is unknown precisely how *M. pneumoniae* causes injury and insult to the respiratory epithelial cells following attachment, but a number of biochemical and immunological traits of the pathogen most likely responsible for its observed cytotoxicity have been described [124-127]. Furthermore, the close association of *M. pneumoniae* to the host cells mediated by the terminal organelle adhesin proteins can lead to localized tissue disruption [33,127].

Additionally, over the past several years it has been found that the organism can produce an ADP-ribosylating and vacuolating toxin named the Community-Acquired-Respiratory-Distress-Syndrome, or CARDS toxin [128]. The CARDS toxin is encoded by the MPN372 gene and was functionally identified as a human surfactant protein A-binding protein [129]. It contains some regions with limited structural homology to the pertussis toxin S1 protein and exhibits dose

dependent vacuolization and cytotoxicity in mouse and baboon bronchiolar and tracheal epithelium models [128]. The exact role of the CARDS toxin in *M. pneumoniae* pathogenicity is yet to be determined.

Another well-characterized virulence factor of *M. pneumoniae* is the hydrogen peroxide (H_2O_2) and superoxide radicals generated as by-products of the organism's metabolism [127]. These products of *M. pneumoniae* metabolism and the host's own endogenous toxic oxygen molecules work in concert to induce oxidative stress in the host cells [125]. The production of H_2O_2 by *M. pneumoniae* is an interesting phenomenon in that, as is consistent with a minimal genome, *M. pneumoniae* lacks enzymes such as superoxide dismutase and catalase to protect itself from the effects of the induced oxidative stress [124]. It is known that *M. pneumoniae* produces H_20_2 during the catabolism of glycerophospholipids via the glycerol-3-phosphate oxidase GlpD and the glycerophosphodiesterase GlpQ [130,131]. Furthermore, GlpQ is essential for H_2O_2 formation in the presence of deacylated phospholipids as the carbon source, and inactivation of GlpQ results in a complete loss of cytotoxicity towards HeLa cells [131]. Furthermore, it has been suggested that superoxide anion produced by *M. pneumoniae* acts to inhibit catalase in host cells, which in turn causes the host cells to become more susceptible to oxidative damage from the low concentrations of toxic oxygen molecules generated by the organism [124]. Another possible source of local injury is the acquisition of host cell lactoferrin by *M. pneumoniae* that generates highly reactive hydroxyl radicals from the introduction of iron complexes into a metabolically rendered acidic microenvironment [125]. How *M. pneumoniae* addresses the issue of oxidative stress generated by its metabolism, however, remains unknown.

On a larger scale, *M. pneumoniae* infection leads to deterioration in number and structure of cilia [33,132,133]. Moreso, some cells may lose their cilia altogether, become vacuolated,

exhibit reduced oxygen consumption, glucose utilization, amino acid uptake, macromolecule synthesis, and ultimately exfoliation of parts or infected cells in their entirety [5,134]. These subcellular events can be correlated with some of the major symptoms of *M. pneumoniae* infection, such as a characteristic chronic, hacking, non-productive cough [33,134].

M. pneumoniae infections trigger an intense local inflammatory response that can be exacerbated upon reinfection and eventually lead to long-term tissue damage [135]. Upon reaching the lower respiratory tract the organism may then be opsonized by complement or antibody binding [136,137]. At this stage, macrophages become activated, begin phagocytosis, and migrate to the site of infection [33]. It is common to see high percentages of neutrophils and lymphocytes in alveolar fluid [33]. Pulmonary infiltrates of CD4+ T lymphocytes, B lymphocytes, and plasma cells manifest radiologically [136,137]. The immune response is further amplified in association with lymphocyte proliferation, immunoglobulin production, release of tumor necrosis factor alpha (TNF-α), gamma interferon (IFN-γ), and a variety of interleukins, specifically interleukin 1-β (IL-1β), IL-2, IL-4, IL-5, IL-6, IL-8, IL-10, IL-17 and IL-18 based upon animal models and clinical and *in vitro* studies [138-145]. Elevated levels of these cytokines will be present in both alveolar fluid and serum, and elevated cold agglutinin levels occur in up to 75% of patients with *M. pneumoniae* infection [33,146,147]. Additionally, Yang et al. reported in 2002 that *M. pneumoniae* infection *in vitro* in human lung epithelial carcinoma cells led to increased levels of IL-8 and TNF-α mRNA's and both proteins were secreted into and detectable in cell medium [148]. Their study also found elevated mRNA levels of IL-1β, which is a major pro-inflammatory cytokine and important mediator in both lung defense and inflammation [148]. IL-1β protein was also synthesized but remained intracellular. Using protease digestion and antibody-blocking methods Yang et al. showed that *M. pneumoniae*

cytadherence is important for the induction of the pro-inflammatory cytokine cascade [148]. The more vigorous the cell-mediated immune response and subsequent cytokine stimulation, the greater the potential is for more severe clinical illness and pulmonary injury, and ultimately the greater the likelihood for immune-mediated lung disease [143,149-154].

Chronic *M. pneumoniae* infection and the exacerbation of asthma. The clinical association between *M. pneumoniae* infection and asthma has been suspected for greater than two decades, though the details and mechanisms of the correlation between the two remain unclear [146]. The first prospective study showing serological evidence of *M. pneumoniae* or respiratory virus infection in 27 of 84 asthma patients was done in 1970 by Berkovich et al. [155]. Not long after that study was published, Huhti et al. reported in 1974 that 19% (n=63) of asthma patients from their study had associated viral or *M. pneumoniae* infections [156]. More recently, in 2004 Biscardi et al. found similar numbers, where 20% (24/119) of patients with previously diagnosed asthma had simultaneous acute *M. pneumoniae* infections and asthma exacerbations [157]. In fact, based on the current literature *M. pneumoniae* appears to be an important factor for the acute exacerbation of asthma, accounting for anywhere from 3.3-50% of exacerbations amongst asthmatic patients [146]. Two of the most influential studies on the subject were done by Kraft et al. and Martin et al., in which they detected *M. pneumoniae* via PCR in the lower airways in 25 of 55 adult patients with chronic stable asthma, compared with just 1 of 11 in the controls [158,159]. However, this phenomenon is not exclusive to adult patients, as Esposito et al. conducted a study in 2000 and found *M. pneumoniae* in children with acute wheezing significantly more often than in the control group [160]. Furthermore, macrolide treatment significantly improved pulmonary function in asthmatics with *M. pneumoniae* infection [161]. Some proposed factors involved with the immune response to *M. pneumoniae*

that may lead to the exacerbation of asthma include the induction of TH2 cytokine, IL-2, IL-4, IL-5, immune cells, and IgE production [162,163]. Other factors possibly related are neutrophil cytokine signaling and degranulation, cell lysis at the respiratory epithelial surface, and increased airway wall thickness [164]. Evidence linking the two is convincing, but the role of *M. pneumoniae* in exacerbation of asthma is unclear as the mechanisms of *M. pneumoniae* interactions with the human airway are highly complex and multifactorial.

Extrapulmonary manifestations. Lastly, extrapulmonary spread is known to occur in up to 25% of *M. pneumoniae* infections, with variable onset of occurrence and in some cases in the absence of initial respiratory symptoms [5,33]. It is suggested that autoimmune reactions are responsible for many of the extrapulmonary complications that are associated with *M. pneumoniae* disease [48]. *M. pneumoniae* has been documented by culture and PCR in extrapulmonary sites such as the blood, synovial fluid of the joints, cerebrospinal fluid, pericardial fluid, and skin lesions [165-169]. The frequency at which direct invasion of these sites occurs is unknown as the organism is rarely diagnosed clinically [33]. Central nervous system (CNS) complications are the most commonly observed and serious extrapulmonary manifestations, and have been reported from as far back as 1943 [170,171]. CNS complications arising from *M. pneumoniae* infection are numerous and have included encephalitis, cerebellar syndrome and polyradiculitis, cranial nerve palsies, aseptic meningitis or meningoencephalitis, coma, mental confusion, and acute psychosis secondary to encephalitis, to name a few [172-179]. The majority of patients with neurological complications experience them 1-2 weeks following the onset of respiratory symptoms, but at least 20% of patients have no preceding or concomitant respiratory diagnosis, and this figure may be even higher in children [180,181]. *M. pneumoniae* associated neurological complications usually resolve entirely, but in some

instances they are severe and life-threatening and can result in chronic debilitating deficits in motor and mental function [170]. It is suspected that immune-mediated pathological mechanisms are the main cause of *M. pneumoniae* associated neurological manifestations due to the presence of cross-reactive antibodies to the brain and other neurologic structures that may develop over the course of infection [182-184]. A second possibility is that they arise from the aforementioned molecular mimicry with carbohydrate moieties of the abundant glycolipids in the *M. pneumoniae* membrane and lipoglycan capsule [33,52,116]. That being said, it cannot be entirely ruled out that direct invasion by the organism itself leads to the extrapulmonary manifestations as evidenced by the detection of *M. pneumoniae* RNA in brain tissue and positive identification by PCR in cerebrospinal fluid [185-189].

Clinical Manifestation and Epidemiology of *Mycoplasma pneumoniae* Infection

As mentioned previously *M. pneumoniae* was isolated and identified in 1944, but the clinical entity of pneumonia caused by the organism was recognized many years prior to its discovery [33,106]. The first clue differentiating *M. pneumoniae* infection from classical pneumococcal pneumonia was the lack of response to antimicrobial treatment with glycopeptides or beta-lactams [33]. As *M. pneumoniae* lacks a cell wall and does not make peptidoglycan, these antibiotics have no effect on the organism's ability to replicate, grow, or divide [32,33]. It was from this atypical therapy response observation that the term "primary atypical pneumonia" was coined [33].

Demographics and spectrum of *M. pneumoniae* infection. *M. pneumoniae* infection is acquired through respiratory secretions, mainly aerosols from person to person, and spreads efficiently within close living quarters such as schools, prisons, or military barracks, for

example, and incubation periods can last as long as three weeks [13,14,132]. Intrafamily spread and transmission is common, with reports that up to 39% of family contacts may eventually become *M. pneumoniae* infected [33,190-192]. *M. pneumoniae* infection has been reported in people of all ages, in both genders, and in otherwise healthy individuals, and *M. pneumoniae* infections occur endemically and epidemically worldwide in both children and adults [5,33,193-195]. Climate and geography do not appear to be of any major significance [33]. Symptoms tend to be nondescript and the disease often has complex and variable presentations, making definitive diagnosis challenging [1,4,15]. As a result, diagnosis of *M. pneumoniae* is often presumptive and relies heavily on the combination of physical findings and elimination of other possible causes [3,5,14]. Diagnostic methods for *M. pneumoniae* detection will be covered in more detail in a later section of this review.

Clinical presentation of *M. pneumoniae* disease. *M. pneumoniae* infections may manifest in the upper respiratory tract, the lower respiratory tract, or both [33]. Though numbers vary amongst numerous studies, it has been reported that up to 50% of patients infected with *M. pneumoniae* present with upper respiratory tract illness [33,196]. Symptomatic disease develops gradually over a period of several days and can persist for as long as weeks or even months [33]. The most commonly reported symptoms are sore throat, hoarseness, fever, non-productive cough occasionally yielding non-bloody sputum, headache, chills, myalgias, coryza, and general malaise [132,179,191,197]. Chest soreness may arise as a result of prolonged coughing, and over time the cough may take on a pertussis-like character [132]. In children under 5 years of age wheezing and coryza are the most common symptoms, and progression to pneumonia is relatively rare [179,191,197]. Older children, however, between the ages of 5-15 are more likely to develop single or bi-lobed bronchopneumonia that can require hospitalization [179,191,197].

In adults *M. pneumoniae* infection is typically mild, with many adult cases being asymptomatic and occur among outpatients, hence the term "walking pneumonia" [33,198]. That being said, *M. pneumoniae* disease can be severe in adults and older persons requiring hospitalization, and is a significant cause of bacterial pneumonia in the United States [199]. Interestingly, subsequent *M. pneumoniae* infections may actually be more common in those with mild initial cases when compared to those in which pneumonia develops, perhaps due to the lesser stimulation of an immune response in the first case [200]. An additional observation of interest is that the likelihood of hospitalization due to *M. pneumoniae* related pneumonia increases with age, and it is the second leading cause of pneumonia after *Streptococcus pneumoniae* in the elderly (**Figure 2.7**) [199]. Furthermore, patients with *M. pneumoniae* infection have an increased incidence of succumbing to a secondary infection(s) with other atypical pneumonia-causing pathogens [149].

Epidemiological trends of *M. pneumoniae* infection. One noteworthy rising trend in *M. pneumoniae* infection is that of macrolide resistance, particularly in children [201-205]. Since *M. pneumoniae* lacks a cell wall and does not produce peptidoglycan, traditional beta-lactams and glycopeptides are ineffective against the pathogen [32,33,206]. Sulfonamides, trimethoprim, polymixins, nalidixic acid, and rifampin are also inactive against *M. pneumoniae* [207]. *M. pneumoniae* is inhibited by tetracyclines, macrolides, ketolides, and fluoroquinolones, with very little variation in MIC's across clinical isolates [208,209]. Agents that target the bacterial ribosome that are effective against *M. pneumoniae* include streptogramins, chloramphenicol, and aminoglycosides, however they are not widely used for therapeutic purposes against the organism [33,132]. Fluoroquinolones have been shown to act with a bacteriocidal mechanism against *M. pneumoniae* whereas macrolides and tetracyclines are primarily bacteriostatic, which is one possible reason for the increase in *M. pneumoniae* resistance to these antibiotics over the

past decade [208,210-212]. It has been shown that macrolide resistance in *M. pneumoniae* arises from a single nucleotide polymorphism (SNP) in the 23S rRNA gene at position 2063 and 2064, which in turn reduces the affinity of macrolide antibiotics for the ribosome [202,213,214].

Another notable aspect of *M. pneumoniae* infection is the periodicity of outbreak epidemics shown to occur in regular patterns of 3-5 years [5,12,33]. Little is known regarding the significance of or factors involved with driving these epidemic cycles, as difficulties in the diagnosis of *M. pneumoniae* have impeded the ability to obtain consistent or comprehensive epidemiological data [3,12]. Also of interest in *M. pneumoniae* infection is the role of strain genotype in pathogenesis and disease epidemiology [3,5,215-217]. Genetic diversity among *M. pneumoniae* is limited, and as such is generally categorized into one of two groups, type I (strain M 129) or type II (strain FH) based on variations within the sequence of the *P1* gene [7,15,18,19,218].

The role of P1 in antigenic variation of *M. pneumoniae* infection. The *P1* gene is approximately 4,900 bp long, and as discussed earlier in this review its gene product, the surface protein P1, plays a significant role in immunogenic response and is also an important virulence factor for *M. pneumoniae* infection [8-10]. There are two well-characterized repetitive regions within the gene, Rep MP2/3 near the 3' end of the gene and Rep MP4 within the 5' end [7]. These sequences are present in the *M. pneumoniae* genome up to 10 and 8 times, respectively, whereas the *P1* gene is present in its fully functional form in just a single copy [7]. Based on sequence analysis of variation within the repetitive element regions, *M. pneumoniae* clinical isolates can be divided into the two main subtypes listed above, with variant strains of the two becoming more and more common [7,15,17-19,56]. In a 20120 study Nilsson et al. found no correlation between the genotype of *M. pneumoniae* infection and the severity of disease as

measured by patient hospitalization [219]. Type-switching between the two major strain types seems to regularly occur in 4-7 year cycles (**Figure 2.8**), though it is unknown whether there is a link between the observed trends in type-switching and outbreak periodicity [12,215-217].

While the variation in the *P1* gene sequence is used to successfully distinguish between type 1, type 2, and variant strains of *M. pneumoniae*, little is known about the exact phenotypic difference(s) arising from the genotype differences that exist between them [220]. Nucleotide and amino acid sequencing of 60 *M. pneumoniae* isolates indicates that trinucleotide short sequence repeats (SSR's) coding for serine can be found in all strain types anywhere from 5-14 times, but appear to be most prevalent in type 1 strains [7]. Serine repeats may form a hinge structure and lead to downstream conformational differences in the P1 protein between the different strain types, which could potentially affect its interaction with the host as a surface antigen [221,222]. In addition, 14 of the 60 isolates in the Zhao study had point mutations in several variant strains corresponding to amino acid changes in P1 to glutamine, proline, asparagine, and isoleucine residues [7]. Furthermore, it was recently observed that type 1 and 2 *M. pneumoniae* strains form biofilms that differ quantitatively and qualitatively [37]. Simmons et al. found that type 1 strain M129 grows well but forms biofilms that are less robust, and with towers that are rougher at the margins than that of type 2 strain UAB PO1, and upon examination of other *M. pneumoniae* isolates it appears that biofilm robustness correlates with strain type (**Figure 2.9**) [37]. A polysaccharide containing *N*-acetylglucosamine (GlcNAc) is secreted by M129 into the culture medium, whereas GlcNAc is found in close association with cells of type 2 strains [37]. They proposed that GlcNAc may have a role in biofilm formation, and as such may contribute to differences in virulence, chronicity, and treatment outcome between strains of *M. pneumoniae* infection [37].

Current Methods for Detecting and Genotyping *Mycoplasma pneumoniae* Infection

Historically, serologic testing has long been considered the foundation for the diagnosis of *M. pneumoniae* infection but has severe limitations in sensitivity and specificity, a high tendency for false negatives, and often must be paired with another diagnostic method [1,3,5,10,14]. Serology diagnoses were initially done via complement fixation using glycolipid extract from *M. pneumoniae* [9,33,223]. However, considerable cross-reactivity with antigens of different origins is known to exist making this method highly inefficient [33,224-226]. Through examination of *M. pneumoniae* infected patient sera, immunoblot techniques identified consistent development of antibodies against P1 protein, which is how the adhesin was identified as the immunodominant antigen of *M. pneumoniae* infection [51,227,228]. From there, the purified protein was successfully used as a defined and specific antigen for *M. pneumoniae* serological diagnoses which overcame the efficiency limitation of the existing method, however, the high cost of isolating P1 prevented the widespread use for diagnostic purposes [9,229,230]. Another particularly limiting factor for serological diagnostic methods is the requirement for both acute and convalescent sera for antibody testing, and the cross-reactivity of IgG, IgA, and/or IgM antibodies against *M. pneumoniae* in healthy blood donors [3,33,231]. Additionally, false negative tests can occur if the serum is collected after the administration of antibiotics [5].

At present, the most effective method for detecting *M. pneumoniae* in clinical samples is qPCR [1,10,14]. There are many assay targets for qPCR detection of *M. pneumoniae*, including 16SrRNA, P1 adhesion gene, ATPase operon gene, *tuf* gene, repetitive element *repMp1*, and the CARDS toxin gene, among others [1,6,10,14,33,232]. Of these, it has been demonstrated that the assay targeting the CARDS toxin gene is the most sensitive and is the gene target currently utilized in CDC outbreak investigations [14]. At present, the only FDA approved qPCR-based

diagnostic test for clinical detection of *M. pneumoniae* is the BioFire FilmArray® Respiratory Panel (BioFire Diagnostics, Inc., Salt Lake City, Utah) [16]. The BioFire test performs nucleic acid purification and nested, multiplex qPCR with high resolution melt analysis on nasopharyngeal swabs to assay for 21 common and emerging viral and bacterial respiratory pathogens, and is capable of detecting *M. pneumoniae* as low as 30 CFU/ml [16]. This method can exhibit high sensitivity and allow for detection in the early stages of infection, but the cost, complexity, and expertise it requires limit the practicality of widespread use in hospitals and reference laboratories [1,3,5,10,14]. These limitations create a critical barrier to the accurate and timely diagnosis of *M. pneumoniae* infection, and a rapid, simple, reliable diagnostic platform would greatly improve the control of *M. pneumoniae* disease.

M. pneumoniae genotyping is currently done by sequencing of the *P1* gene, restriction length fragment polymorphism, or by qPCR in combination with high-resolution melt analysis [3,5,15,17-19]. These assays target regions within the *P1* gene containing the repetitive element RepMP2/3, where the major point of variance between strain types occurs [111,233]. While the application of these PCR-based typing assays has greatly facilitated the study of *M. pneumoniae* epidemiology, both require a great deal of cost, technical expertise, and additional testing beyond clinical detection that limit their practicality for widespread, point-of-care use [13,234]. Therefore, a biosensing platform with the ability to simultaneously detect and type clinical specimens in a single assay would be of great value from both diagnostic and epidemiological standpoints.

Another available diagnostic test based on qPCR in combination with high-resolution melt analysis exists for detection of macrolide resistance [235]. This assay was developed by Wolff et al. in 2008 and detects the dominant mutations conferring macrolide resistance in *M.*

pneumoniae [235]. While this is a valuable assay in that it provides a way for clinicians to evaluate the macrolide susceptibility of *M. pneumoniae* from a patient specimen and proceed accordingly with treatment, it is yet another entirely separate assay in addition to those required for confirmation of the presence of *M. pneumoniae* within the patient sample and to subsequently establish the strain type.

Essentially, the key diagnostic question for clinicians is to establish the source of infection in order to determine the appropriate antibiotic regimen to administer. However, the ability to answer the questions (1) is the organism present, (2) what strain-type is present, and (3) what macrolide susceptibility profile is present in the organism within a single, point-of-care test would be invaluable for epidemiological purposes such as monitoring strain type periodicity and virulence, determining the true prevalence of the pathogen within the population, macrolide resistance trends, frequency of concomitant and/or secondary infection with other respiratory pathogens, the effects of chronic infection, finding the natural reservoir of infection for *M. pneumoniae*, and accurately tracking outbreak occurrences and frequencies. At present there is an unmet need for a rapid, robust, cost-effective, point-of-care platform for the detection, typing, and characterization of *M. pneumoniae* within a single test.

Evolution of NA-SERS for Biosensing Purposes

Vibrational spectroscopy has an inherent biochemical specificity that led to its consideration as a next-generation platform for the rapid detection, characterization, and identification of infectious agents [20-23]. Raman spectroscopy in particular has several advantages for application to biological samples, including narrow bandwidths, good spatial resolution, and the ability to analyze aqueous samples due to the absence of interference by water

molecules [20,21,24]. Additionally, Raman spectra provide detailed structural information on the chemical composition of a sample, which can serve as a characteristic molecular fingerprint for pathogen identification [23,24]. Despite these advantages, standard Raman spectra are inherently limited by low scattering cross-sections, which translate to weak signals for detection, and initially made the application of traditional Raman spectroscopy for biosensing applications impractical and inefficient [13,21,24]. However, over time the technique has evolved to be a very powerful tool for analytical detection of biological samples.

History of Raman spectroscopy. Sir C. V. Raman first described that light is inelastically scattered in 1928 [236]. When a monochromatic light source such as a laser is used to excite a sample, the energy of the photon is transferred to the sample as it strikes the molecules that make up the sample [236]. Most of the transferred energy will be elastically scattered at the same frequency as the incoming incident frequency, which is known as Rayleigh scattering [236]. However, a small proportion of the light, approximately 1 in 10^8 photons, is scattered inelastically at frequencies that differ from that of the incident frequency, known as Raman scattering [236]. According to the Tyndall effect, it has been shown that the intensity of Raman scattering is inversely proportional to the fourth power of the wavelength of the incident light [237]. There are two types of Raman scattering, Stokes and anti-Stokes [236]. In Stokes Raman scattering, the molecule in the sample absorbs energy from a photon, and the vibrational mode energy of the sample is emitted with less energy at a lower frequency than the incident energy state [236]. Therefore, the wavenumber of the Raman shift for Stokes scattering will be less than that of the incident photon [236]. In anti-Stokes Raman scattering, the frequency of the vibrational mode energy emitted from the molecule is greater than that of the incident light, and so the subsequent wavenumber of the Raman shift will be greater than that of the incident photon

[236]. Raman spectra are described by the observed wavenumber shift in the unit cm^{-1} resulting from excitation by an external source [236]. Measuring vibrational energy based on the polarizability of the electron clouds from a sample allows for the generation of Raman spectra over a range of wavenumbers creating a total biological fingerprint (Raman shifts between 400-1800 cm^{-1}) [24,238,239]. Furthermore, the assignment of individual peaks within spectral data corresponding to specific biological input has also been prevalent in the literature, and vast spectral libraries have been compiled from classic analytical chemistry analyses on purified single components [240-244]. However, traditional Raman scattering of biological samples was considered a bulk sampling technique and was severely limited by the weak cross-section of the scattering signal [245].

Capabilities, applications, and limitations of early SERS platforms. In the late 1970s, Raman spectroscopy evolved upon the discovery that adsorption of molecules onto nanoscopically roughened metallic surfaces resulted in significant enhancements in Raman signal and spectral intensity, referred to as surface-enhanced Raman spectroscopy, or SERS [23-25]. A cartoon schematic of the principle behind SERS is given in **Figure 2.10A**. Certain noble metals (for example Au, Ag, and Cu) can amplify the Raman signal as much as 15 orders of magnitude when in close proximity to a compound of interest, which can allow for collection of a signal that is rich in chemical and structural information about the sample of interest [246]. The enhancement effect is attributed to a combination of two factors, (1) the surface Plasmon resonance (also known as the electromagnetic effect) of the metal electrons and (2) the charge-transfer resonance between the molecules of the sample and the electrons of the metallic substrate [247,248]. The electromagnetic effect is thought to be the most significant contributor to signal amplification, with typical signal enhancements ranging from 10^4 to 10^{14} with respect to

normal Raman intensities [20,21]. This phenomenon arises from the transfer of energy from the incoming light source to the metal atoms of the substrate, which stimulates a polarization of the electron clouds in the surface atoms to generate an oscillating dipole of the conducting electrons of the metal surface [249,250]. Another important contributor to SERS enhancement is the proximity of the analyte to the nanostructures [251]. The distance-dependent nature of the surface enhancement effect has been previously calculated to define an intimate proximity factor of 10^{-10} indicating that even the slightest separation between the sample and the nanostructure is enough to nullify SERS enhancement [251]. SERS allows a sample to be analyzed rapidly by simply placing the sample on the substrate and scanning, without the need of incubating or complex sample preparation and handling [20]. In addition to this experimental ease, SERS also offers a high degree of sensitivity and specificity, with single molecule detection previously reported [252,253]. Most importantly, SERS retains all the advantages of standard Raman spectroscopy in addition to markedly improving sensitivity and allowing for considerable success in whole organism molecular fingerprinting, capable of not only species level discrimination of bacteria and viruses but also strain discrimination within species [20,24,26,27]. SERS has been applied for biosensing purposes in numerous fields of study, for example optical probing in live cells, cancer detection, geology and mineralogy, forensic science, homeland security and biodefense, applied, environmental, and for chemistry, pharmaceutical, and cosmetic sciences purposes [26,245].

However, inconsistency and lack of reproducibility in the preparation of SERS-active substrates and metal colloid solutions originally prevented the widespread use of SERS for biosensing applications [20,21,24]. Problems arose as colloidal solutions, while easily prepared, were often variable and unstable in their SERS enhancement factors [21,254]. Other

disadvantages include the effect of temperature, pH, and the presence of adsorbates on colloidal stability [254]. Early research on SERS-active particles was driven by the search for "hot spots" that result in high signal amplification and the development of nano-structured surfaces [21,22]. These limitations initially made further advancement of SERS technology for clinical diagnostic purposes impractical.

Development of nanorod array-SERS. In 2005, a technique for fabricating reproducible metallic nanorod arrays was developed called oblique angle deposition (OAD) [255]. OAD yields highly ordered silver nanorod array (NA) substrates with stable, consistent, reproducible SERS enhancement factors of around 10^8, with less than 15% variation between substrate batches [21]. Schematics of the physical parameters of the nanorod array substrates are shown in **Figure 2.10B**. The silver nanorods generated using the OAD method were fabricated using a custom-designed electron-beam/sputtering evaporation system [255]. Briefly, three sequential layers are deposited onto pre-cleaned 1×3'' glass microscope slides as follows: a 20-nm Ti film, a 500-nm Ag film, and a layer of Ag nanorods obliquely angled at 86° with respect to the surface normal [20,21,255]. Average specifications for optimized SERS enhancements are nanorod lengths of 895 ± 95 nm and widths of 85-100 nm, at a density of 13 nanorods/μm^2 [20,21,255]. Furthermore, the nanorods have been optimized to enhance signals from 785 nm incident light [256]. In addition, the reproducibility of OAD-prepared substrates can be improved even further when patterned into a multiwell format with polydimethylsiloxane (PDMS) using the protocol established by Abell et al. (**Figure 2.11**). [20]. Upon optimization of the physical parameters and signal enhancement of the nanorod substrates, the application of the platform for biological detection was investigated [256]. Viral agents were studied initially due to their size, which was predicted to be of importance for the intimate association of the analyte and the nanostructure

required for the SERS enhancement effect to occur [251]. The highly reproducible detection capabilities of NA-SERS substrates have been demonstrated for multiple infectious agents, including but not limited to respiratory syncytial virus (RSV), rotavirus, influenza, HIV, adenovirus, SARS, and *M. pneumoniae* [13,22,27-29].

Chemometric analysis of spectral data. A second critical aspect of NA-SERS biosensing applications is the analytical method used to interpret the intrinsically multivariate SERS spectral data [257,258]. Chemometric analysis was introduced in the 1970's by Svante Wold to address the complex spectral data from NMR and UV-VIS instruments [259]. Chemometric analysis uses statistical algorithms for specialized feature selection in order to analyze the entire spectral profile, which is an absolute necessity as discrete patterns of multiple bands rather than individual peaks are used for identification [258,260,261]. Furthermore, chemometric analysis reduces the dimensionality of the dataset allowing for the highly selective discrimination and detection of pathogens based upon their unique NA-SERS spectral profiles [13,26,27,29,262].

With spectral data the scientific paradigm of one dependent variable per experiment is impractical and of limited usefulness, as spectral data represents the vibrational energies of many different types of molecules and chemical structures within a sample [257]. To further increase the complexity of spectral data, a large number of wavenumbers are collected for each sample, which produces a matrix of linear, independent columns [257]. These columns often display colinearity with one another, that is to say one or more wavenumbers are linearly dependent in their response to incident energy, and chemometric software programs can extract a large amount of information out of the spectra by optimizing this similarity of the data structure [257]. The

following paragraphs will discuss the common features of chemometric analysis and the most relevant techniques employed for *M. pneumoniae* detection by NA-SERS.

Pre-processing of sample spectra. Pre-processing is a standard practice in spectral data handling prior to proceeding with chemometric analyses. The intensity of multiple spectra collected within a single experiment can vary due to instrument fluctuations, background interference, or poor signal-to-noise ratios, which can be improved by simple mathematical corrections [257]. For example, spectral data is frequently derivatized to reduce noise and sharpen peaks, and can then be further normalized to the unit vector or the area under the curve to allow for comparison of peak-wise intensities [260]. In 1964 Savitsky and Golay described a smoothing algorithm for pre-processing spectra that uses a calculated "best fit" line with a moving window of data points, and the result is re-plotted to produce a new spectrum with least squares residuals minimized to optimize the slope of the new line [263]. Spectra can subsequently be mean-centered to further improved chemometric modeling performance of the spectra [258].

Principal component analysis (PCA). A common data mining approach that utilizes the total variance present in the dataset to find patterns for classification is PCA [264,265]. PCA deconstructs the data and reduces the dimensionality of the dataset by finding the vector in multivariate space that both captures the maximum variance and redraws the space with that component as a new x-axis [257,264,265]. Next, the next dimension is found that captures the second highest variance at an independent and orthogonal vector to the initial vector [257,264,265]. Principal components are ordered by decreasing eigenvalues, which reflects the reduction in captured variance by each subsequent component [257,264,265]. In this way, PCA allows for a dataset spanning 2,796 wavenumbers (variable dimensions), for example, to be

greatly reduced in number of dimensions, and facilitates establishing patterns and grouping of similar spectra present in the dataset without any *a priori* knowledge of sample class or identity [257].

Partial least squares-discriminatory analysis (PLS-DA). PLS-DA is a full-spectrum, multivariate, supervised chemometric method whereby prior knowledge of classes is used to yield more robust discrimination by minimizing variation within classes while emphasizing latent variables arising from spectral differences between classes [266,267]. In this approach, a training set (y-block) is used and can be applied to the multivariate x-block containing the pre-processed spectral data, usually in combination with the class assignment [266,268]. However, one of the dangers of classification by PLS-DA is over-fitting the data, and therefore it is essential to cross-validate the model to assess its goodness of fit [266,268]. Internal cross-validation is performed by algorithms that withhold a portion of the dataset [257,269]. A common algorithm for cross-validation of PLS-DA models is Venetian blinds, which withholds several samples from the model and then tests the model's accuracy with the withheld samples [266], and is the cross-validation method of choice for classification of *M. pneumoniae* NA-SERS spectra.

NA-SERS for the detection of *M. pneumoniae.* Hennigan et al. previously developed an NA-SERS-based assay capable of detecting *M. pneumoniae* in both simulated and true clinical backgrounds with statistically significant sensitivity and specificity [13]. Specifically, three *M. pneumoniae* strains were reproducibly differentiated by NA-SERS with 95-100% specificity and 94-100% sensitivity, with a lower endpoint for detection that exceeded conventional PCR [13]. Furthermore, throat swab samples spiked with *M. pneumoniae* were also analyzed and yielded detection in a clinically relevant background of >90% cross-validated statistical accuracy [13].

In addition, NA-SERS was able to correctly classify ten true clinical throat samples previously established to be positive or negative by qPCR and culture with 97% cross-validated statistical accuracy [13].

Their initial evaluation of the NA-SERS biosensing platform capabilities indicate the potential for application as a next-generation diagnostic tool for the clinical detection of *M. pneumoniae*, but a more comprehensive analysis of the assay is needed prior to proceeding with clinical validation [13]. The studies discussed in the following chapters of this dissertation further explore and define the clinically relevant parameters and limits of the Hennigan et al. assay in order to continue the development of NA-SERS as a next-generation platform for the detection of *M. pneumoniae* in clinical samples.

Figure 2.1: Phylogeny of mycoplasmas. Reconstructed from 16S rRNA sequence comparisons. Branch lengths are proportional to evolutionary-distance (the number of base changes per 1,000 nucleotides). The scale at the bottom denotes the branch distance corresponding to 5 base changes per 100 nucleotides. Modified from [270].

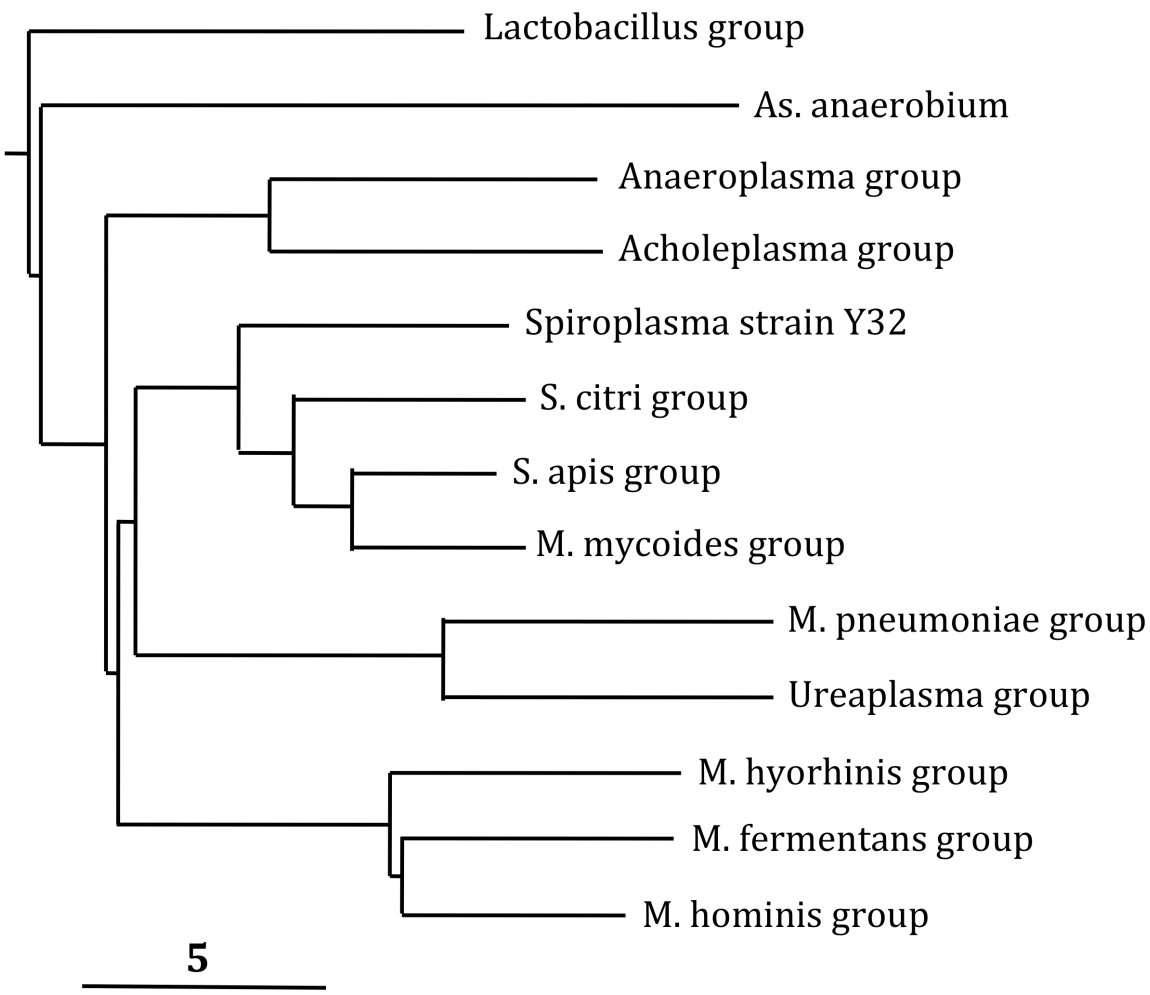
Lactobacillus group
As. anaerobium
Anaeroplasma group
Acholeplasma group
Spiroplasma strain Y32
S. citri group
S. apis group
M. mycoides group
M. pneumoniae group
Ureaplasma group
M. hyorhinis group
M. fermentans group
M. hominis group
5

Figure 2.2: Microscopic imaging of *M. pneumoniae.* (A) Stereomicroscope image of typical *M. pneumoniae* colonies growing on SP4 agar. Magnification x95. Examples of individual colonies of *M. pneumoniae* are indicated by red arrows. **(B)** Scanning electron micrograph (SEM) image of individual wild type *M. pneumoniae* cells. Whole mycoplasmas are shown with terminal attachment organelles indicated by red arrows. Modified from [33,135].

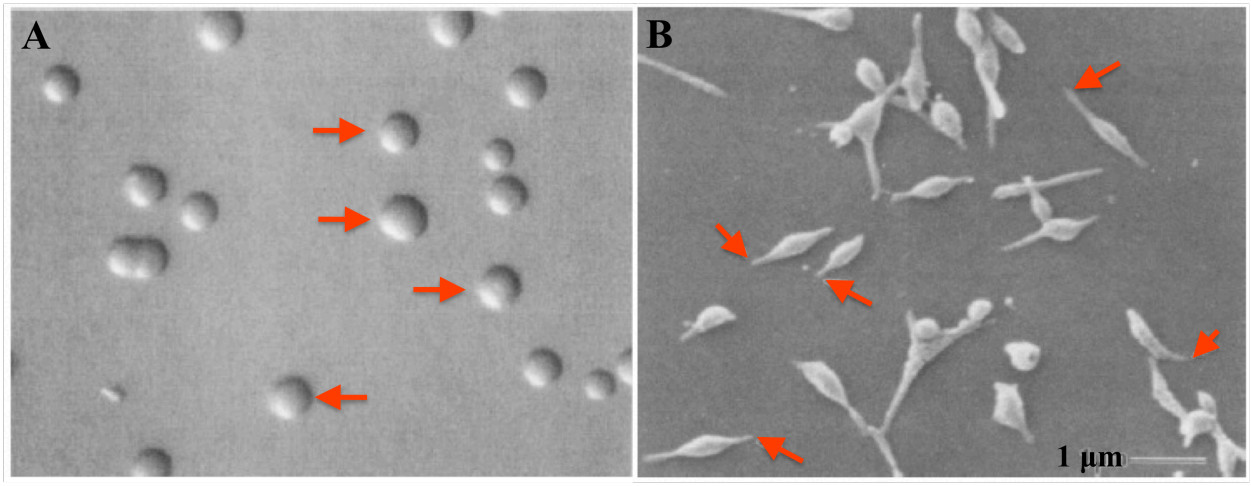
A
B
1 µm

Figure 2.3: Schematic of *M. pneumoniae* terminal organelle. Shapes represent localization of key terminal organelle substructures and protein components associated therewith. White shapes represent P41, P24, and HMW1; black shapes represent HMW2 and HMW3; and light gray ovals represent P1, P30, P65, B, and C. Modified from [55].

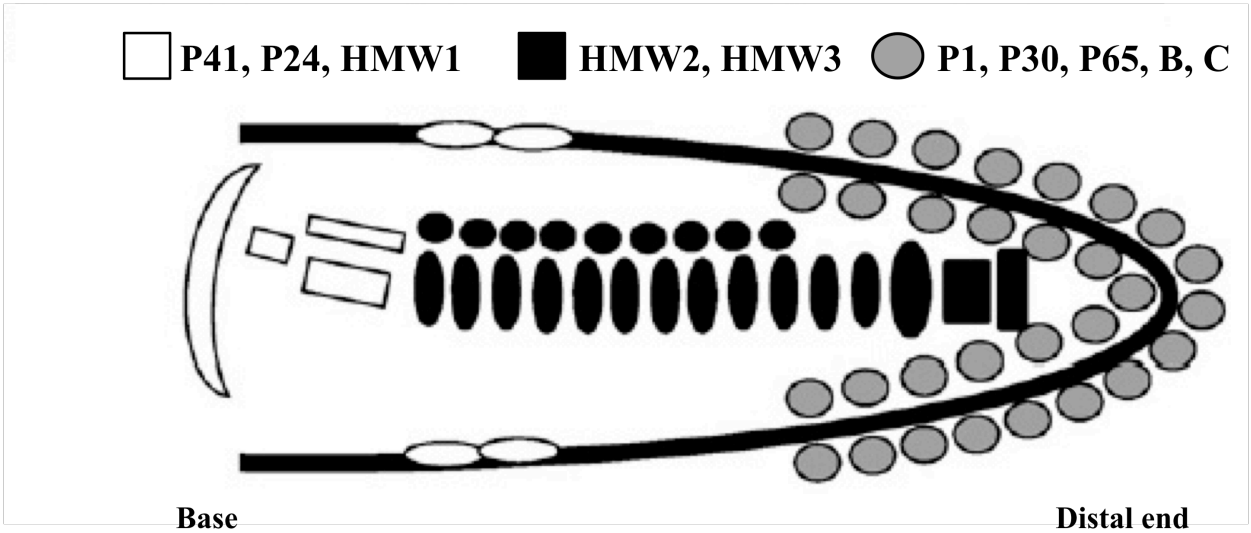
P41, P24, HMW1
HMW2, HMW3
P1, P30, P65, B, C
Base
Distal end

Figure 2.4: Structure of sialylated oligosacharride compound most effective for inhibition of *M. pneumoniae* binding and gliding motility. Modified from [50].

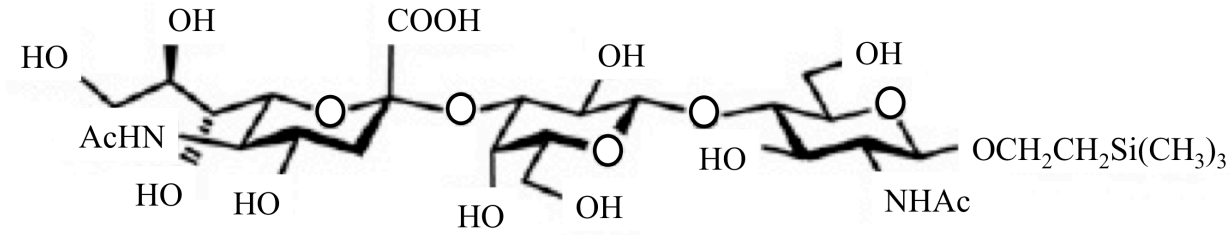

Neu5Ac-α-2,3-LacNAc

Figure 2.5: Transmission electron micrograph (TEM) of *M. pneumoniae*-infected hamster tracheal ring. Demonstration of the close association of *Mycoplasma pneumoniae* to the host epithelium mediated by the terminal organelle (*M. pneumoniae* cell indicated by red arrow, terminal organelle attaching to the epithelium indicated by red circle). Image modified from [33].

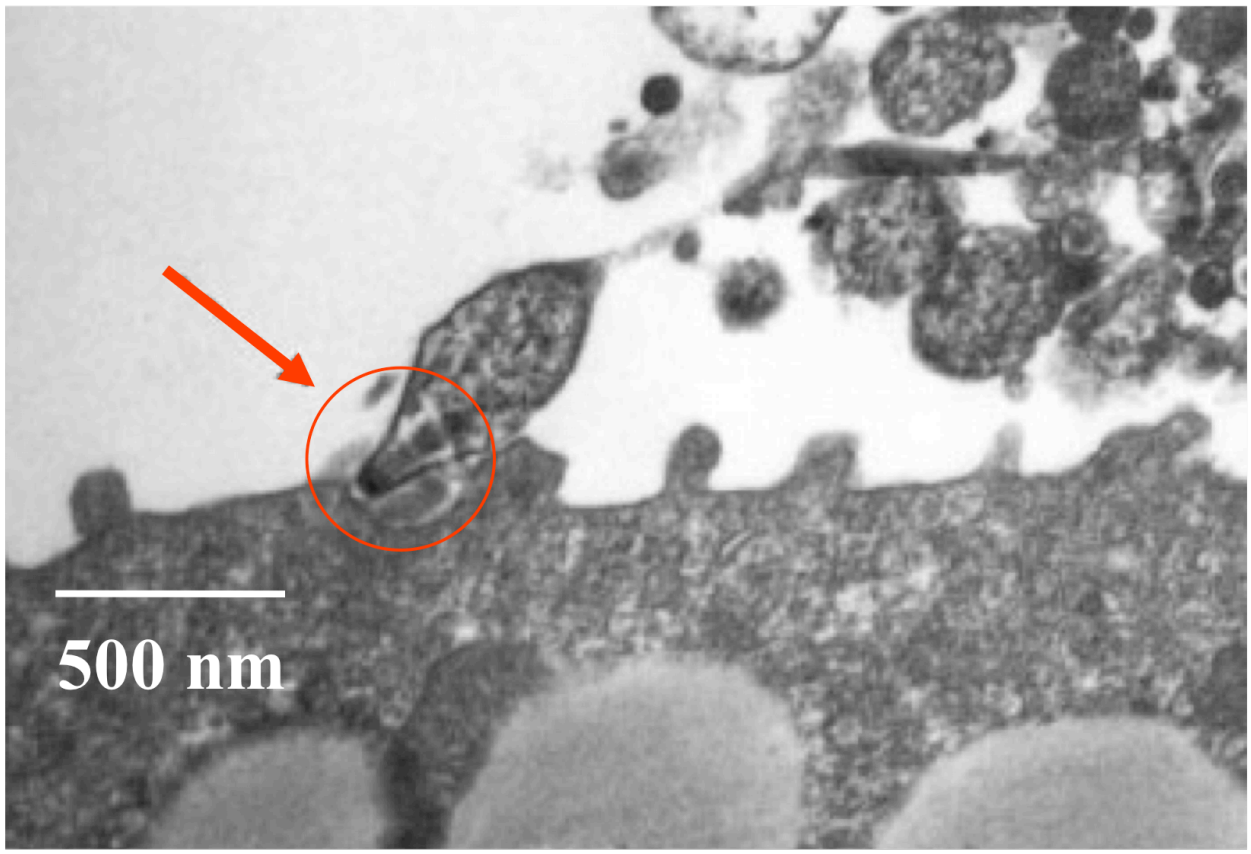
500 nm

Figure 2.6: Schematic of P1 adhesin. The molecule is divided into domains I, II, and III, which are linked by predicted flexible hinges. Domain I is highly conserved. The transmembrane segment is labeled TM. The N-terminal 59 residues are removed during the maturation process at the position marked by an open triangle. The regions homologous to paralogs are indicated by lines marked as RepMP4 and RepMP2/3. The binding sites of inhibitory antibodies, which should indicate exposed regions of the protein, are represented by filled triangles [8]. Domain III is inside the cell and likely interacts with other cytoplasmic proteins. Two molecules of P1 are predicted to fold into a globular complex with two molecules of P90. Modified from [56].

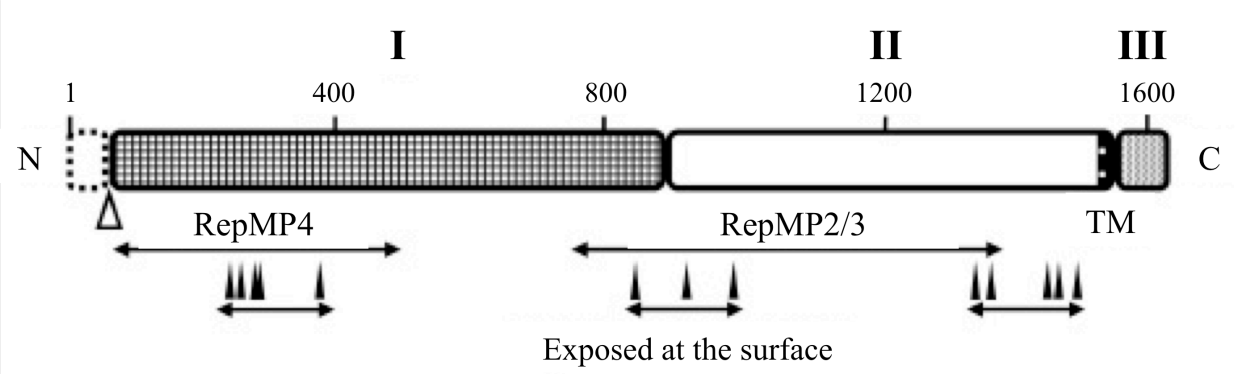
I
II
III
1
400
800
1200
1600
N
C
RepMP4
RepMP2/3
TM
Exposed at the surface

Figure 2.7: Epidemiological data for incidence of *M. pneumoniae* infection. Data from an active surveillance study performed in Ohio in 1991, showing age-specific rates of community acquired pneumonia due to the major bacterial pathogens. *M. pneumoniae* infections were diagnosed by seroconversion, using complement fixation tests. Due to the high degree of inaccuracy and propensity for false negatives of the complement fixation tests, it is likely that these numbers are actually an underrepresentation of *M. pneumoniae* infection statistics. Sp, *Streptococcus pneumoniae*; Mp, *Mycoplasma pneumoniae*; Lp, *Legionella pneumophila*; Cp, *Chlamydia pneumoniae* [199]. Image modified from [33].

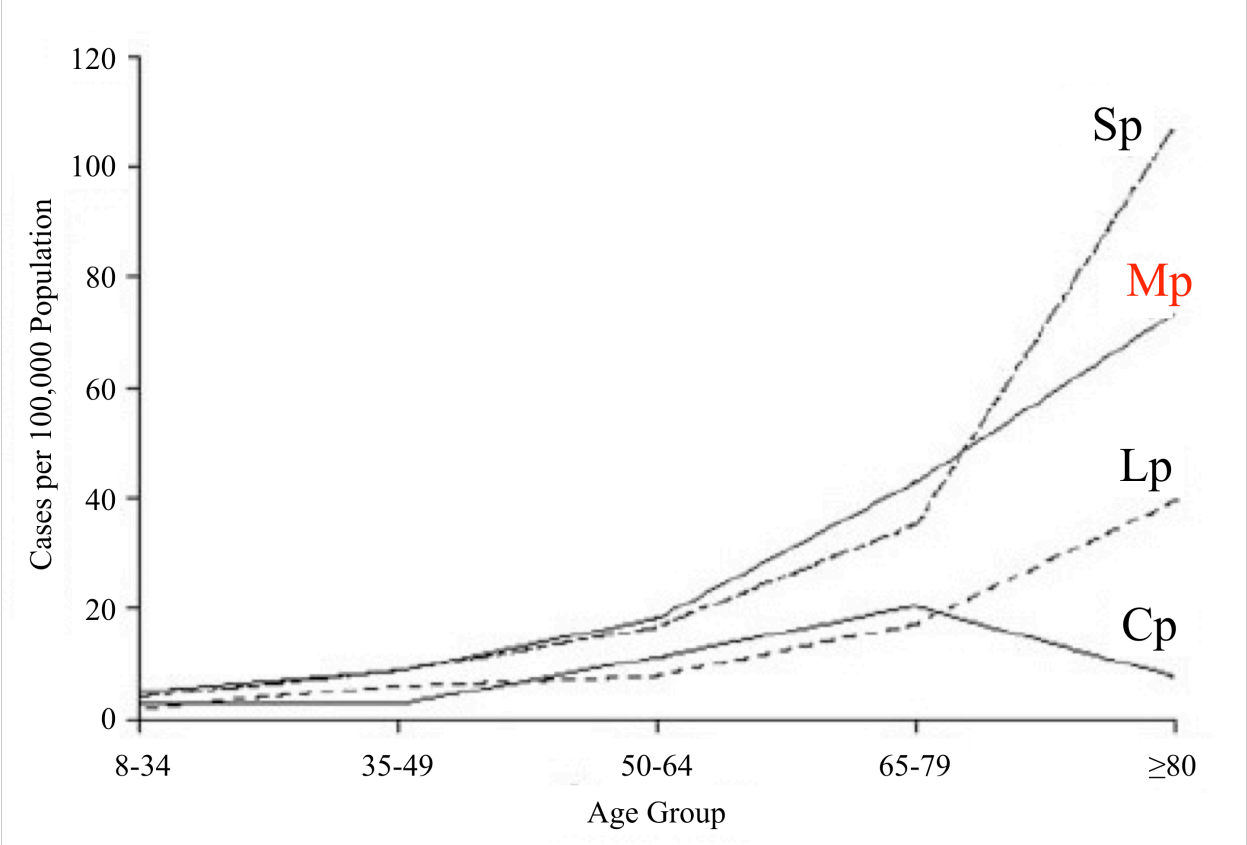
120
100
80
60
40
20
0
Cases per 100,000 Population
Sp
Mp
Lp
Cp
8-34
35-49
50-64
65-79
≥80
Age Group

Figure. 2.8: Type-switching periodicity of *M. pneumoniae* infection. Integrated data from *M. pneumoniae* typing in Japan between 1976 and 2005. Typing results of *M. pneumoniae* clinical strains (1976-2005) and the genotyping results of *p1* genes from throat swabs (1997-2000) and sputum samples (2000-2005) are integrated. Frequencies of type 1 strain infections are indicated at the top of the graph by black bars. Frequencies of type 2 strain infections are indicated by light gray bars in the middle of the graph. Frequencies of type 2 variant strain infections are indicated by dark gray bars at the bottom of the graph. Modified from [218].

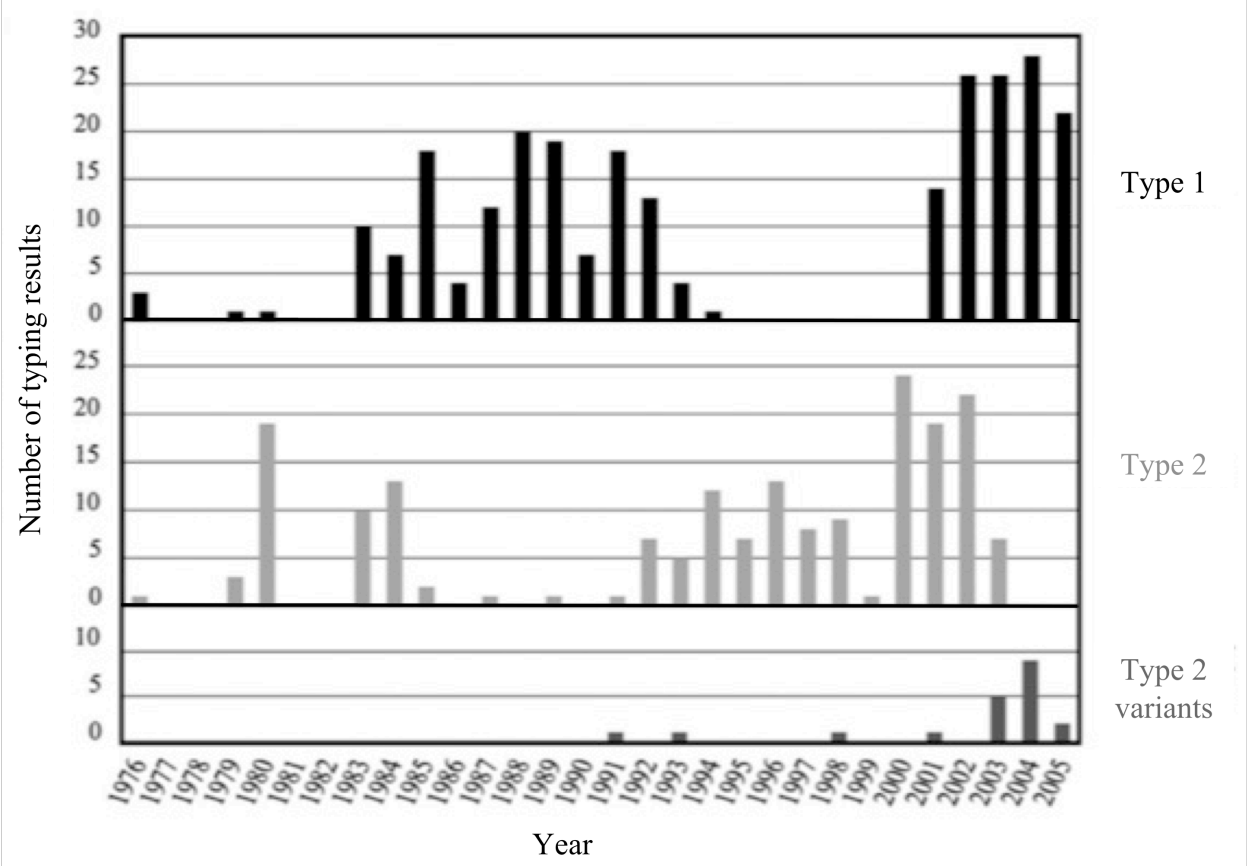
Number of typing results
30
25
20
15
10
5
0
Type 1
Type 2
Type 2 variants
1976
1977
1978
1979
1980
1981
1982
1983
1984
1985
1986
1987
1988
1989
1990
1991
1992
1993
1994
1995
1996
1997
1998
1999
2000
2001
2002
2003
2004
2005
Year

Figure 2.9: Differences in biofilm formation between *M. pneumoniae* strain types. Biofilms formed by strains M129 (type 1) and UAB PO1 (type 2). 3D reconstructions made from confocal microscopic images of biofilms grown for 7 days and stained with Syto 64. Biofilms of UAB PO1: **a, c, e, g**; Biofilms of M129: **b,d,f,h**. Overhead views: **a, b.** Views looking down on the biofilm from an angle: **c,d**. Side views: **e, f**. Examples of towers are indicated by white arrows. The honeycombed region of the biofilm formed by UABPO1 is shown by the green arrow in panel **a**. A close-up, overhead view of the towers of UAB PO1 **(g)** and M129 **(h)**. The towers are pseudo-colored in cyan while the honeycomb associated mycoplasmas are shown in red. In panels **a** and **b** major and minor ticks represent 50 and 10 μm, respectively. Modified from [37].

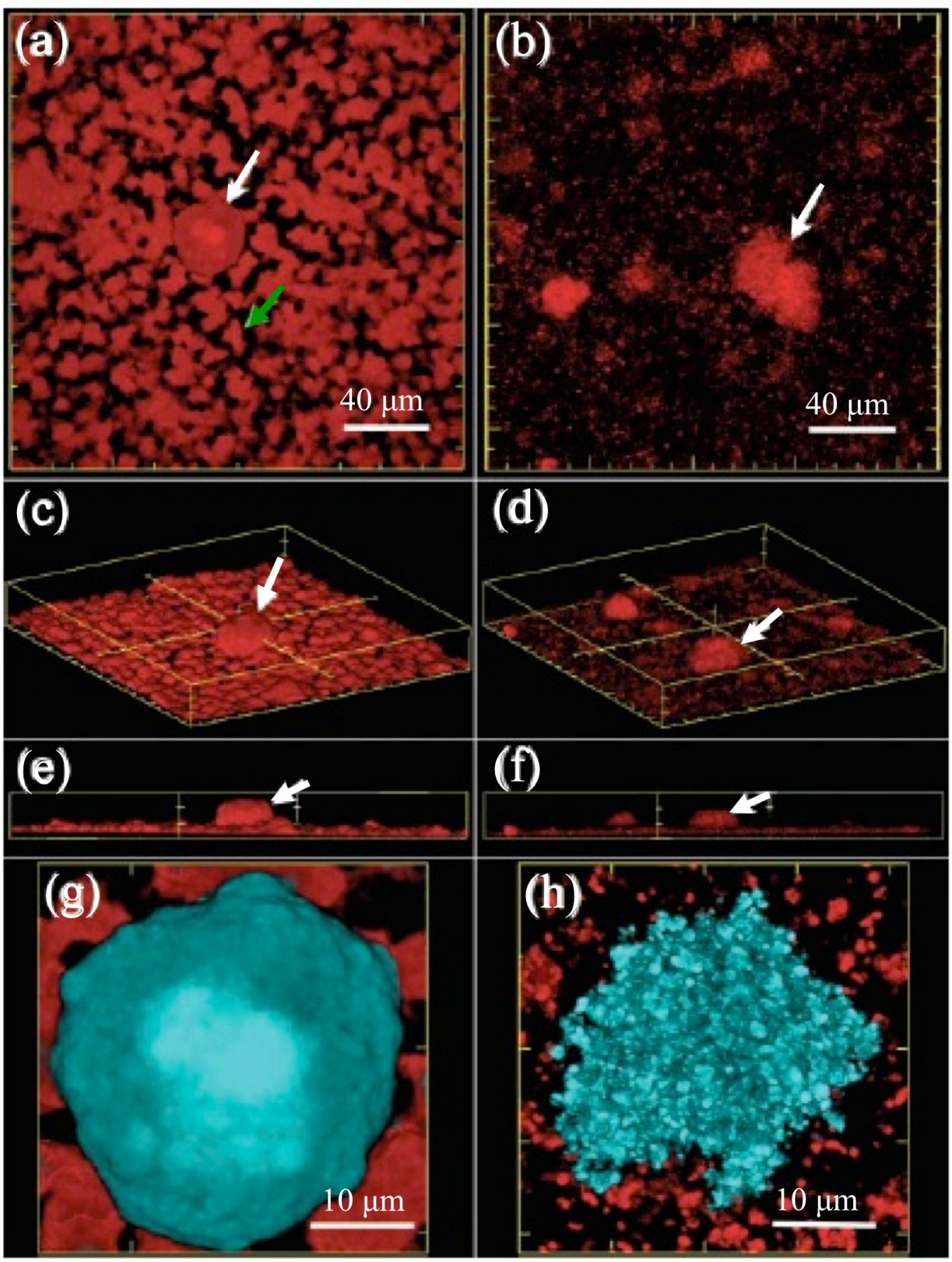
(a)
40 μm
(b)
40 μm
(c)
(d)
(e)
(f)
(g)
10 μm
(h)
10 μm

Figure 2.10: Schematic of SERS and NA-SERS substrate composition. Cartoon schematics of the principle of **(A)** surface enhanced-Raman spectroscopy (SERS) and **(B)** physical parameters of oblique angle deposition (OAD) silver nanorod substrates. Modified from [21].

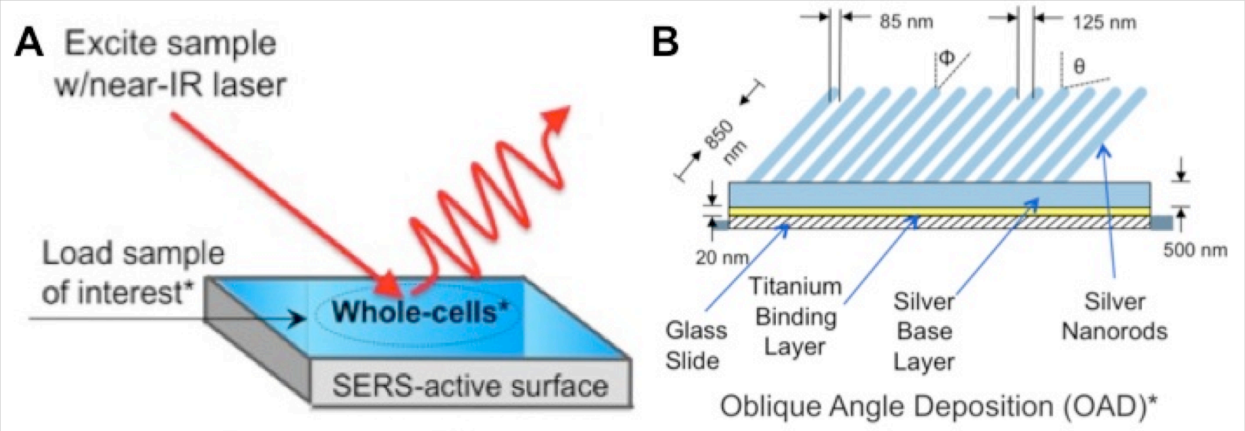
A Excite sample w/near-IR laser
Load sample of interest*
Whole-cells*
SERS-active surface
B
85 nm
125 nm
Φ
θ
850 nm
20 nm
500 nm
Glass Slide
Titanium Binding Layer
Silver Base Layer
Silver Nanorods
Oblique Angle Deposition (OAD)*

Figure 2.11: Image of PDMS multi-well array and TEM of NA-SERS substrate. (A) Image of NA-SERS substrate patterned using PDMS multi-well protocol and **(B)** Transmission electron micrograph (TEM) of nanorod-array SERS substrate. Modified from [20,21].

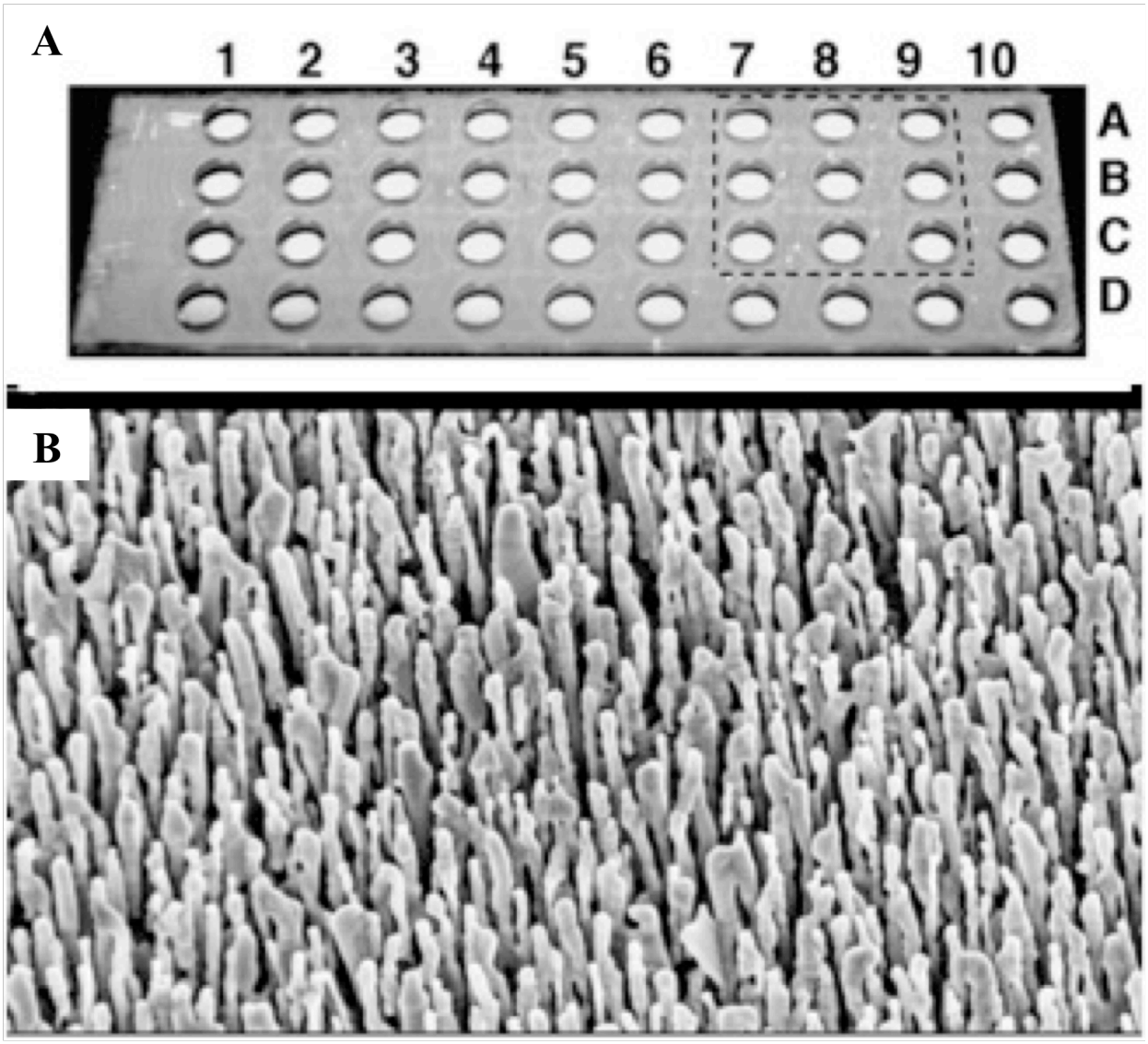
A
1 2 3 4 5 6 7 8 9 10
A
B
C
D
B

CHAPTER 3

COMPARISON OF THE ENDPOINTS FOR DETECTION OF *MYCOPLASMA PNEUMONIAE* BY NANOROD ARRAY-SURFACE ENHANCED RAMAN SPECTROSCOPY AND QPCR

Kelley C. Henderson, Edward S. Sheppard, Omar E. Rivera-Betancourt, Richard A. Dluhy, Kathleen A. Thurman, Jonas M. Winchell, and Duncan C. Krause. Submitted to *The Analyst*, 06/24/14.

Abstract

Mycoplasma pneumoniae is a cell wall-less bacterial pathogen of the human respiratory tract that accounts for up to 20% of community-acquired pneumonia (CAP). Detection and diagnosis of mycoplasma infections is limited by several factors, including poor success at culture from clinical samples. At present, the standard for detection and genotyping is quantitative polymerase chain reaction (qPCR), which can exhibit excellent sensitivity but lacks standardization and has limited practicality for widespread, point-of-care use. We have developed and previously described a silver nanorod array-surface enhanced Raman spectroscopy (NA-SERS) biosensing platform capable of detecting *M. pneumoniae* in simulated and true clinical throat swab samples with statistically significant specificity and sensitivity. Here we ascertained that differences in sample preparation influence the integrity of mycoplasma cells for NA-SERS analysis, which in turn impacts the resulting spectral signature. Furthermore we established the lower endpoint of detection by NA-SERS for *M. pneumoniae* intact-cell sample preparations. Using partial-least squares discriminatory analysis of sample spectra, we found that NA-SERS consistently detected intact *M. pneumoniae* to 0.66 genome equivalents (cells/µl) with 90% cross-validated statistical accuracy. By comparison, qPCR of samples in parallel yielded a lower endpoint of detection of 2.5 cells/µl.

Introduction

The cell wall-less prokaryote *Mycoplasma pneumoniae* is a major cause of respiratory disease in humans, accounting for 20% to 40% of all cases of community-acquired pneumonia (CAP), and the leading cause of CAP in older children and young adults [1-5]. In adults alone the annual economic burden of CAP exceeds $17 billion, and the incidence of infection in the very young and elderly is on the rise [4,6]. Furthermore, extra-pulmonary sequelae occur in up to 25% of cases, and chronic *M. pneumoniae* infection can play a contributing role in the onset, exacerbation, and recurrence of asthma [5].

M. pneumoniae infection is transmitted through aerosolized respiratory secretions and spreads efficiently but slowly within close living quarters, with incubation periods as long as three weeks [13,14]. Symptoms tend to be nondescript, and the disease often has complex and variable presentations, making definitive diagnosis challenging [1,4,15]. As a result, diagnosis is often presumptive and relies heavily on the combination of physical findings and elimination of other possible causes [3,5,14]. Serologic testing has historically been considered the foundation for diagnosis of *M. pneumoniae* infection but has severe limitations in sensitivity and specificity, a high tendency for false negatives, and often must be paired with another diagnostic method [1,3,5,10,14]. Of the currently existing methods, the most efficient means for detection is quantitative polymerase chain reaction (qPCR). At present, the only FDA approved qPCR-based diagnostic test for clinical detection of *M. pneumoniae* is the BioFire FilmArray® Respiratory Panel (BioFire Diagnostics, Inc., Salt Lake City, Utah). The BioFire test performs nucleic acid purification and nested, multiplex qPCR with high resolution melt analysis on nasopharyngeal swabs to assay for 21 common and emerging viral and bacterial respiratory pathogens, and is capable of detecting *M. pneumoniae* as low as 30 CFU/ml [16]. This method can exhibit high

sensitivity and allow for detection in the early stages of infection, but the cost, complexity, and expertise required limit the practicality of widespread use in hospitals and reference laboratories or point-of-care testing [1,3,5,10,14]. These limitations create a critical barrier to the accurate and timely diagnosis of *M. pneumoniae* infection, and a rapid, simple, diagnostic platform would greatly improve the control of *M. pneumoniae* disease.

Vibrational spectroscopy has an inherent biochemical specificity that led to its consideration as a next-generation platform for the rapid detection, characterization, and identification of infectious agents [20-23]. Raman spectroscopy in particular has several advantages for application to biological samples, including narrow bandwidths, good spatial resolution, and the ability to analyze aqueous samples due to the absence of interference by water molecules [20,21,24]. Additionally, Raman spectra provide detailed structural information on the chemical composition of a sample and can serve as a characteristic molecular fingerprint for pathogen identification [23,24]. Despite these advantages, standard Raman spectra are inherently limited by low scattering cross-sections, which translate to weak signals for detection, and initially made the application of traditional Raman spectroscopy for biosensing applications impractical and inefficient [13,21,24]. However, in the late 1970s it was discovered that adsorption of molecules onto nanoscopically roughened metallic surfaces results in significant enhancements in Raman signal and spectral intensity [23-25]. The enhancement is attributed to the increased electromagnetic field experienced by molecules in close proximity to the metallic surface, with typical signal enhancements of 10^4 to 10^{14} with respect to normal Raman intensities [20,21]. Most importantly, for biomedical applications, surface-enhanced Raman spectroscopy (SERS) retains the advantages of standard Raman spectroscopy, in addition to markedly improving sensitivity and allowing for considerable success in whole organism molecular

fingerprinting [20,24,26,27]. However, inconsistency and lack of reproducibility in the preparation of SERS-active substrates has hindered the widespread use of SERS for biosensing applications [20,21,24].

Highly ordered silver nanorod array (NA) substrates fabricated using oblique angle deposition (OAD) yield consistent SERS enhancement factors of around 10^8, with less than 15% variation between substrate batches [21]. In addition, the reproducibility of OAD-prepared substrates can be improved further when patterned into a multiwell format with polydimethylsiloxane (PDMS) [20]. The highly reproducible detection capabilities of NA-SERS substrates have been demonstrated for multiple infectious agents, including respiratory syncytial virus (RSV), rotavirus, influenza, HIV, adenovirus, SARS, and *M. pneumoniae* [13,22,27-29].

Hennigan et al. previously described an NA-SERS-based assay capable of detecting *M. pneumoniae* in both simulated and true clinical throat swab samples, with statistically significant sensitivity and specificity [13]. Their initial evaluation of the NA-SERS biosensing platform capabilities indicate the potential for application as a next-generation diagnostic tool for the clinical detection of *M. pneumoniae*, but a more comprehensive analysis is needed prior to proceeding with clinical validation [13]. In addition, the initial study analyzed samples prepared in water, and we hypothesize that as a result the content of the analyte on the substrate consisted predominately of lysed cells, cytoplasmic content, and membrane debris. In the present study we further explored the impact of differences in sample preparation, defined the lower endpoint of detection for *M. pneumoniae* intact-cell preparations by NA-SERS, and evaluated in parallel the endpoint of detection by qPCR, in order to continue the development of NA-SERS as a next-generation platform for the detection of *M. pneumoniae* in clinical samples.

Materials and Methods

Preparation of *M. pneumoniae* samples for SERS analysis. Wild type *M. pneumoniae* strain M129 was used in this study. Mycoplasma samples were cultured in SP4 medium [1,30] in tissue culture flasks with a 1µl/ml inoculation, incubated at 37°C, and harvested at log phase when the phenol red indicator turned an orange color upon reaching a pH of ~6.5. At time of harvest, spent growth medium was decanted and cells were scraped into 0.1× volume of SP4. Cells were then syringe-passaged 10× with a 25 gauge needle and aliquots made for determination of protein content, plating on PPLO agar [271] for colony-forming unit (CFU) determination, DNA extraction for qPCR analysis, and SERS analysis.

We used two protocols for preparation of *M. pneumoniae* samples for NA-SERS analysis. Initially we followed the protocol described previously [13]. Briefly, the spent SP4 medium was decanted and cells collected by scraping into 0.1× volume sterile deionized (DI) water and centrifuged (20,000×g for 25 min at 4°C). Mycoplasmas were then washed 3× in DI water, suspended in a final volume of 500 µl DI water, syringe-passaged 10× with a 25-gauge needle to disperse clumps, fixed with the addition of 500 µl of 8% formaldehyde in DI water, and stored at 4°C until time of SERS analysis. We anticipated that this protocol would yield significant lysis of the mycoplasma cells and therefore we also prepared samples by adding to a 500-µl aliquot of mycoplasma in SP4, 500 µl of 8% formaldehyde in SP4 (pH 7.0-7.5) and stored at 4°C until SERS analysis. Three independent M129 cultures were prepared for intact-cell SERS analysis. Growth medium control samples were prepared in parallel for the intact-cell sample preparation method. Briefly, uninoculated SP4 medium was incubated in the same volume as was used for *M. pneumoniae* cell growth. The SP4 medium-only control samples were treated identically as *M. pneumoniae* positive samples at time of harvest, washing, and fixation, as described above.

At time of SERS analysis, mycoplasma and growth medium only control samples were serially diluted in DI water in ten-fold or hundred-fold increments to encompass and extend below the clinically relevant range of *M. pneumoniae* concentrations in order to determine the endpoint of the NA-SERS detection capabilities.

Preparation of *M. pneumoniae* samples for protein, DNA, and qPCR analysis. Aliquots designated for protein content and DNA extraction were prepared by centrifugation at 4°C and 20,000×g for 25 min. The supernatants were removed and the samples washed 2× in sterile PBS, pH 7.2. After the second wash the samples were suspended in 1 ml sterile PBS and analyzed for protein content via the colorimetric Bicinchoninic acid (BCA) assay [272], or DNA extraction by the QIAamp DNA Blood Minikit (Qiagen, Valencia, CA) using the blood and body fluids protocol, including Rnase A treatment. 200 µl of sample were used for DNA extraction, with a final elution volume of 200 µl for use to quantitate DNA content and in qPCR analyses. Quantitation of genomic DNA concentration was performed using a NanoDrop instrument (Model ND-1000, Thermo Scientific, Wilmington, DE) and analyzed by NanoDrop software V3.5.2. Genome equivalents of *M. pneumoniae* were calculated from DNA concentration obtained from this analysis and using the previously determined weight of the *M. pneumoniae* genome, 5.3×10^7 Daltons [32].

Parallel analyses of the endpoint of detection by qPCR were done on three independent *M. pneumoniae* cultures using the CARDS toxin gene target [14] and assay cycling parameters developed by the U.S. Centers for Disease Control and Prevention (CDC) [14]. DNA was extracted from the three independent cultures and serial dilutions of extracted DNA were made in nuclease free water prior to qPCR analysis using an ABI 7500 real-time PCR system (Applied Biosystems, Foster City, CA) and SDS v1.4 software platform (Applied Biosystems, Foster City,

CA) for analysis of fluorescence amplification. Briefly, qPCR mastermix reactions contained 12.5 µl 2× PerfeCTa® qPCR FastMix (Quanta Biosciences, Gaithersburg, MD, USA), forward and reverse primers (1µmol/L each), labeled probe (200 nmol/L), 5 µl of total nucleic acid extract, and nuclease free water to a final reaction volume of 25 µl [273]. Cycling conditions were as follows: 1 cycle of 95°C for 5 min followed by 45 cycles of 95°C for 15 sec and 60°C for 1 min. Upon completion of the cycling, positive amplification of a sample was defined as a sigmoidal fluorescence increase above the cycle threshold (Ct) limit assigned to the raw fluorescence data by the user [274]. The endpoint for detection capability by qPCR was defined for each culture using Ct values from the fluorescence amplification analysis and defined as the lowest concentration for which positive amplification occurred in at least one of three replicates tested per individual dilution.

Scanning Electron Microscopy (SEM) characterization of *M. pneumoniae* samples. SEM images of the bacteria were obtained using a Zeiss 1450EP (Carl Zeiss MicroImaging, Inc., Thornwood, NY). The samples were fixed as previously described [72], with modifications. As a control, cells grown on glass coverslips were fixed in 2% glutaraldehyde in sodium cacodylate buffer for one hr. Briefly, lysed- and intact-cell samples were dried onto glass coverslips, fixed with glutaraldehyde, washed twice in sodium cacodylate buffer for five min each wash, post-fixed in 1% OsO_4 in sodium cacodylate buffer for one hr, washed once with sodium cacodylate buffer for ten min, and rinsed twice with water for five min. The SEM coverslips were then treated with an ethanol dehydration series sequentially (five min each step) with 25, 50, 75, 85, 95 and three 100% washes, critical point dried, and sputter coated with 20-nm diameter gold.

NA-SERS measurements and chemometric analysis. Silver nanorod array substrates were prepared for reproducible enhancement of the Raman signal using OAD [21,29,256,275].

Briefly, an electron beam evaporation system was used to deposit three sequential layers onto 1×3'' glass microscope slides as follows: a 20-nm Ti film, a 500-nm Ag film, and an obliquely angled (86° with respect to the surface normal) as specified for optimum signal production [256]. Prior to their use, the nanorod substrates were cleaned for five minutes in an Ar^+ plasma using a plasma cleaner (Model PDC-32G, Harrick Plasma, Ithaca, NY) to remove any surface contamination [276]. The 1×3'' NA substrates were then patterned into 40 3mm diameter PDMS-formed wells. Raman spectra were acquired using a Renishaw inVia Reflex multi-wavelength confocal imaging microscope (Hoffman Estates, IL). A Leicha apochromatic 5× objective (NA 0.12) illuminated a 1265 μm^2 area on the substrate, which allows spatial averaging and minimization of the effect of potential random hot spots. A 785-nm near-infrared diode laser (Renishaw) operating at 10% power capacity (28 mW) provided the incoming radiation, and spectra were collected in 10-sec acquisitions.

A dilution series from each of the three *M. pneumoniae* NA-SERS cultures fixed in SP4 and their respective growth medium controls were analyzed on a single substrate. Each individual test dilution was analyzed in duplicate wells, and two wells were left blank on each substrate to obtain a background SERS reading on the naked nanorod substrate only. All samples were applied to the nanorod substrates in a volume of 1 µl per individual well. Samples were dried onto the nanorods overnight and spectra collected from five random locations within each sample spot for analysis. Ten spectra were collected per dilution (five spectra per well per µl of sample) for both experimental and control samples, with n=200 spectra per substrate. Three separate substrates were analyzed, resulting in a total of n=600 spectra collected over the course of the EOD experiments. Raman spectra between 400-1800 cm^{-1} were acquired using

Renishaw's WiRE 3.4 software. Instrument settings were optimized to maximize signal and minimize saturation or sample degradation arising from laser stimulation.

Raman spectra were first averaged using GRAMS32/A1 spectral software package (Galactic Industries, Nashua, NH) in order to assess signal-to-noise quality, and baseline-corrected using a concave rubberband algorithm which performed ten iterations on 64 points to aid in preliminary evaluation of the spectra and peak assignment (OPUS, Bruker Optics, Inc., Billerica, MA). Chemometric analysis was carried out with MATLAB version 7.10.0 (The Mathworks, Inc., Natick, MA) using PLS-Toolbox version 7.5.1 (Eigenvector Research Inc., Wenatchee, WA). Raw spectra were pre-processed using the first derivative of each spectrum and a fifteen-point, 2^{nd}-order polynomial Savitsky-Golay algorithm. Each dataset was then vector- normalized and mean-centered. Due to the inherently complex nature of the spectral data, multivariate statistical analysis of the datasets was performed using principal component analysis (PCA), hierarchical cluster analysis (HCA), and partial least squares-discriminatory analysis (PLS-DA), using the PLS Toolbox software. The calculated principal components were used as inputs to the HCA algorithm, which used the K-nearest neighbor and Mahalanobis distance to evaluate minimum variances within clusters.

Results and discussion

SERS sample preparation and its effect on SERS spectra of *M. pneumoniae*. Previous studies [13] indicated a sub-CFU lower endpoint for detection by NA-SERS. In the initial development of the NA-SERS assay, mycoplasma samples were prepared in DI water rather than salt-based buffer in order to avoid potential damage to the Ag nanorods. As such, we hypothesized that the majority of cells in our sample were lysed, and consequently cytoplasmic

contents and cell membrane debris encompassed the bulk of our analyte on the substrate, accounting for the sub-CFU detection limits observed. To investigate this point we compared the SERS sample preparation method used previously with a modified protocol expected to yield intact mycoplasma cells, visualizing each sample by SEM (**Figure 3.1a** and **3.1c**). As expected, we observed predominately intact cells with the characteristic flask shape of *M. pneumoniae* [33,277] when samples were fixed prior to dilution in DI H_20 **(Figure 3.1a**), and an abundance of membrane vesicles characteristic of cell lysis were present when samples were washed with DI H_20 prior to fixation (**Figure 3.1c**). For comparison we also examined *M. pneumoniae* cells grown on coverslips and fixed in place. Those cells exhibited the expected elongated morphology of *M. pneumoniae* attached to an inert surface (**Supplementary Figure 3.2**) [277].

Mycoplasmas are phylogenetically unique bacteria in that they lack a cell wall and are instead bound by only a cell membrane; this membrane has numerous surface-exposed membrane proteins and glycolipids [32,135]. As such, the SERS spectra of intact-cell preparations should predominately originate from membrane lipids, glycolipids, and exposed regions of surface proteins accessible for interaction with the Ag nanorods. In contrast, SERS spectra from lysed-cell samples should also contain bands from a multitude of internal cellular components and membrane debris.

The SERS spectra of the two sample preparation types (**Figure 3.1b** and **3.1d**) exhibited both similarities and differences. Qualitatively, the key peaks found within the intact-cell spectra (**Figure 3.1b**) consisted of a broad peak at 895 cm^{-1}, a sharper peak at 1051 cm^{-1}, and three more broad peaks at 1402, 1613, and 1645 cm^{-1}. For the lysed-cell spectra (**Figure 3.1d**) the peaks were more numerous, sharper, and of an overall greater intensity, with the strongest bands falling at 607, 767, 932, 959, 1051, 1137, 1402, 1613, and 1645 cm^{-1}. Several peaks were present in

both intact- and lysed-cell samples, including those at approximately 465, 1051, 1284, 1402, 1613, and 1645 cm^{-1}, though the intensity of the bands was different between the two sample types at all peaks other than 465 cm^{-1}.

Vibrational mode assignments for the major Raman shift peaks observed in Fig. 1 are given in **Table 3.1**. The region between 550-1000 cm^{-1} contained the majority of the spectral variation between the two sample types. Bands present in both the intact- and lysed-cell samples were more frequently associated with bond vibrations present in amino acids and lipids, whereas the lysed-cell spectra contained additional peaks that commonly correspond with nucleotide, amino acid, and lipid/carbohydrate bond vibrations [240-244,278,279]. The spectral differences seen in **Figure 3.1b** and **Figure 3.1d** are likely explained by the differences in the two sample preparation types. The sharper band profile seen in **Figure 3.1d** may also be due to the small vesicle size in lysed-cell preparations, which allows greater surface contact with the Ag nanorod array, with correspondingly greater signal enhancement.

NA-SERS endpoint of detection for intact-cell *M. pneumoniae* preparations. Because clinical samples are likely to have predominantly intact mycoplasmas present, we next assessed the sensitivity of NA-SERS for detection of intact-cell *M. pneumoniae* preparations. Due to sample heterogeneity, we were unable to utilize classical statistical methods for defining limit of detection. Instead, PLS-DA was applied here to determine a statistically significant endpoint for detection by NA-SERS. PLS-DA is a full-spectrum, multivariate, supervised method whereby prior knowledge of classes is used to yield more robust discrimination by minimizing variation within classes while emphasizing latent variables arising from spectral differences between classes [266,267]. When using PLS-DA, it is important to include an appropriate negative control to avoid over- or under-fitting the statistical models. For this purpose a mycoplasma-free

growth medium control was processed in parallel, in accordance with the intact-cell sample preparation, and serially diluted to match the corresponding *M. pneumoniae* dilution series. This allowed us to build PLS-DA models for each dilution that included both media and substrate negative controls to ensure that any differences in growth medium and nanorod background signal within the substrate did not affect the ability of the model to discriminate between the presence or absence of *M. pneumoniae.*

For each individual dilution for all three dilution series, PLS-DA models were generated to discriminate between three classes: a positive control *M. pneumoniae* dilution (10^3 CFU/ml) and each individual *M. pneumoniae* test sample; the growth medium control; and the substrate background. PLS-DA models for all individual dilutions contained a total of n=30 to 40 pre-processed NA-SERS spectra (10 spectra per class for substrate background and negative-media control samples, 20 spectra for *M. pneumoniae* control and test sample dilution class) and were cross-validated using a Venetian blinds algorithm with five to six data splits. Full PLS-DA modeling statistics for all intact-cell dilution ranges can be found in Supplementary **Tables 3.6-3.8.**

For clinical detection platforms, the most critical question is whether the pathogen is present in the sample or not, and so with this parameter in mind the endpoint for detection by NA-SERS was defined as the concentration at which the PLS-DA modeling was unable to correctly discriminate between positive *M. pneumoniae* and growth medium control dilutions. The cross-validated measure of acceptable accuracy cut-off was set at 90%, consistent with the performance capabilities of existing platforms for *M. pneumoniae* detection [5,14]. An example of the PLS-DA modeling system used herein is shown in **Supplementary Figure 3.3**.

To assess NA-SERS sensitivity we used PLS-DA modeling to analyze three dilution series of *M. pneumoniae*, each on independent substrates. Three separate dilution series with concentration ranges from 10^{8} to 10^{-4} CFU/ml were analyzed on three independent NA-SERS substrates. Due to the propensity for mycoplasma cells to clump, a confounding factor in using CFU values to define endpoints for detection is the potential discrepancy between CFU value and actual cell number, which can differ by as much as three logs [280]. Furthermore, clumping and small cell size prevents quantifying cell number by direct microscopic count [32,33]. To account for this potential issue, analyses to determine total protein and genomic DNA concentration and calculate genomic equivalents were included to supplement the CFU values for each culture and better define the content of the samples at each detection endpoint. Sample content for all three cultures fell within comparable ranges (**Table 3.2**). The molecular content of our samples is consistent with published values for bacterial cells. For example, Zubkov, *et al*. reported an average of 60-330 fg total protein per bacterial cell [281]. *M. pneumoniae* is much smaller than model bacteria, roughly 5% by volume the size of *E. coli*, corresponding to 3-16 fg of protein per *M. pneumoniae* cell based on the Zubkov, *et al*. study, and in good agreement with our results of 5.6 fg protein per *M. pneumoniae* cell (**Table 3.2**). As expected, the greatest variation observed between cultures was for CFU values, whereas the remaining measures were more consistent among independently prepared samples. As such, for the purposes of describing the dilutions within the PLS-DA models and comparing endpoints for detection, genomic equivalents in cells/ml will be used for consistency and ease of reference.

The lower endpoints for detection by NA-SERS as defined by CFU, protein content, and genome equivalents are shown in Table 3. On average this corresponded to 2.6 CFU/ml, 3.7 fg protein, and 660 cells per ml, corresponding to 0.66 cells and 3.7 fg protein per 1 μl applied to

the NA-SERS substrate. While the standard deviation was higher for some measures than for others, it is important to keep in mind that these values are representative of the very endpoint of the dilution series and range, which is where the greatest amount of variation is to be expected. Significantly, we also consistently observed an upper endpoint for detection, with PLS-DA classification power dropping below the 90% threshold for samples with concentrations > 10^8 cells/ml (**Supplementary Tables 3.6-3.8**). This is to be expected at high concentrations of analyte, as these samples form visible films on the substrate, which can prevent direct contact of the analyte with the nanorods while also obscuring access to the nanorods by the laser, thus diminishing sensitivity and quenching the SERS signal [29]. However, the clinically relevant concentration of *M. pneumoniae* in respiratory secretions is ~ 10^3 – 10^5 organisms/ml,[1] and NA-SERS consistently detected *M. pneumoniae* at this and flanking levels.

Endpoint of detection by qPCR analysis. At present, the most reliable and rapid test for detecting *M. pneumoniae* in a clinical sample is real-time PCR [5]. To compare detection capabilities, a highly sensitive assay developed and employed by the CDC for outbreak detection was chosen. A singleplex version of the assay was used for this study, and qPCR experiments were conducted in the Pneumonia Response and Surveillance Laboratory at the CDC in Atlanta, Georgia [14]. Quality control data for the three datasets used for qPCR analysis are given in **Table 3.4**.

In accordance with the NA-SERS LOD experiments, dilution series were generated for three independent cultures ranging from 10^7 to 10^0 cells/ml for qPCR analysis. All samples were tested in triplicate, and positive vs. negative amplification of each sample was compared to crossing threshold (Ct) values of positive and negative template controls. Samples amplifying above the Ct value with the *M. pneumoniae* template control were considered positive and those

failing to amplify were considered negative. All Ct value data are given in **Supplementary Tables 3.9-3.11**, and the endpoint of detection for qPCR is summarized in **Table 3.5**.

On average, the lower endpoint for detection by qPCR was 2.45 CFU/ml, 44.7 fg of genomic DNA, and 2,533 cells/ml, corresponding to 223.5 fg of genomic DNA or 12.67 cells per 5 µl of sample examined by qPCR. Our findings are consistent with those established by the CDC of approximately 1-5 CFU/ml and 50 fg of DNA [14]. Furthermore, the qPCR assay performed very similarly to the NA-SERS assay, keeping in mind that NA-SERS analysis used a 1 µl volume of sample whereas qPCR analysis required a 5 µl sample. This is reflected in the genome equivalent limits for each technique, where qPCR exhibited a four-fold higher endpoint than did NA-SERS (2.5 vs. 0.66 cells/µl, respectively). A key consideration in comparing the two technologies arises from the fact that they detect fundamentally different things. NA-SERS detects any cell component of *M. pneumoniae* that interacts with the nanorods upon adsorption to the substrate, whereas qPCR amplifies only *M. pneumoniae* DNA.

Conclusions

M. pneumoniae is a significant human respiratory tract pathogen in both incidence of infection and public health impact, but diagnostic strategies are complicated by the atypical and complex presentation of disease, non-descript symptoms, and the numerous challenges posed by direct culture. Serologic testing was historically the gold standard for detection but suffers from severe limitations that make it both unreliable and impractical for widespread use. Advances in qPCR technologies have overcome many issues with sensitivity and reliability, but the cost of reagents and requirement for technical expertise is still high, limiting diagnosis by qPCR to advanced laboratory facilities and making it impractical for point-of-care use. Here we have shown that

NA-SERS has a sensitivity that equals qPCR for *M. pneumoniae* detection. Additionally, our findings stress the significance of sample preparation when using NA-SERS technology. However, the question of whether cell lysis improves or hinders the detection capabilities of NA-SERS in the presence of a complex clinical background remains to be determined. In addition, NA-SERS is an extremely flexible technology that can be adapted to meet the needs of the user, be it epidemiological investigations in a laboratory or clinical diagnostics in a physician's office. Another important advantage of NA-SERS technology is the existence of handheld Raman instruments that have the potential to be employed for point-of-care clinical detection [282-284]. In combination with the minimal sample preparation requirements and expedient detection, NA-SERS shows great promise for future application as a potential platform to apply for point-of-care *M. pneumoniae* diagnostics.

Acknowledgments

This work was supported by Public Health Service research grant AI096364 from the National Institute of Allergy and Infectious Diseases to D.C.K.

Manuscript data

Figure 3.1: **Scanning electron micrograph (SEM) image of lysed- and intact-cell *M. pnemoniae* sample preparations and their respective SERS spectra**. **(a)** SEM image of intact *M. pneumoniae* cells fixed in suspension; **(b)** corresponding SERS spectrum of intact *M. pneumoniae* cells fixed in suspension; **(c)** SEM image of lysed-cell *M. pneumoniae* preparations; **(d)** corresponding SERS spectrum of lysed-cell *M. pneumoniae* preparation. For **(b)** and **(d)**, spectra were averaged (n=10), baseline-corrected, and normalized; initial concentrations were $2x10^3$ CFU/ml **(b)** and $6.2x10^3$ CFU/ml **(d)**, respectively.

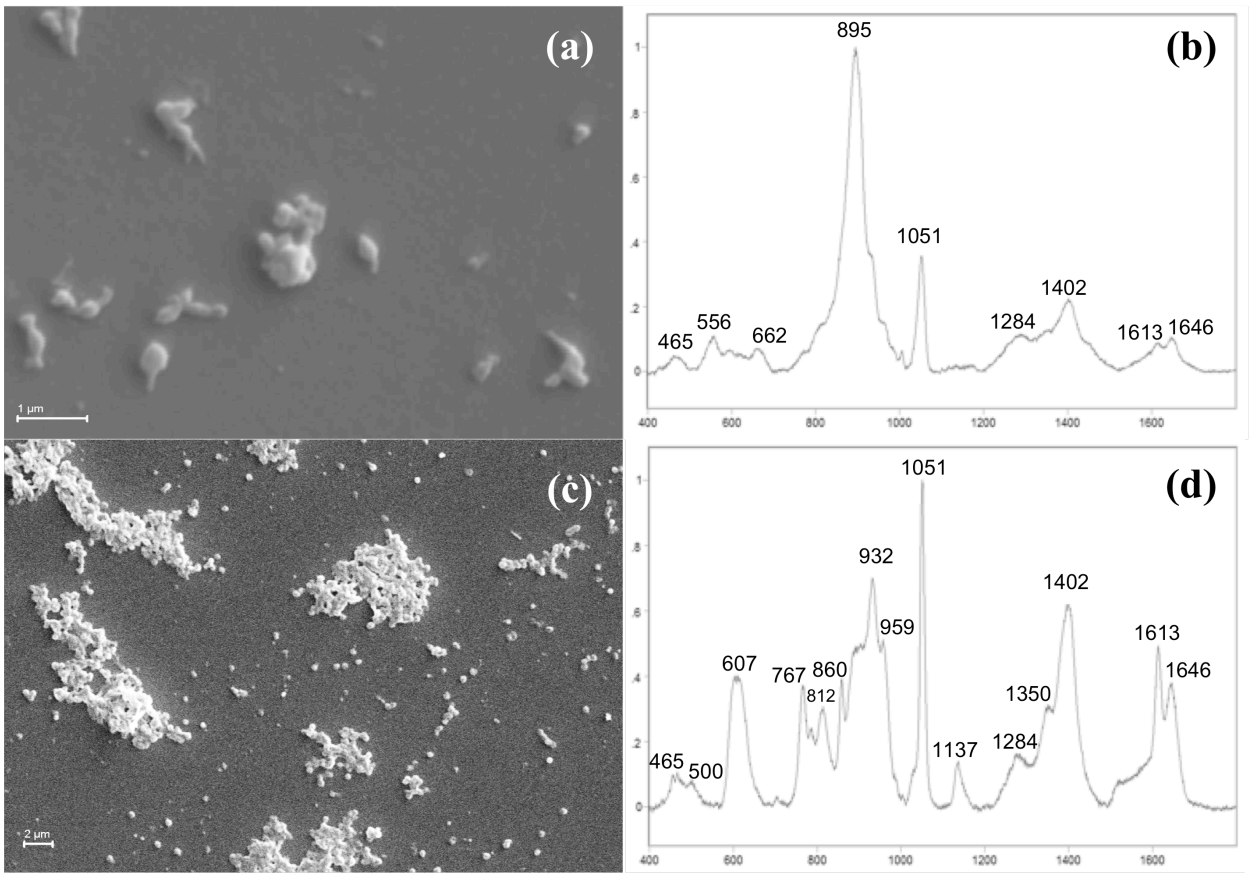
(a)
1 µm
(b)
895
1051
1402
556
662
465
1284
1613
1646
(c)
2 µm
(d)
1051
932
1402
959
1613
607
767
860
812
1646
1350
1284
1137
465
500
400
600
800
1000
1200
1400
1600

Table 3.1: **Representative Raman bands appearing in the NA-SERS spectra of intact- and lysed- cell *M. pneumoniae* samples.** Peaks present in both sample types are shown in green; peaks present in lysed-cell only are shown in blue; peaks found in only the intact cells are shown in black.

Raman Shift (cm-1)	Vibrational mode assignment
1646	Amide I [285]
1613	Tyr [286]
1402	COH bend; $(CH_2)_n$ in-phase twist, COC str [286]
1350	Amide III [286], Trp [242]
1284	COH bend, Amide III [278], CH in-plane (lipid) [278]
1137	C-N and C-C stretch [286], deoxyribose phosphate [240,278]
1051	Gln, C-N stretch [244]
1005	Phenylalanine [286]
959	C-C stretch [242], PO_4 [279]
932	Thr, Trp, Glu, Gln, Asp, Met, His C-COO stretch Tyr [244]
895	COC str[286]
860	C-C str, COC-1,4 glycosidic link [286]
812	Xylose [241], O-P-O [278]
786	Cystosine, Uracil (stretch, ring) [286], O-P-O symmetric stretch [240]
767	Trp [244]; Glucose, Galactose [241]
662	Guanine [286], C-S [242]
607	COO – wag [244]
556	Trp, C-SS-C [242,278]
500	Deoxyribose phosphate [240]
465	Protein S-S stretching [287]

Table 3.2: Initial culture information for *M. pneumoniae* NA-SERS datasets.

Culture prep type	CFU/ml	Protein conc. (μg/ml)	Genome Equivalents (cells/ml)	DNA conc. (μg/ml)
Intact (a)	$8x10^{7}$	310	$7.3x10^{10}$	6.47
Intact (b)	$5x10^{8}$	250	$5.4x10^{10}$	4.77
Intact (c)	$2x10^{8}$	540	$7.1x10^{10}$	6.27
Mean ± Std. deviation	$2.6x10^{8} \pm 2.2x10^{8}$	370 ± 153	$6.6x10^{10} \pm 1.0x10^{10}$	5.48 ± 0.93

Table 3.3: NA-SERS lower endpoint of detection (EOD) for *M. pneumoniae* datasets. Extrapolated from initial culture data presented in Table 3.2.

Intact-cell culture dataset	EOD by CFU/ml	EOD by Protein conc. (fg/µl)	EOD by Genome equivalents (cells/ml)	EOD by DNA conc. (fg)
(a)	0.8	3.1	730	32.5
(b)	5	2.5	540	24
(c)	2	5.4	710	31.5
Mean ± Std. deviation	2.6 ± 2.2	3.7 ± 1.5	660 ± 104	29.3 ± 4.6

Table 3.4: Initial culture information for qPCR analysis.

qPCR dataset	CFU/ml	Protein conc. (µg/ml)	Genome equivalents (cells/ml)	DNA content (µg/ml)
(a)	2.03×10^{8}	190	2.3×10^{11}	19.95
(b)	2.53×10^{8}	175	2.8×10^{11}	25.03
(c)	2.79×10^{8}	220	2.5×10^{11}	22.33
Mean ± Std. deviation	$2.45 \times 10^{8} \pm 3.86 \times 10^{7}$	195 ± 23	$2.5 \times 10^{11} \pm 2.5 \times 10^{10}$	22.45 ± 2.54

Table 3.5: Lower EOD of *M. pneumoniae* by qPCR analysis. Extrapolated from initial culture data presented in Table 3.4

qPCR dataset	EOD by CFU/ml	EOD by genome equivalents (cells/ml)	EOD by DNA concentration (fg)
(a)	2.03	2300	39.8
(b)	2.53	2800	49.8
(c)	2.79	2500	44.4
Mean ± Std. deviation	2.45 ± 0.39	2533 ± 251	44.7 ± 5.00

Supplementary Information

Supplementary Figure 3.2: Scanning electron micrograph image of intact *M. pneumoniae* cells grown on glass coverslips.

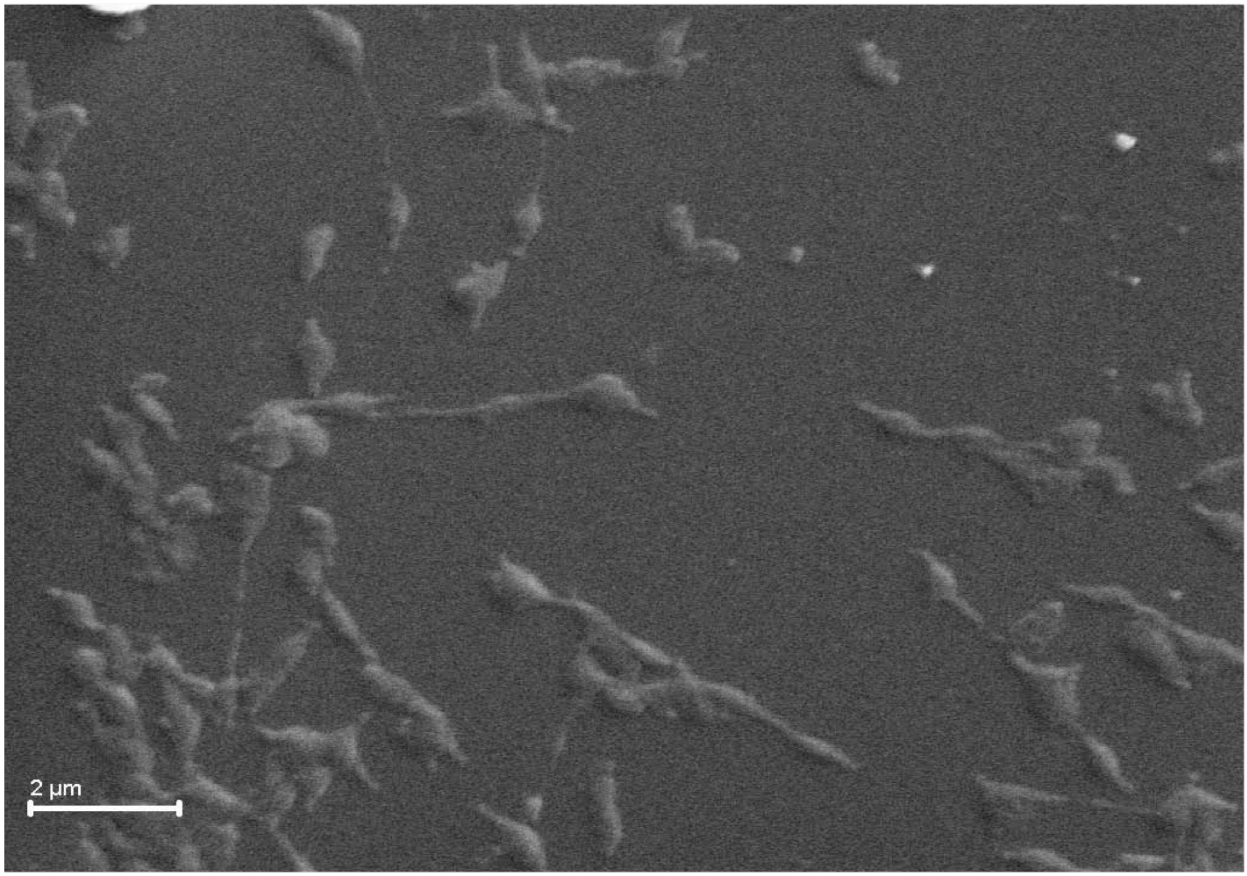
2 µm

Supplementary Figure 3.3: Example of PLS-DA modeling scheme used to determine NA-SERS endpoint of detection (EOD) for intact-cell *M. pneumoniae* samples. This PLS-DA modeling scheme was used generate the statistics given in Supplementary Tables 1-3. Each individual shape represents a single pre-processed NA-SERS spectrum. Each panel represents a cross-validated class prediction score for **(a)** class 1, substrate background spectra; **(b)** class 2, *M. pneumoniae* control and test dilution spectra; and **(c)** class 3, growth medium control spectra. For all panels, substrate background spectra are represented by upside-down dark-gray triangles, *M. pneumoniae* control and test dilution spectra by black asterisks, and growth medium control spectra by light gray squares. The red-dotted line indicates the classification threshold line for positive class prediction. Cross-validated statistics for the model **(d)** were obtained using Venetian blinds with 6 data splits and represent the prediction performance of the PLS-DA plots shown in a-c.

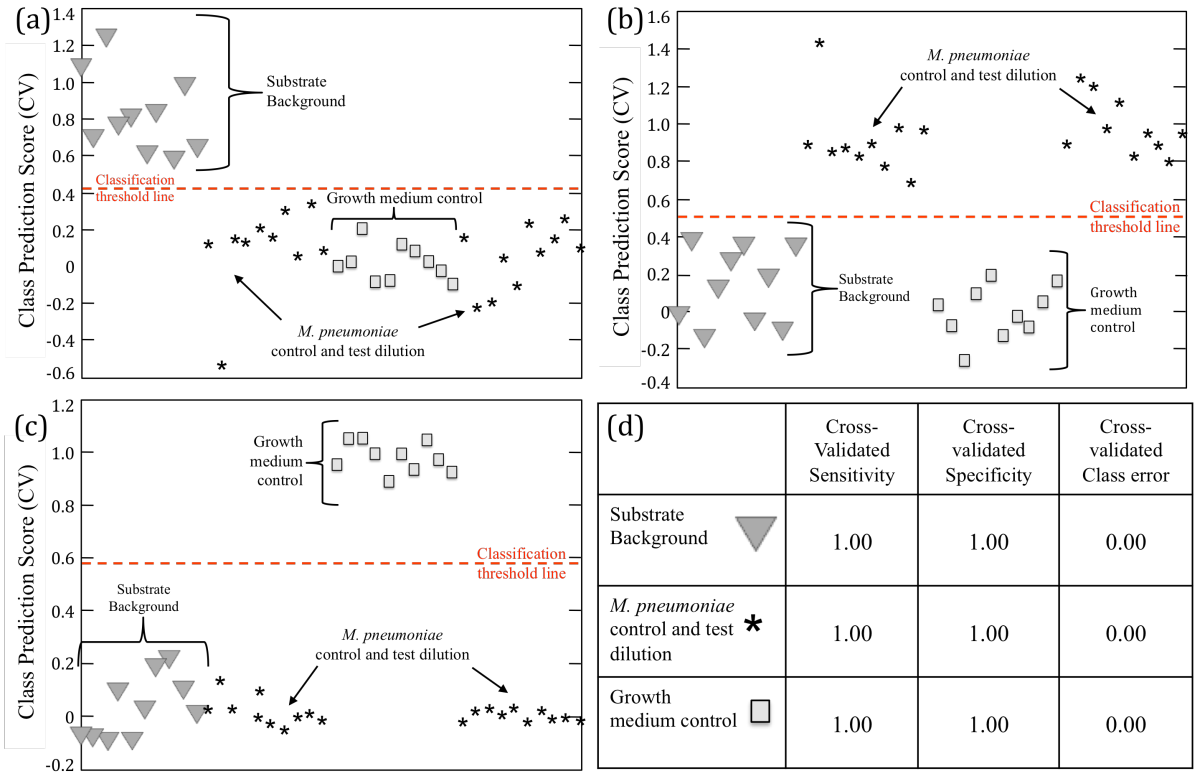

(d)

	Cross-Validated Sensitivity	Cross-validated Specificity	Cross-validated Class error
Substrate Background ▽	1.00	1.00	0.00
M. pneumoniae control and test dilution *	1.00	1.00	0.00
Growth medium control □	1.00	1.00	0.00

Supplementary Table 3.6: PLS-DA modeling statistics for NA-SERS detection of intact-cell *M. pneumoniae* dataset (a). Class 1: Mpn = *M. pneumoniae* control and test dilution; class 2: SP4 = growth medium control dilution; class 3: Subs. bkg = nanorod substrate background; CV stands for cross-validated; RMSECV stands for root mean square error cross-validated.

Dilution by Genome equivalents (cells/ml)	PLS-DA Sensitivity CV	PLS-DA Specificity CV	PLS-DA Class Error CV	PLS-DA RMSECV	Meets 90% PLS-DA threshhold
1: Mpn $7.3x10^{8}$ 2: SP4 10^{-2} 3: Subs. bkg	0.9 0.9 1	0.95 0.95 0.97	0.075 0.075 0.02	0.24 0.27 0.14	Yes
1: Mpn $7.3x10^{6}$ 2: SP4 10^{-4} 3: Subs. bkg	0.9 0.9 1	1 1 1	0.05 0.05 0	0.25 0.24 0.13	Yes
1: Mpn $7.3x10^{5}$ 2: SP4 10^{-5} 3: Subs. bkg	1 1 1	1 1 1	0 0 0	0.22 0.16 0.21	Yes
1: Mpn $7.3x10^{4}$ 2: SP4 10^{-6} 3: Subs. bkg	0.9 1 1	0.9 0.93 0.97	0.1 0.03 0.02	0.32 0.28 0.24	Yes
1: Mpn $7.3x10^{3}$ 2: SP4 10^{-7} 3: Subs. Bkg	0.95 0.9 1	0.95 0.9 0.97	0.05 0.1 0.02	0.24 0.29 0.18	Yes
1: Mpn $7.3x10^{2}$ 2: SP4 10^{-8} 3: Subs. bkg	0.95 1 1	0.9 0.97 1	0.075 0.02 0	0.30 0.26 0.23	Yes
1: Mpn $7.3x10^{1}$ 2: SP4 10^{-9} 3: Subs. Bkg	0.95 0.7 1	1 0.97 0.93	0.025 0.17 0.03	0.23 0.32 0.26	No
1: Mpn $7.3x10^{0}$ 2: SP4 10^{-10} 3: Subs. Bkg	0.9 0.56 0.9	0.89 0.93 1	0.10 0.25 0.05	0.35 0.33 0.17u	No
1: Mpn $7.3x10^{-1}$ 2: SP4 10^{-11} 3: Subs. bkg	0.95 0.9 0.9	0.9 0.97 0.86	0.075 0.06 0.11	0.31 0.34 0.31	No

Supplementary Table 3.7: PLS-DA modeling statistics for NA-SERS detection of intact-cell *M. pneumoniae* dataset (b). Class 1: Mpn = *M. pneumoniae* control and test dilution; class 2: SP4 = growth medium control dilution; class 3: Subs. bkg = nanorod substrate background; CV stands for cross-validated; RMSECV stands for root mean square error cross-validated.

Dilution by Genome equivalents (cells/ml)	PLS-DA Sensitivity CV	PLS-DA Specificity CV	PLS-DA Class Error CV	PLS-DA RMSECV	Meets 90% PLS-DA threshhold
1: Mpn $5.4x10^{10}$ 2: SP4 10^{0} 3: Subs. bkg	0.9 0.67 1	0.84 0.95 1	0.13 0.19 0	0.34 0.34 0.07	No
1: Mpn $5.4x10^{8}$ 2: SP4 10^{-2} 3: Subs. bkg	1 1 1	1 1 1	0 0 0	0.16 0.10 0.11	Yes
1: Mpn $5.4x10^{6}$ 2: SP4 10^{-4} 3: Subs. Bkg	1 0.9 1	0.95 1 1	0.025 0.05 0	0.23 0.25 0.11	Yes
1: Mpn $5.4x10^{4}$ 2: SP4 10^{-6} 3: Subs. bkg	1 0.9 1	0.9 0.95 0.95	0.05 0.075 0.025	0.20 0.29 0.19	Yes
1: Mpn $5.4x10^{3}$ 2: SP4 10^{-7} 3: Subs. Bkg	1 0.9 1	1 0.95 1	0 0.075 0	0.21 0.26 0.20	Yes
1: Mpn $5.4x10^{2}$ 2: SP4 10^{-8} 3: Subs. Bkg	0.9 0.9 1	0.95 0.95 1	0.075 0.075 0	0.25 0.27 0.14	Yes
1: Mpn $5.4x10^{1}$ 2: SP4 10^{-9} 3: Subs. Bkg	0.7 0.9 1	0.8 0.9 1	0.25 0.1 0	0.41 0.31 0.22	No
1: Mpn $5.4x10^{0}$ 2: SP4 10^{-10} 3: Subs. Bkg	0.7 0.7 1	0.8 0.85 1	0.25 0.225 0	0.52 0.49 0.16	No
1: Mpn $5.4x10^{-1}$ 2: SP4 10^{-11} 3: Subs. bkg	0.9 0.9 1	0.86 0.95 0.95	0.11 0.075 0.025	0.27 0.27 0.25	No

Supplementary Table 3.8: PLS-DA modeling statistics for NA-SERS detection of intact-cell *M. pneumoniae* dataset (c). Class 1: Mpn = *M. pneumoniae* control and test dilution; class 2: SP4 = growth medium control dilution; class 3: Subs. bkg = nanorod substrate background; CV stands for cross-validated; RMSECV stands for root mean square error cross-validated.

Dilution by Genome equivalents (cells/ml)	PLS-DA Sensitivity CV	PLS-DA Specificity CV	PLS-DA Class Error CV	PLS-DA RMSECV	Meets 90% PLS-DA threshhold
1: Mpn $7.1x10^{9}$ 2: SP4 10^{-1} 3: Subs. Bkg	0.9 0.9 1	0.5 0.6 1	0.25 0.17 0	0.45 0.44 0.12	No
1: Mpn $7.1x10^{7}$ 2: SP4 10^{-3} 3: Subs. Bkg	0.9 1 1	0.95 0.95 1	0.075 0.025 0	0.26 0.25 0.12	Yes
1: Mpn $7.1x10^{5}$ 2: SP4 10^{-5} 3: Subs. Bkg	1 1 1	1 1 1	0 0 0	0.09 0.11 0.12	Yes
1: Mpn $7.1x10^{4}$ 2: SP4 10^{-6} 3: Subs. bkg	1 1 1	1 1 1	0 0 0	0.17 0.15 0.18	Yes
1: Mpn $7.1x10^{3}$ 2: SP4 10^{-7} 3: Subs. Bkg	1 1 1	0.95 1 1	0.025 0 0	0.18 0.08 0.16	Yes
1: Mpn $7.1x10^{2}$ 2: SP4 10^{-8} 3: Subs. Bkg	1 0.9 0.9	0.95 0.95 1	0.025 0.075 0.05	0.24 0.27 0.25	Yes
1: Mpn $7.1x10^{1}$ 2: SP4 10^{-9} 3: Subs. Bkg	1 1 1	0.95 0.85 1	0.025 0.075 0	0.27 0.27 0.20	No
1: Mpn $7.1x10^{0}$ 2: SP4 10^{-10} 3: Subs. Bkg	0.8 1 1	0.9 0.95 0.95	0.15 0.025 0.025	0.24 0.19 0.14	No

Supplementary Table 3.9: Crossing threshold values for qPCR EOD dataset (a).

- indicates detectable amplification was not observed for this replicate

Dilution (cells/ml)	Rep 1	Rep 2	Rep 3
$2.3x10^7$	24.04	24.20	24.24
$2.3x10^6$	26.30	26.52	26.60
$2.3x10^5$	29.32	29.26	29.49
$2.3x10^4$	32.23	32.43	32.61
$2.3x10^3$	36.50	35.16	37.09
$2.3x10^2$	-	-	-
$2.3x10^1$	-	-	-
$2.3x10^0$	-	-	-

Supplementary Table 3.10: Crossing threshold values for qPCR EOD dataset (b).

- indicates detectable amplification was not observed for this replicate.

Dilution (cells/ml)	Rep 1	Rep 2	Rep 3
$2.8x10^7$	23.58	23.38	23.50
$2.8x10^6$	28.00	26.11	26.71
$2.8x10^5$	30.16	30.06	29.86
$2.8x10^4$	34.57	34.14	33.30
$2.8x10^3$	-	-	39.26
$2.8x10^2$	-	-	-
$2.8x10^1$	-	-	-
$2.8x10^0$	-	-	-

Supplementary Table 3.11: Crossing threshold values for qPCR EOD dataset (c).

- indicates detectable amplification was not observed for this replicate.

Dilution (cells/ml)	Rep 1	Rep 2	Rep 3
$2.5x10^7$	23.58	23.49	23.53
$2.5x10^6$	26.76	26.84	26.71
$2.5x10^5$	29.98	29.85	30.20
$2.5x10^4$	33.27	32.65	33.03
$2.5x10^3$	35.6	-	35.45
$2.5x10^2$	-	-	-
$2.5x10^1$	-	-	-
$2.5x10^0$	-	-	-

CHAPTER 4

SPECIFICITY AND STRAIN-TYPING CAPABILITIES OF NANOROD ARRAY-SURFACE ENHANCED RAMAN SPECTROSCOPY FOR *MYCOPLASMA PNEUMONIAE* DETECTION AND GENOTYPING

Kelley C. Henderson, Alvaro J. Benitez, Amy E. Ratliff, Donna M. Crabb, Edward S. Sheppard, Jonas M. Winchell, Richard A. Dluhy, Ken B. Waites, T. Prescott Atkinson, and Duncan C. Krause. To be submitted to *PLoS One.*

Abstract

Mycoplasma pneumoniae is a cell wall-less bacterial pathogen of the human respiratory tract that accounts for up to 20% of all community-acquired pneumonia (CAP). At present the most effective means for detection and genotyping is quantitative polymerase chain reaction (qPCR), which can exhibit excellent sensitivity and specificity but requires separate tests for detection and genotyping, lacks standardization between available tests, and has limited practicality for widespread, point-of-care use. We have developed and previously described a silver nanorod array-surface enhanced Raman Spectroscopy (NA-SERS) biosensing platform capable of detecting *M. pneumoniae* with statistically significant specificity and sensitivity in simulated and true clinical throat swab samples, and the ability to distinguish between reference strains of the two main genotypes of *M. pneumoniae*. Furthermore, we have established a lower endpoint of detection for NA-SERS of < 1 genome equivalent (cell/μl). Here using partial least squares- discriminatory analysis (PLS-DA) of sample spectra, we demonstrate that NA-SERS detected 30 clinical isolates from globally diverse origins and *M. pneumoniae* reference strain controls, and could distinguish all *M. pneumoniae* clinical isolates and reference strains from a panel of 12 other human commensal and pathogenic mycoplasma species with 100% cross-validated statistical accuracy. Furthermore, PLS-DA correctly classified by genotype all 30 clinical isolates with 96% cross-validated accuracy for type 1 strains, 98% cross-validated accuracy for type 2 strains, and 90% cross-validated accuracy for type 2V strains.

Introduction

The cell wall-less prokaryote *Mycoplasma pneumoniae* is a major cause of respiratory disease in humans, accounting for 20% to 40% of all community acquired pneumonia (CAP), and in addition is the leading cause of CAP in older children and young adults [1-5]. For adults alone the annual economic burden of CAP is > $17 billion, and the incidence of infection in the very young and the elderly is on the rise [4,6]. Macrolide resistance is a growing concern, particularly in children [5], and extra-pulmonary sequelae occur in up to 25% of infections. Finally, evidence continues to indicate a contributing role for *M. pneumoniae* infection in the onset, exacerbation, and recurrence of asthma [5].

An area of growing interest is the role of *M. pneumoniae* genotype in pathogenesis and disease epidemiology. Genetic diversity is relatively limited among *M. pneumoniae* strains and can be categorized into two major groups (type 1 or type 2) based on variation within sequence of the *P1* (MPN141) gene, with variant strains of the two becoming increasingly more common [7]. The P1 protein is an important virulence factor and plays a significant role in the immunogenic response to *M. pneumoniae* infection [8-10]. P1 must complex with several other proteins in order to localize to the tip of the terminal organelle, where it mediates receptor binding for attachment to the respiratory epithelium, an essential step in successful colonization of the airways [9,11]. Variation in the *P1* gene sequence is used to distinguish between type 1 and type 2 strains of *M. pneumoniae*, but little is known about phenotypic differences arising from this genetic variation. Perhaps notable in regard to strain variation is the periodicity of type-switching between the two major genotypes that occurs in regular patterns every 4-7 years [12].

M. pneumoniae infection is transmitted through aerosolized respiratory secretions and spreads slowly but efficiently through close living quarters, with incubation periods up to three

weeks [13,14]. Symptoms tend to be non-descript, often with complex and variable clinical presentations, which makes definitive diagnosis challenging [1,4,15]. As a result, diagnosis is often presumptive and relies heavily on the combination of physical findings and the elimination of other possible causes [3,5,14]. The success rate for laboratory culture is poor, even for experienced labs, while serologic testing, historically considered the foundation for diagnosis of *M. pneumoniae* infection, has limited sensitivity and specificity, a high tendency for false-negatives, and must often be paired with another diagnostic method [1,3,5,10,14]. Of the currently existing methods, the most efficient means for detection is quantitative polymerase chain reaction (qPCR). At present, the only FDA approved qPCR-based test is the FilmArray® Respiratory Panel (BioFire Diagnostics Inc., Salt Lake City, Utah), providing nested, multiplex qPCR with high resolution melt analysis on nasopharyngeal swabs for 21 different viral and bacterial respiratory pathogens, and capable of detecting *M. pneumoniae* as low as 30 colony-forming units (CFU)/ml [16]. The current standard for *M. pneumoniae* genotyping is PCR-restriction fragment length polymorphism but can also be done by nested PCR and sequencing, or by qPCR and high resolution melt curve analysis [15,17-19]. These methods for detection and genotyping exhibit high sensitivity and specificity for all known strain variants, can allow for detection in the early stages of infection, and can be performed in hospitals and reference laboratories [1,3,5]. However, the requirement of separate tests for detection and genotyping, as well as the cost, complexity, and expertise required, limits the practicality for widespread, point-of-care use [1,3-5,14]. These limitations create a critical barrier to the accurate and timely diagnosis of *M. pneumoniae* infection, and a rapid, simple, diagnostic platform capable of simultaneous detection and genotyping would greatly improve the control of *M. pneumoniae* disease.

Vibrational spectroscopy has an inherent biochemical specificity that led to its consideration as a next-generation platform for the rapid detection, characterization, and identification of infectious agents [20-23]. Raman spectroscopy in particular has several advantages for application to biological samples, including narrow bandwidths, good spatial resolution, and the ability to analyze aqueous samples due to the absence of interference by water molecules [20,21,24]. Furthermore, Raman spectra provide detailed structural information on the chemical composition of a sample and can serve as a characteristic molecular fingerprint for pathogen identification [23,24]. Despite these advantages, standard Raman spectra are inherently limited by weak signals for detection. As a result, the application of traditional Raman spectroscopy for biosensing applications was impractical and inefficient [13,21,24] until the discovery that sample adsorption onto nanoscopically roughened metallic surfaces results in significant enhancements in Raman signal and spectral intensity [23-25]. This enhancement by factors up to 10^{14}-fold, is attributed to the increased electromagnetic field for molecules in close proximity to the metallic surface [20,21]. Surface-enhanced Raman spectroscopy (SERS) retains the advantages of standard Raman spectroscopy, in addition to markedly improved sensitivity, allowing for considerable success at whole organism molecular fingerprinting [20,24,26,27].

Inconsistency and lack of reproducibility in the preparation of SERS-active substrates has hindered its widespread use for biosensing applications [20,21,24]. However, highly ordered silver nanorod array (NA) substrates fabricated using oblique angle deposition (OAD) yield consistent SERS enhancement factors of around 10^{8}, with less than 15% variation between substrate batches [21]. The reproducibility of NA-SERS substrates can be improved further when patterned into a multiwell format with polydimethylsiloxane (PDMS) [20]. The highly reproducible detection capabilities of NA-SERS have been well demonstrated for multiple

infectious agents, including RSV, rotavirus, influenza, HIV, adenovirus, SARS coronavirus, and *M. pneumoniae* [13,22,28-30].

Hennigan et al. described an NA-SERS-based assay capable of detecting *M. pneumoniae* with statistically significant sensitivity and specificity in both simulated and true clinical throat swabs, with the potential to detect and type *M. pneumoniae* within a single test [13]. We recently determined the sensitivity of the NA-SERS assay for *M. pneumoniae* detection to be < 1 genome equivalent (cell/μl) [288]. Initial evaluation of the NA-SERS biosensing platform capabilities indicates the potential for application as a next-generation diagnostic tool for the clinical detection of *M. pneumoniae*, but a more comprehensive analysis is needed prior to proceeding with clinical validation. In the present study we further explored the specificity of NA-SERS for *M. pneumoniae* detection with a panel of 30 *M. pneumoniae* isolates collected from representative global outbreaks and spanning clinically relevant genotypes. Furthermore, since NA-SERS has inherent biochemical specificity, we analyzed a panel of 12 other human commensal and pathogenic mycoplasmas to demonstrate that this biosensing platform could distinguish *M. pneumoniae* from its clinically relevant closest phylogenetic relatives. Finally, we evaluated the ability of the NA-SERS platform to correctly genotype the 30 *M. pneumoniae* clinical isolates relative to known reference strains of *M. pneumoniae*.

Methods

Preparation of *M. pneumoniae* controls and clinical isolates for SERS analysis. Wild type *M. pneumoniae* reference strains M129 (type 1) and FH (type 2) were grown, harvested, and prepared at the University of Georgia (UGA) for this study. A panel of 30 clinical isolates consisting of 13 type 1 strains, 11 type 2 strains, and 6 type 2 variant strains were grown,

harvested, and prepared for SERS and quality control analysis at the Pneumonia Response and Surveillance Laboratory at the Centers for Disease Control and Prevention (CDC) in Atlanta, Georgia. All mycoplasma isolates and controls were cultured in SP4 medium [1,30] in tissue culture flasks with a 1µl/ml inoculation and incubated at 37°C. Samples grown at UGA were harvested at log phase when the phenol red indicator turned an orange color upon reaching a pH of ~6.5. Samples grown at the CDC were harvested 14 days from the date of inoculation to ensure adequate growth for all isolates. At time of harvest, the spent growth medium was decanted for each flask and 0.1× volume of sterile PBS (pH 7.2) was added to wash the adherent mycoplasmas. The PBS wash was then decanted and the PBS wash repeated 3× before the cells were scraped into 1 ml sterile PBS. Cells were then syringe-passaged 10× with a 25 gauge needle and aliquots made for determination of protein content, plating on PPLO agar [271] for CFU determination (for select isolates and controls), DNA extraction for genome equivalent determination, and SERS analysis.

M. pneumoniae samples for SERS analysis were syringe-passaged 10× with a 25-gauge needle to disperse clumps, fixed with the addition of 1× volume of 8% formaldehyde in sterile PBS (pH 7.0), and stored at 4°C. Growth medium control samples were prepared in parallel under the same conditions as the *M. pneumoniae* reference strains as described previously [288]. At the time of SERS analysis, mycoplasma and growth medium control samples were diluted in sterile DI water to a concentration of 10^5 cells/µl and then immediately loaded onto the NA-SERS substrate.

Preparation of non-*M. pneumoniae* human commensal and pathogenic species for NA-SERS analysis. 12 human commensal and pathogenic *Mollicutes* species closely related [289] to *M. pneumoniae* were grown and harvested at the University of Alabama at Birmingham

(UAB). These included: *Acholeplasma laidlawii* (ATCC 23206), *Mycoplasma amphoriforme* (ATCC A39, M6123), *Mycoplasma fermentans* (ATCC 19989), *Mycoplasma genitalium* (ATCC 49897), *Mycoplasma hominis* (ATCC Mh132), *Mycoplasma orale* (ATCC 23714), *Mycoplasma penetrans* (UAB reference strain collection, year 1995), *Mycoplasma pirum* (ATCC 25960), *Mycoplasma salivarium* (ATCC 23064), *Mycoplasma spermatophilum* (ATCC 49695), *Ureaplasma parvum* (ATCC Up1), and *Ureaplasma urealyticum* (ATCC Uu11). For each culture, 500 µl to 1 ml of stock culture was inoculated into approximately 30 ml of SP4, Hayflick's, or 10B medium and incubated until the pH indicator turned a peach color for *M. genitalium, M. penetrans, M. pirum,* and *M. fermentans*; a rose color for *M. hominis, M. orale,* and *M. salivarium*; a pink color for *U. parvum,* and *U. urealyticum*; until a clearing of the media occurred for *A. laidlawii;* and for 72 hr for *M. spermatophilum*. At the time of harvest the cells and spent media were poured into 50 ml polycarbonate tubes and centrifuged at 8,000 RPM for 15 min, except for *Ureaplasma* species, which were centrifuged for 1 hr. The supernatants were decanted and the pellets suspended in 30 ml sterile PBS. The cells were washed by centrifugation at 8,000 RPM for 15 min as above, or 10,000 RPM for 1 hr for *Ureaplasma* species. The supernatants were then decanted and the pellets suspended in 1 ml sterile PBS, transferred to a 1.5 ml vial, and centrifuged at 14,000 RPM for 20 min. The supernatants were again decanted and the pellets suspended in 1 ml sterile PBS and syringe-passaged using a 26-gauge needle to disperse clumps. Aliquots were then made for spotting onto a blood agar plate to test for contamination, and plating for CFU and color-changing unit (CCU) determination. Two 400 µl aliquots for each were centrifuged at 14,000 RPM for 20 min, the supernatant was removed, and the pellets were frozen for shipment to UGA, where they were stored at -80°C.

For SERS and quality control analysis, cell pellets were suspended in 1 ml sterile PBS (pH 7.2) and syringe-passaged 10× with a 25 gauge needle to disperse clumps. Aliquots were then made for DNA extraction and genome equivalent determination, protein assay, and NA-SERS analysis. SERS samples were prepared by fixing 500 µl of suspended cells with 500 µl of 8% formaldehyde in sterile PBS (pH 7.0), and stored at 4°C until time of SERS analysis. At time of NA-SERS analysis, the samples were diluted in sterile DI water to a concentration of 10^3 to 10^4 cells/µl and then immediately loaded onto the NA-SERS substrate. A negative SP4 medium control and *M. pneumoniae* strain M129 samples were prepared as described above for comparison.

Preparation of samples for determination of protein content and genome equivalents. All samples were analyzed for protein content via the Bicinchoninic acid assay [272]. DNA was extracted by the QIAamp DNA Blood Minikit (Qiagen, Valencia, CA) using the blood and body fluids protocol, including RNase A treatment. 200 µl of sample were used for DNA extraction, with a final elution volume of 200 µl for use to quantify DNA content and genome equivalents. Genomic DNA concentration and absorbance measurements for the Bicinchoninic acid assay for protein content were performed on a NanoDrop instrument (Model ND-1000, Thermo Scientific, Wilmington, DE) using software V3.5.2. Genome equivalents of *M. pneumoniae* samples were calculated from the DNA concentration obtained from this analysis and using the previously determined weight of the *M. pneumoniae* genome, 5.3×10^7 Daltons [32]. For all non-*M. pneumoniae* samples, genome equivalents were determined using DNA concentrations obtained from this analysis and a genome weight calculated for this study based on published genome lengths and known G+C contents from the GenBank database.

NA-SERS measurements and chemometric analysis. NA-SERS substrates were prepared by OAD as described [21,29,256,275]. Prior to their use, substrates were cleaned for 5 min in an Ar+ plasma using a plasma cleaner (Model PDC-32G, Harrick Plasma, Ithaca, NY) to remove any surface contamination [276] and then patterned into 40 3mm diameter PDMS-formed wells. 1,2-bis(4-pyridyl)ethylene (BPE; 10^{-4} Molar in methanol) was used as an external control to ensure consistency between substrates. Raman spectra were acquired using a Renishaw inVia Reflex multi-wavelength confocal imaging microscope (Hoffman Estates, IL). A Leicha apochromatic 5× objective (NA 0.12) illuminated a 1265 μm^2 area on the substrate, which allows spatial averaging and minimization of the effect of potential random hot spots. A 785-nm near-infrared diode laser (Renishaw) operating at 10% power capacity (28 mW) provided the incoming radiation, and spectra were collected in 3 10-sec acquisitions. An internal silicon standard measurement was obtained at the beginning of each SERS analysis as an internal control for instrument performance.

All samples were applied to the NA substrates at the concentrations specified, in a volume of 1 µl per well, and analyzed in duplicate wells. Samples were dried onto the nanorods overnight and spectra collected from 5 random locations within each sample spot for analysis. 10 spectra were collected per sample (5 spectra per well per µl of sample), and *M. pneumoniae* reference strain and negative media controls were independently prepared and analyzed for each substrate. 2 wells were intentionally left blank on each substrate to obtain a background SERS reading on the naked nanorod substrate only. A total of 3 separate NA substrates were used for these experiments; 2 for the analysis of the *M. pneumoniae* isolates with n=390 spectra, and 1 for the analysis of other human and commensal *Mollicutes* species with n=150 spectra, resulting in a total of n=540 spectra. Raman spectra between 400-1800 cm^{-1} were acquired using Renishaw's

WiRE 3.4 software. Instrument settings were optimized to maximize signal and minimize saturation or sample degradation arising from laser stimulation.

Raman spectra were first averaged using GRAMS32/A1 spectral software package (Galactic Industries, Nashua, NH) in order to assess signal-to-noise quality, and baseline-corrected using a concave rubberband algorithm which performed 10 iterations on 64 points to aid in preliminary evaluation of the spectra and peak assignment (OPUS, Bruker Optics, Inc., Billerica, MA). Chemometric analysis was carried out with MATLAB version 7.10.0 (The Mathworks, Inc., Natick, MA) using PLS-Toolbox version 7.5.1 (Eigenvector Research Inc., Wenatchee, WA). Raw spectra were pre-processed using the 1st derivative of each spectrum and a 15-point, 2nd order polynomial Savitsky-Golay algorithm. Each dataset was then vector-normalized and mean-centered. Due to the inherently complex nature of spectral data, multivariate statistical analysis of the datasets was performed using principal component analysis (PCA) and partial least squares-discriminatory analysis (PLS-DA), using the PLS Toolbox software. Unless otherwise specified, all PLS-DA models were cross-validated using a Venetian blinds algorithm with 10 data splits.

Results and Discussion

Detection of *M. pneumoniae* clinical isolates. We analyzed 32 clinical isolates, including reference strains M129 (type 1) and FH (type 2), alongside a growth medium control prepared in parallel with the *M. pneumoniae* samples. Full details regarding isolate origin, year isolated, P1 genotype, macrolide susceptibility, protein content, DNA content, and genome equivalents for *M. pneumoniae* clinical isolates and reference strains are given in **Table 4.1**. CFU values were determined for both reference strains and six randomly chosen additional

isolates to assess cell viability at time of fixation and ranged from $1x10^5$ to $1x10^7$ CFU/ml. Due to the propensity for mycoplasma cells to clump, a confounding factor in using CFU values as a metric for sample content is the potential discrepancy between CFU value and actual cell number, which can differ by as much as 10^3-fold [280]. Therefore, protein content and genome equivalents were determined in order to better define the content of the samples at the concentration analyzed by SERS. Sample content for all *M. pneumoniae* samples fell within comparable ranges, and the molecular content of all samples was consistent with published values for bacterial cells [281]. A five to ten-fold increase in protein concentration per cell was observed in *M. pneumoniae* isolates harvested during stationary phase relative to those harvested during log phase (growth phase based on the color of the pH indicator in the SP4 medium), but no notable differences in genome equivalents or SERS spectra were observed between *M. pneumoniae* samples relative to growth phase at time of harvest (data not shown). Average SERS spectra of the nanorod substrate background, growth medium control, and *M. pneumoniae* samples are shown in **Figure 4.1**, with each class exhibiting a distinct band pattern.

PLS-DA was applied here to determine statistically significant detection of *M. pneumoniae* by NA-SERS. PLS-DA is a full-spectrum, multivariate, supervised statistical method whereby prior knowledge of classes is used to yield more robust discrimination by minimizing variation within classes while emphasizing latent variables arising from spectral differences between classes [266,267]. A PLS-DA model was generated to discriminate between three classes: the nanorod substrate background (**Figure 4.2A**); the growth medium control (**Figure 4.2B**); and all *M. pneumoniae* strains (**Figure 4.2C**). The inclusion of substrate background and growth medium controls allowed us to ensure that any differences in growth medium and nanorod background signal within the substrate did not affect the ability of the

model to discriminate between the presence or absence of *M. pneumoniae*. Two nanorod substrates were used for these experiments, with each containing duplicate wells of the bare nanorod substrate, independently prepared M129, FH, and growth medium controls, and 15 additional clinical isolates of *M. pneumoniae* per substrate. A total of n=390 pre-processed NA-SERS spectra collected from both substrates were included in the model, consisting of 20 nanorod substrate background spectra, 20 growth medium control spectra, 25 M129 spectra, 25 FH spectra, and 10 spectra per additional clinical isolate. The cross-validated statistics for the model are given in **Figure 4.2D** and show that NA-SERS was able to correctly classify all 32 clinical isolates as *M. pneumoniae* regardless of global origin, year isolated, genotype, or macrolide susceptibility phenotype, and distinguish them from the substrate background and the growth medium control with 100% cross-validated sensitivity and specificity.

Differentiation of *M. pneumoniae* samples and 12 other human commensal and pathogenic *Mollicutes* species. A critical question for clinical detection platforms is specificity for the pathogen of interest, particularly in the context of other organisms potentially present in a clinical sample. SERS is a structure-based technique that generates a Raman fingerprint or barcode based on the unique molecular content of the sample, and as such, the most likely organisms to generate false positives would be those most closely resembling *M. pneumoniae* structurally. To evaluate the specificity of the NA-SERS biosensing platform, 12 human commensal and pathogenic *Mollicutes* species closely related to *M. pneumoniae* in *rpoB* β-subunit nucleotide and amino acid sequence phylogenies and 16S rDNA phylogeny were chosen for analysis alongside *M. pneumoniae* strain M129 and a growth medium control [289]. In order to best define the content of the sample at the concentration used for SERS, analyses were done to determine total protein and DNA content, the latter allowing calculation of genome

equivalents based on known genome sizes and G+C content (**Table 4.2**). All sample contents fell within comparable ranges and were consistent with published values for bacterial cells [281].

A total of n = 150 pre-processed NA-SERS spectra were collected on a single nanorod substrate consisting of n = 10 substrate background spectra, n = 10 growth medium control spectra, n = 10 *M. pneumoniae* spectra, and 10 spectra each per other *Mollicutes* species. The first PLS-DA model generated was used to discriminate between two classes, the nanorod substrate background and all other biological samples, which it did with 100% cross-validated sensitivity and specificity (data not shown). The purpose of this model was to ensure that the nanorod background signal within the substrate was significantly different than all other samples in order to exclude the background spectra from our future models. The second PLS-DA model was generated using a total of n = 140 pre-processed NA-SERS spectra, consisting of n= 10 growth medium control spectra, n = 10 *M. pneumoniae* spectra, and 10 spectra each per other *Mollicutes* species categorized into three classes: the growth medium control; *M. pneumoniae* strain M129; and all 12 other human commensal and pathogenic *Mollicutes* species. This model distinguished the three classes with 100% cross-validated sensitivity and specificity (data not shown). The third PLS-DA model was generated using pre-processed NA-SERS spectra from all three nanorod substrates analyzed during these experiments and contained a total of n = 495, consisting of 25 growth medium control spectra, 25 M129 spectra, 25 FH spectra, 10 spectra each per other *M. pneumoniae* clinical isolates (30 isolates total), and 10 spectra each per other human commensal and pathogenic *Mollicutes* species (12 species total). This model was also categorized into three classes: the growth medium control (**Figure 4.3A**); all *M. pneumoniae* clinical isolates, including reference strains (**Figure 4.3B**); and all human commensal and pathogenic *Mollicutes* species (**Figure 4.3C**). PLS-DA was able to distinguish all *M.*

pneumoniae strains from all 12 other human commensal and pathogenic *Mollicutes* species and the growth medium control with 100% cross-validated sensitivity and specificity (**Figure 4.3D**).

***M. pneumoniae* genotyping capabilities of NA-SERS.** A key advantage of SERS for biosensing is the potential to detect and genotype an organism within a single test, especially of interest here since there is currently no existing platform capable of the simultaneous detection and typing of *M. pneumoniae*. To evaluate this capability we applied PLS-DA to the *M. pneumoniae* strain spectra above. Our panel of clinical isolates contained 3 distinct and clinically relevant genotypes of *M. pneumoniae*: 13 type 1 strains, 11 type 2 strains, and 6 type 2 variant (2V) strains. *M. pneumoniae* strains M129 (type 1) and FH (type 2) were used as reference strain controls, as they have been previously applied in this manner for evaluation of *M. pneumoniae* genotyping assays [19].

For the type 1 strains a PLS-DA model was generated using 180 pre-processed NA-SERS spectra consisting of the 25 M129 spectra and the 25 FH spectra as controls, and all 130 other type 1 clinical isolate spectra (10 spectra per isolate). The model was built to discriminate between 2 classes, either type 1 or type 2. PLS-DA was able to correctly classify all other 13 type 1 strains with the type 1 reference strain with 96.8% sensitivity and 96% specificity (**Figure 4.4A** and **4.4B**). For the type 2 strains a second PLS-DA model was generated using 160 pre-processed NA-SERS spectra consisting of the 50 type 1 and 2 reference strain control spectra and all 110 other type 2 strain spectra (10 spectra per isolate). As for the type 1 isolates, this model was built to discriminate between 2 classes, type 1 or type 2. PLS-DA was able to correctly classify all 11 other type 2 isolates with the type 2 reference strain control with 99.3% sensitivity and 100% specificity (**Figure 4.4C** and **4.4D**).

For type 2V clinical isolates, a third PLS-DA model was generated using 110 pre-processed NA-SERS spectra consisting of the 50 type 1 and 2 reference strain control spectra and all 60 type 2V clinical isolate spectra (10 spectra per isolate). However, this model was built to discriminate between 3 classes: type 1 reference strain control; type 2 reference strain control; or type 2V clinical isolate spectra. A third class was necessary for classification of this genotype as existing methods are capable of identifying variant strains as unique from type 1 and 2 isolate strains [18], and as such for clinical purposes NA-SERS genotyping should be able to do the same. PLS-DA correctly classified the type 1 reference strain control as distinct from the type 2 control and the type 2V clinical isolates with 100% cross-validated sensitivity and 98.8% cross-validated specificity (**Figure 4.5A** and **4.5D**). Furthermore, PLS-DA distinguished the type 2 reference strain control from the type 1 control and 2V clinical isolates with a cross-validated sensitivity and specificity of 92% and 90.6%, respectively (**Figure 4.5B** and **4.5D**). Lastly, PLS-DA correctly classified all 6 type 2V strains as distinct from the type 1 and 2 reference strain controls with 100% cross-validated sensitivity and specificity (**Figure 4.5C** and **4.5D**). The drop in sensitivity and specificity observed for the type 2 reference strain control is likely due to the fact that these are variant strains of the type 2 parent strain, and variant strains tend to be more similar to their respective parent strains genetically than either are to the opposite strain type [18,256].

To further evaluate the strain typing capabilities of NA-SERS, PLS-DA models were generated using the M129 and FH reference strains alongside each clinical isolate individually. 30 PLS-DA models were built using the 25 type 1 M129 spectra and 25 type 2 FH spectra as reference strain control classes, and 10 clinical isolate spectra treated as an unknown class. For type 1 and 2 clinical isolates, 2 categories were used for cross-validation of the model, while for

type 2V isolate strains, 3 categories were incorporated to cross-validate the model, as described above. For all clinical isolate types cross-validation of the model was done using a Venetian blinds algorithm with 7 data splits. These PLS-DA models were incorporated to simulate a potential strategy for future application of NA-SERS for *M. pneumoniae* genotyping wherein known strain type controls are used to predict the genotype of an unknown clinical sample. Full cross-validated statistics for all 30 PLS-DA models are given in **Table 4.3**. Overall, PLS-DA performance was consistent with the models shown in **Figures 4.4** and **4.5**. The only notable difference in performance was a decrease in cross-validated specificity in the individual modeling for type 1 clinical isolates K20, NM2, and FL1, but this likely arises due to the decreased sample size (n = 60) used to build the individual PLS-DA models.

Additionally, we compared averaged, baseline-corrected, and normalized spectra of all three genotypes to look for any differences in band pattern between the three genotypes that could be contributing to the classification capabilities demonstrated in the PLS-DA modeling (**Figure 4.6**). The majority of the spectral fingerprint was identical for all three strain types, which is to be expected since they are all the same species and classify as such in the PLS-DA models shown in Figures 2 and 3. However, several visible differences in band pattern are present in the spectra for each genotype of *M. pneumoniae*, which could account for the ability of NA-SERS to distinguish between the three genotypes with statistically significant sensitivity and specificity. The averaged type 1 spectrum has two unique peaks, one at 1636 cm^{-1} that does not appear in the averaged type 2 or 2V spectra, and one at 959 cm^{-1} which appears as more distinct and shifted slightly right in the type 1 spectrum when compared to the type 2 spectrum, and does not appear in the type 2V spectrum. The averaged type 2 strain spectrum is very similar to the type 1 strain spectrum aside from the differences mentioned above and the presence of a doublet

at 767 and 778 cm^{-1}, which appears as more distinct than that present in the type 2V spectrum and as a broad singlet in the type 1 spectrum. The averaged type 2V spectrum appears to be the most distinct of the three, with a doublet at 875 and 890 cm^{-1} that appears as a single peak at 890 in type 1 and 2 spectra, and a small peak at 521 that is also absent in type 1 and 2 spectra. While these spectral differences are extremely subtle, chemometric analysis is highly capable of discerning differences such as these with substantial discriminatory classification power [257].

Although little is known about the phenotypic effects of strain type beyond observable differences in biofilm formation [37], the genotypic differences between them are very well characterized. Briefly, homologous recombination within the *P1* gene of repetitive element sequences located both in and outside the *P1* gene is known to be the source of sequence variation between the strain types [7]. Nucleotide and amino acid sequencing of 60 *M. pneumoniae* isolates indicates that trinucleotide short sequence repeats (SSR's) coding for serine can be found in all strain types anywhere from 5-14 times, but appear to be most prevalent in type 1 strains [7]. Serine repeats may form a hinge structure and lead to downstream conformational differences in the P1 protein between the different strain types which could potentially affect its interaction with the host as a surface antigen [221,222]. In addition, 14 of the 60 isolates in the Zhao et al. study had point mutations in several variant strains corresponding to amino acid changes in P1 to glutamine, proline, asparagine, and isoleucine residues [7].

In our study, the peaks unique to the type 1 spectrum are commonly associated with vibrational mode bonds present in lysine (959 cm^{-1}) and amide I or alpha helix (1636 cm^{-1}) molecular structures [242,244,278]. The peaks unique to the type 2 spectral fingerprint located at 767 and 778 cm^{-1} are commonly associated with vibrational modes found in histidine,

tryptophan, or carbohydrate bonds [241,242,244]. Finally, the peaks unique to the type 2V clinical isolates found at 521, 875 and 890 cm^{-1} are frequently associated with bonds present in histidine, tryptophan, ribose, indole, asparagine, methionine, glutamine, and S-S and C-C stretching vibrational modes [241,242,244]. Interestingly, all the unique peaks present in the average spectra for the strain types analyzed in this study are predominately associated with protein backbone, amino acid residue, and DNA bond vibrations. Furthermore, spectral features in the averaged spectrum of the 2V variant strains are consistent with the point mutations identified in the Zhao et al. study [7], and our overall spectral interpretation of the averaged spectra for each strain type is consistent with what is known about the differences between strain types of *M. pneumoniae* infection.

Unsupervised chemometric analysis of *M. pneumoniae* strain types and *Mollicutes* species. We applied principal component analysis (PCA) to supplement the PLS-DA modeling of sample spectra and evaluate the total variance present in our *M. pneumoniae* typing and other human commensal and pathogenic *Mollicutes* datasets. PCA is an unsupervised form of chemometric analysis, which reduces the dimensionality of the dataset and facilitates establishing patterns and grouping of similar spectra without any *a priori* knowledge of sample class [257]. PCA explains successively smaller proportions of the variance, with the first few principal components explaining the greatest percentage of total variance present in the dataset [290].

Pre-processed SERS spectra from *M. pneumoniae* reference strain type 1 and 2 controls and all other type 1 clinical isolates were used to generate a PCA plot comparing principle components 1, 2, and 3, which captured 54.3% of the total variance present in the 180 spectra used to build the model (**Figure 4.7A**). Type 2 control strain FH clustered in the bottom right

corner, and the clustering pattern for all type 1 strains was predominately below and to the left, though some overlap between the two strain types was present. The PCA model of the type 1 clinical isolates supports the PLS-DA modeling of the spectra shown in **Figure 4.4A**.

A second PCA model was built using pre-processed SERS spectra (n=160) consisting of type 1 and 2 reference strain controls and all other type 2 clinical isolates of *M. pneumoniae.* Principal components 1-3 captured 57.99% of the total variance and when plotted orthogonally showed a distinct separation between the type 1 reference strain control and all type 2 reference strain and other isolates, with very little overlap of clusters (**Figure 4.7B**). PCA modeling for the type 2 clinical isolate dataset was consistent with the PLS-DA modeling of the data shown in **Figure 4.4B**.

In addition, a PCA model was built using the pre-processed SERS spectra from the type 2V clinical isolate dataset (n=110). Principal components 1-3 captured 54.12% of the total variance and when plotted orthogonally showed distinctly separated clusters for the type 1 control, the type 2 control, and the type 2V clinical isolates, with some overlap present between the type 2 and type 2V clusters (**Figure 4.7C**). This clustering pattern further supports the PLS-DA classification performance shown in **Figure 4.5**.

Finally, a PCA model was built using the full *M. pneumoniae* and *Mollicutes* species dataset consisting of pre-processed spectra from all 3 nanorod array substrates (n=495). Principal components 1-3 captured 50.09% of the total variance and when plotted orthogonally showed three distinctly separated clusters for growth medium control spectra, all *M. pneumoniae* spectra, and all other *Mollicutes* species spectra, with no overlap between clusters (**Figure 4.7D**). This supports the PLS-DA model of the data shown in **Figure 4.3**.

Conclusions

M. pneumoniae is a significant human respiratory tract pathogen in both incidence of infection and public health impact, but diagnostic strategies are complicated by the atypical and complex presentation of disease, non-descript symptoms, the requirement for separate tests for detection and genotyping, and the numerous challenges posed by direct culture. Serologic testing was historically the gold standard for diagnosis but suffers from severe limitations that make it both unreliable and impractical for rapid detection. Advances in qPCR technologies have overcome many issues with sensitivity and reliability, but the cost of reagents and requirement for technical expertise are still high, and independent tests must be done for detection and genotyping, limiting diagnosis by qPCR to hospital or advanced laboratory facilities and making it impractical for point-of-care use.

We previously established that the NA-SERS biosensing platform was capable of statistically significant detection of *M. pneumoniae* in true and simulated throat swabs, and that it has an endpoint of detection for *M. pneumoniae* of < 1 cell/μl, a sensitivity exceeding that of qPCR [13,288]. Here, NA-SERS showed statistically significant specificity for *M. pneumoniae* detection regardless of clinical isolate origin, year of isolation, macrolide susceptibility phenotype, or strain type, and was also able to distinguish all *M. pneumoniae* clinical isolates and control strains from 12 other human commensal and pathogenic *Mollicutes* species. Furthermore, NA-SERS discriminated between the two major strain types of *M. pneumoniae* with a high degree of statistically significant accuracy and correctly identified variant strains as different from the two major genotypes. Most importantly, NA-SERS was capable of detecting and genotyping *M. pneumoniae* within the same dataset, although the effect of the presence of a clinical background on the platform's ability to genotype *M. pneumoniae* and distinguish it from

other human commensal and pathogenic *Mollicutes* species remains to be determined. Nevertheless, NA-SERS is the first biosensing platform with the potential to simultaneously detect and genotype *M. pneumoniae* within a single test, which has significant implications and potential for the advancement of *M. pneumoniae* epidemiology. This capability would facilitate tracking epidemiological trends, such as type-switching and outbreak periodicity [12]. Additionally, from a point-of-care clinical standpoint, the ability to detect *M. pneumoniae* rapidly is critical to informing appropriate treatment regimens consistent with the responsible use of antimicrobials. This feature is underscored by the availability of handheld Raman instruments having the potential for point-of-care use [282-284]. In combination with the minimal sample preparation requirements and expedient detection, NA-SERS shows great promise for future application as a potential platform to apply for point-of-care *M. pneumoniae* diagnostics.

Acknowledgments

This work was supported by Public Health Service research grant AI096364 from the National Institute of Allergy and Infectious Diseases to D.C.K.

Manuscript data

Table 4.1: Strain/isolate information for all *M. pneumoniae* specificity cultures.

Isolate	Location	Year	P1 type	Macrolide phenotype	Protein content (µg/µl)	DNA content (ng/µl)	Genomic equivalents (cells/µl)	fg of protein/ cell
E1	Egypt	2009	2	S	0.149	2.0	$4.49x10^6$	26
E16	Egypt	2010	1	S	0.057	1.7	$4.34x10^6$	11
K3	Kenya	2010	2	S	0.065	2.3	$6.5x10^6$	10
K20	Kenya	2010	1	S	0.044	1.2	$3.39x10^6$	12.9
G6	Guatemala	2010	1	S	0.078	2.6	$7.36x10^6$	10.6
NM2	New Mexico	2010	1	R	0.074	1.1	$3.11x10^6$	23.8
RI1	Rhode Island	2011	2	S	0.071	1.5	$4.24x10^6$	16.7
OR1	Oregon	2011	1	R	0.076	1.3	$3.68x10^6$	20.7
WV1	W. Virginia	2011	2	S	0.094	1.9	$5.34x10^6$	17.6
WV9	W. Virginia	2012	1	R	0.071	1.3	$3.68x10^6$	19.3
FL1	Florida	2012	1	S	0.098	2.3	$6.5x10^6$	15
WI11	Wisconsin	2014	2V	S	0.085	1.6	$4.53x10^6$	18.8
WI17	Wisconsin	2014	2V	S	0.047	1.8	$5.09x10^6$	9.2
CO12	Colorado	2014	2V	S	0.077	1.6	$4.53x10^6$	16.9
CO44	Colorado	2014	2V	R	0.073	1.3	$3.68x10^6$	19.8
SA18	S. Africa	2013	2V	S	0.35	1.7	$4.81x10^6$	72.8
SA19	S. Africa	2013	2	S	0.47	1.1	$3.11x10^6$	151.0
SA22	S. Africa	2013	1	S	0.44	1.1	$3.11x10^6$	141.5
1005	New York	1999	2	S	0.28	1.5	$4.24x10^6$	66.0
1134	Indiana	1999	2	S	0.30	2.2	$6.22x10^6$	70.8
988	Canada	1992	1	S	0.12	2.0	$5.65x10^6$	19.3
678	Denmark	1962	1	S	0.12	3.5	$9.9x10^6$	12.1
682	Denmark	1988	2	S	0.16	2.1	$5.94x10^6$	26.9
983	S. Carolina	1988	2	S	0.16	1.6	$4.53x10^6$	35.3
386	Texas	1994	2	S	0.10	2.9	$8.2x10^6$	12.1
519	California	1995	2	S	0.28	1.5	$4.24x10^6$	63.6
GA1	Georgia	2012	1	S	0.22	3.5	$9.9x10^6$	22.2
GA3	Georgia	2012	2V	S	0.46	3.3	$9.33x10^6$	49.3
IL1	Illinois	2012	1	R	0.12	1.7	$4.81x10^6$	24.9
IL2	Illinois	2012	1	R	0.10	1.8	$5.09x10^6$	19.6
M129	N/A	N/A	1	S	0.169	4.1	$1.13x10^7$	14
M129	N/A	N/A	1	S	0.168	4.3	$1.20x10^7$	14
FH	N/A	N/A	2	S	0.046	2.1	$5.94x10^6$	7.7
FH	N/A	N/A	2	S	0.046	2.2	$6.30x10^6$	7.3

Figure 4.1: Comparison of averaged, baseline-corrected, and normalized SERS spectra for the nanorod substrate, growth medium control, and *M. pneumoniae* reference strain controls and clinical isolates. SERS spectra of the nanorod substrate (top), growth medium control (middle), and *M. pneumoniae* reference strains and other clinical isolates (bottom). Raw spectra of the three sample classes were averaged, baseline-corrected, and normalized using GRAMS32/A1 spectral software package (Galactic Industries, Nashua, NH). For the nanorod substrate background class, n = 20; for the growth medium control class, n = 20; and for the *M. pneumoniae* class, n = 350.

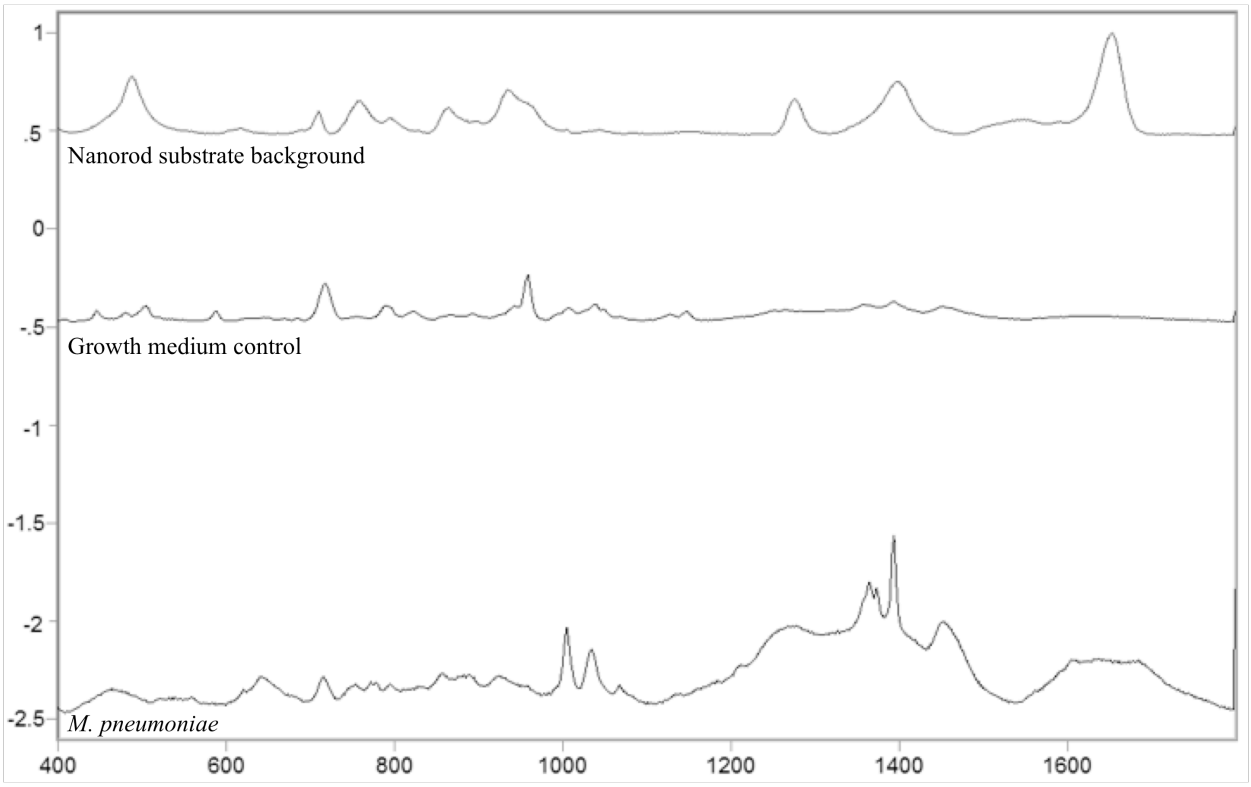
1
.5
0
-.5
-1
-1.5
-2
-2.5
Nanorod substrate background
Growth medium control
M. pneumoniae
400
600
800
1000
1200
1400
1600

Figure 4.2: PLS-DA of 32 *M. pneumoniae* clinical isolates, including reference strains M129 and FH. Each panel represents a cross-validated class prediction score for **(A)** class 1, substrate background; **(B)** class 2, growth medium control; and **(C)** class 3, all *M. pneumoniae* strains. For panels **A-C**, each individual shape represents a single pre-processed NA-SERS spectrum. The substrate background spectra are represented by gray diamonds, the growth medium control spectra by solid black squares, and the *M. pneumoniae* spectra by open shapes that differ by cluster to indicate the different individual strains and isolates. The red-dotted line indicates the classification threshold line for positive class prediction, and the black-dotted line indicates the 95% confidence interval. **(D)** Cross-validated sensitivity, specificity, and class error for the plots shown in A-C obtained using Venetian blinds with 10 data splits to represent the prediction performance of the PLS-DA model for *M. pneumoniae* detection.

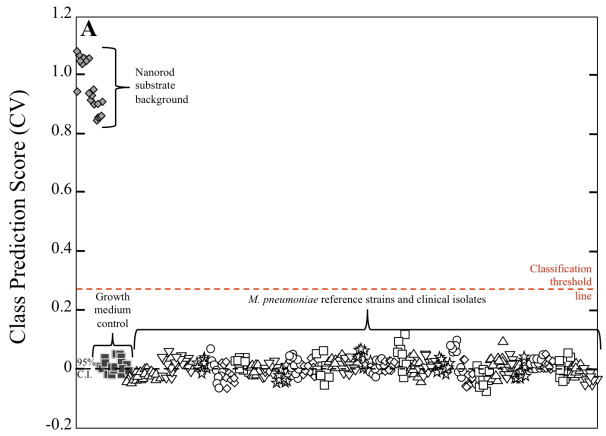

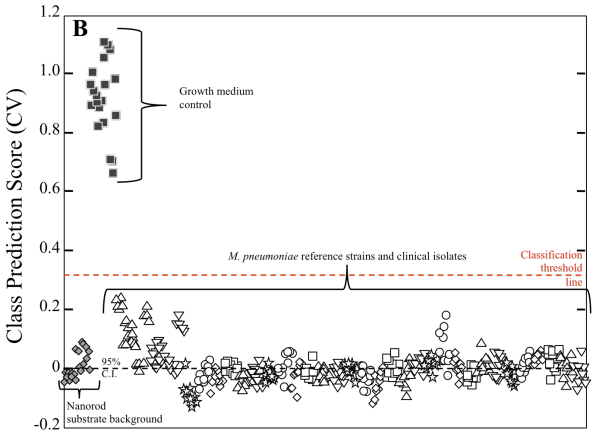

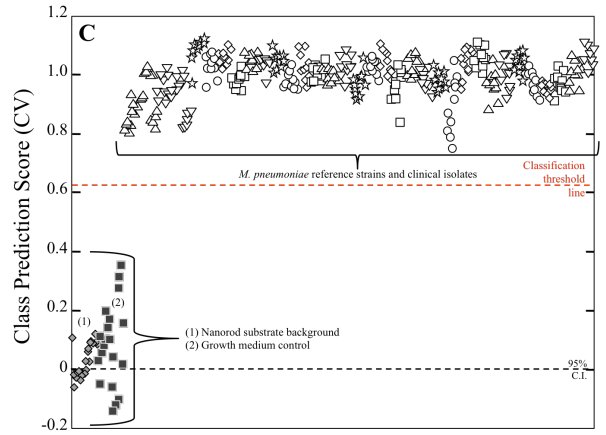

D

CLASS	Sensitivity (CV)	Specificity (CV)	Class Error (CV)
Nanorod substrate background	1.00	1.00	0.00
Growth medium control	1.00	1.00	0.00
M. pneumoniae	1.00	1.00	0.00

Table 4.2: Quality control and sample information for *Mollicutes* species and *M. pneumoniae* control cultures.

Commensal organism	Genome Size (Bp)	Protein content (µg/µl)	DNA content (ng/µl)	Genomic equivalents (cells/µl)	fg protein/cell	CFU/µl
Acholeplasma laidlawii	1,496,992	0.247	16.2	$1.9x10^6$	130	$4.55x10^5$
Mycoplasma amphoriforme	1,029,022	0.072	2.4	$4.3x10^5$	167	ND
Mycoplasma fermentens	1,118,751	0.374	23.8	$3.9x10^6$	95.9	$2.6x10^6$
Mycoplasma genitalium	580,073	0.099	2.6	$8.2x10^5$	121	$1.75x10^4$
Mycoplasma hominis	665,445	0.454	10.7	$2.9x10^6$	157	$2.2x10^5$
Mycoplasma orale	710,549	0.114	8.1	$2.1x10^6$	54.3	$9.9x10^4$
Mycoplasma penetrans	1,358,633	0.813	19	$2.6x10^6$	313	$1.7x10^6$
Mycoplasma pirum	510,593	0.384	20	$7.2x10^6$	53.3	$3.85x10^6$
Mycoplasma salivarium	710,000	0.558	32.1	$8.32x10^6$	67.1	$1x10^5$
Mycoplasma spermatophilum	846,000	0.068	1.2	$2.6x10^5$	261	ND
Ureaplasma parvum	727,289	0.068	1.7	$4.3x10^5$	158	$4.5x10^4$
Ureaplasma urealyticum	874,478	0.067	2	$4.2x10^5$	159	$5.6x10^3$
Mycoplasma pneumoniae	816,394	0.061	1	$2.24x10^6$	27.2	$8.4x10^4$

Figure 4.3: PLS-DA distinguishing *M. pneumoniae* strains from other human commensal and pathogenic *Mollicutes* species. Each panel represents a cross-validated class prediction score for **(A)** class 1, growth medium control; **(B)** class 2, all *M. pneumoniae* strains; and **(C)** class 3, all other human commensal and pathogenic *Mollicutes* samples. For panels **A-C**, each individual shape represents a single pre-processed NA-SERS spectrum. The growth medium control spectra are represented by gray diamonds, the *M. pneumoniae* spectra by open shapes that differ by cluster to indicate the different individual strains and isolates, and the human commensal and pathogenic *Mollicutes* species are represented by light gray shapes that differ by cluster to indicate the individual species. The red-dotted line indicates the classification threshold line for positive class prediction, and the black-dotted line indicates the 95% confidence interval. **(D)** Cross-validated sensitivity, specificity, and class error for the plots shown in A-C obtained using Venetian blinds with 10 data splits to represent the prediction performance of the PLS-DA model for *M. pneumoniae* detection.

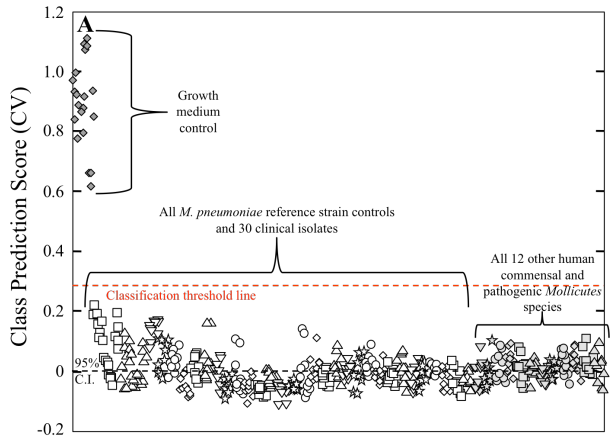

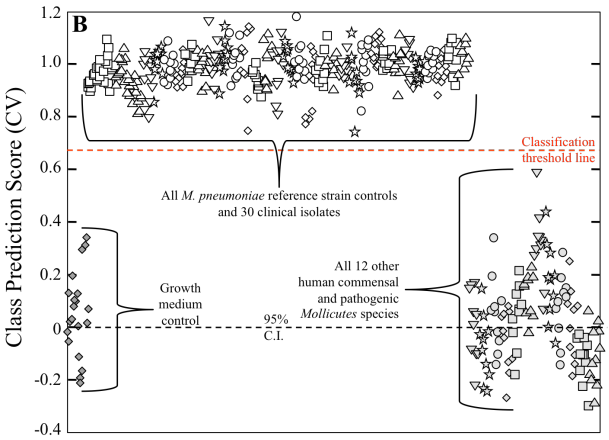

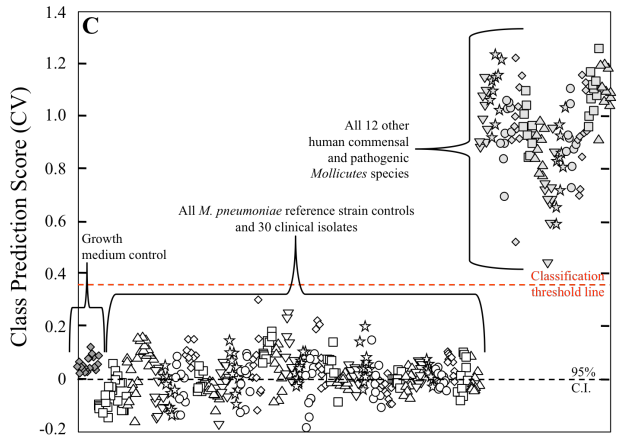

D

CLASS	Sensitivity (CV)	Specificity (CV)	Class Error (CV)
Growth medium control	1.00	1.00	0.00
All *M. pneumoniae* controls and clinical isolates	1.00	1.00	0.00
All 12 other human commensal and pathogenic *Mollicutes* species	1.00	1.00	0.00

Figure 4.4: PLS-DA for NA-SERS genotyping of type 1 and 2 *M. pneumoniae* strains. Cross-validated class prediction scores for **(A)** all 13 type 1 clinical isolates, and **(C)** all 11 type 2 clinical isolates. The cross-validated sensitivity, specificity and class error was obtained using Venetian blinds with 10 data splits to represent the prediction performance of models for classification of **(B)** type 1 strains and **(D)** type 2 strains. For panels A and C, each individual shape represents a single pre-processed NA-SERS spectrum. *M. pneumoniae* type 1 reference strain control and other clinical isolates are represented by dark gray diamonds, while the type 2 reference strain control and other clinical isolates are represented by open shapes. Shapes differ by cluster to indicate the individual clinical isolates and samples, and the strain/isolate designation is indicated above the brackets for each cluster. The red-dotted line indicates the classification threshold line for positive class prediction, and the black-dotted line indicates the 95% confidence interval.

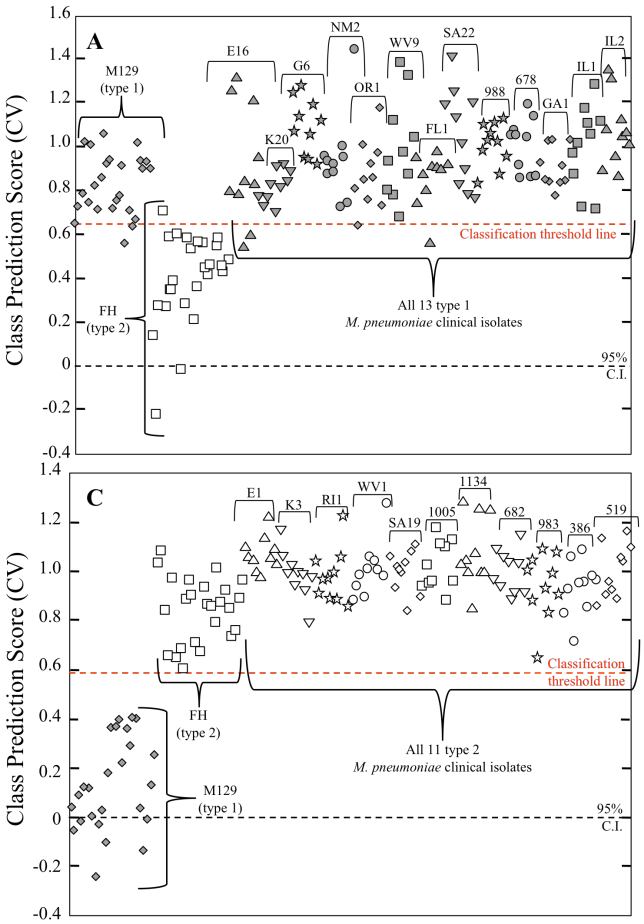

B

CLASS	Sensitivity (CV)	Specificity (CV)	Class Error (CV)
Type 1	0.968	0.96	0.04
Type 2	0.96	0.968	0.04

D

CLASS	Sensitivity (CV)	Specificity (CV)	Class Error (CV)
Type 1	1.00	0.993	0.004
Type 2	0.993	1.00	0.004

Figure 4.5: PLS-DA for NA-SERS genotyping of type 2V *M. pneumoniae* clinical isolates. Cross-validated class prediction scores for **(A)** class 1, the type 1 reference strain control; **(B)** class 2, the type 2 reference strain control; and **(C)** class 3, all 6 type 2V clinical isolates. The cross-validated sensitivity, specificity and class error for panels A-C was obtained using Venetian blinds with 10 data splits to represent the prediction performance of models for classification of type 2V strains **(D)**. For the panels **A-C**, each individual shape represents a single pre-processed NA-SERS spectrum. The *M. pneumoniae* type 1 reference strain control is represented by dark gray diamonds, the type 2 reference strain control is represented by open squares, and the type 2V clinical isolates are represented by light gray shapes. The light gray shapes differ by cluster to indicate the individual clinical isolates, and the strain/isolate designation is indicated above the brackets for each cluster. The red-dotted line indicates the classification threshold line for positive class prediction, and the black-dotted line indicates the 95% confidence interval.

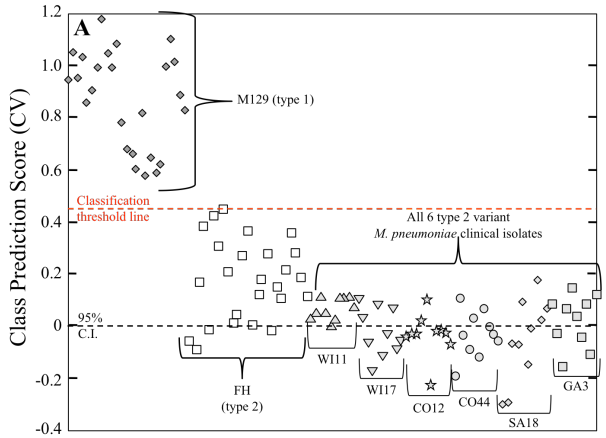

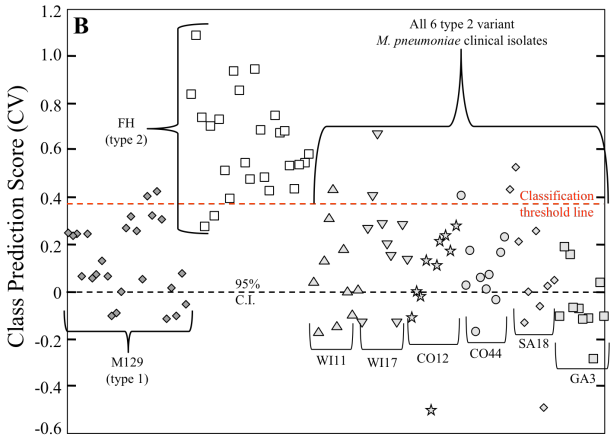

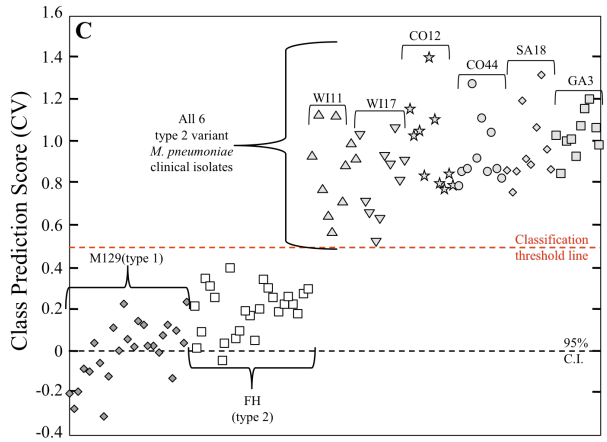

D

CLASS	Sensitivity (CV)	Specificity (CV)	Class Error (CV)
Type 1	1.00	0.988	0.006
Type 2	0.92	0.906	0.08
Type 2V	1.00	1.00	0.00

Table 4.3: Cross-validated PLS-DA individual modeling statistics representing the prediction performance for NA-SERS genotyping of type 1 and 2 *M. pneumoniae* clinical isolates. For type 1 and type 2 isolates, 2 categories were used for cross-validation of the model, either category 1, type 1; or category 2, type 2. Clinical isolates were treated as an unknown class and cross-validated sensitivity, specificity, and class error was based on their classification prediction score with their respective reference strain control class. CV, cross-validated.

Isolate	P1 Type	CV Sensitivity	CV Specificity	CV class error
E16	1	0.943	0.92	0.06
K20	1	1	0.84	0.08
G6	1	1	0.92	0.04
NM2	1	1	0.88	0.06
OR1	1	0.914	0.92	0.08
WV9	1	0.914	0.96	0.06
FL1	1	0.971	0.84	0.09
SA22	1	0.971	1	0.01
988	1	0.971	1	0.01
678	1	1	1	0
GA1	1	1	1	0
IL1	1	1	1	0
IL2	1	0.971	1	0
E1	2	1	0.971	0.01
K3	2	1	1	0
RI1	2	1	1	0
WV1	2	1	1	0
SA19	2	1	1	0
1005	2	1	1	0
1134	2	1	0.971	0.01
682	2	1	1	0
983	2	1	1	0
386	2	1	1	0
519	2	1	1	0

Table 4.4: **Cross-validated PLS-DA individual modeling statistics representing the prediction performance for NA-SERS genotyping of type 2V *M. pneumoniae* clinical isolates.** For type 2V isolate strains, 3 categories were incorporated to cross-validate the model, either category 1, type 1; category 2, type 2; or category 3, neither. Clinical isolates were treated as an unknown class and cross-validated sensitivity, specificity, and class error was based on their classification prediction score as neither type 1 or type 2 reference control strains (i.e. category [61]). CV, cross-validated.

Isolate	P1 Type	CV Sensitivity	CV Specificity	CV class error
1: M129	2V	1	0.971	0.01
2: FH		0.8	0.943	0.13
3: WI11		1	0.98	0.01
1: M129	2V	1	1	0
2: FH		0.88	0.943	0.08
3: WI17		1	0.98	0.01
1: M129	2V	1	0.971	0.01
2: FH		0.84	1	0.08
3: CO12		1	1	0
1: M129	2V	1	1	0
2: FH		0.92	0.971	0.05
3: CO44		1	0.98	0.01
1: M129	2V	1	1	0
2: FH		1	0.943	0.03
3: SA18		1	1	0
1: M129	2V	1	1	0
2: FH		0.96	1	0.02
3: GA3		1	1	0

Figure 4.6. Comparison of averaged, baseline-corrected, and normalized SERS spectra for type 1, type 2, and type 2V genotypes. Raw spectra of all type 1 (n=155), type 2 (n=135), and type 2V (n=60) clinical isolates and controls were averaged, baseline-corrected, and normalized using GRAMS32/A1 spectral software package (Galactic Industries, Nashua, NH). Red, average spectrum of all type 1 *M. pneumoniae* strains; green, average spectrum of all type 2 *M. pneumoniae* strains; blue, average spectrum of all type 2V *M. pneumoniae* strains. Peaks unique to a specific genotype of *M. pneumoniae* are indicated by arrows and identified above the spectral fingerprint. Type 1 peaks, red arrows; type 2 peaks, green arrows; and type 2V peaks, blue arrows.

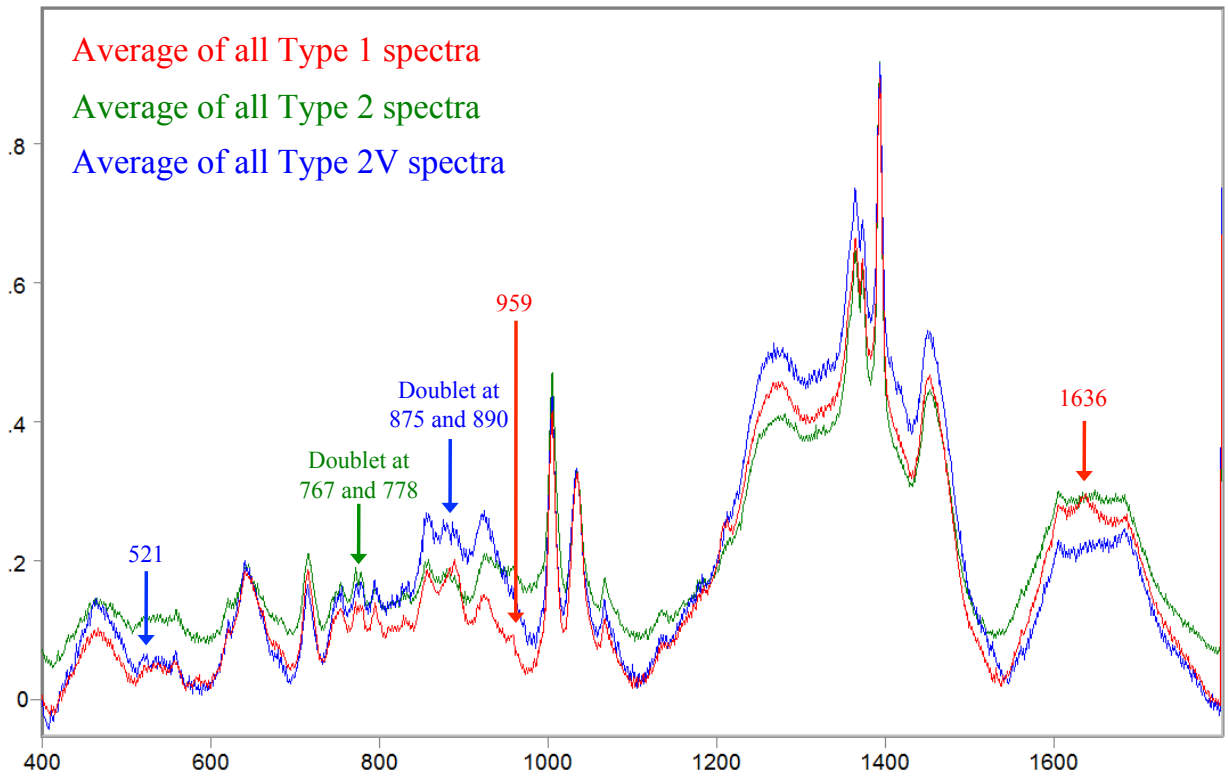
Average of all Type 1 spectra
Average of all Type 2 spectra
Average of all Type 2V spectra
.8
.6
.4
.2
0
400
600
800
1000
1200
1400
1600
959
Doublet at
875 and 890
Doublet at
767 and 778
521
1636

Figure 4.7: Principle component analysis of *M. pneumoniae* strain typing and other human commensal and pathogenic *Mollicutes* species. For all panels, each individual shape represents a single sample spectrum. PC scores plots of 1 vs. 2 vs. 3 of: **(A)** *M. pneumoniae* reference strains and all 13 other type 1 clinical isolates; **(B)** *M. pneumoniae* reference strains and all 11 other type 2 clinical isolates; **(C)** *M. pneumoniae* type 1 reference strain, type 2 reference strain, and all 6 type 2V clinical isolates; and **(D)** growth medium control, all *M. pneumoniae* strains, and all 12 other human commensal and pathogenic *Mollicutes* species. For panels **A-C**, dark gray diamonds represent type 1 sample spectra whereas open squares represent the type 2 sample spectra. In panel **C**, type 2V clinical isolate spectra are represented by light gray triangles. For panel **D**, growth medium control spectra are represented by dark gray diamonds, *M. pneumoniae* spectra by open squares, and all 12 other *Mollicutes* species by light gray triangles. For panels **A-D**, clustering of samples is indicated by black circles or brackets.

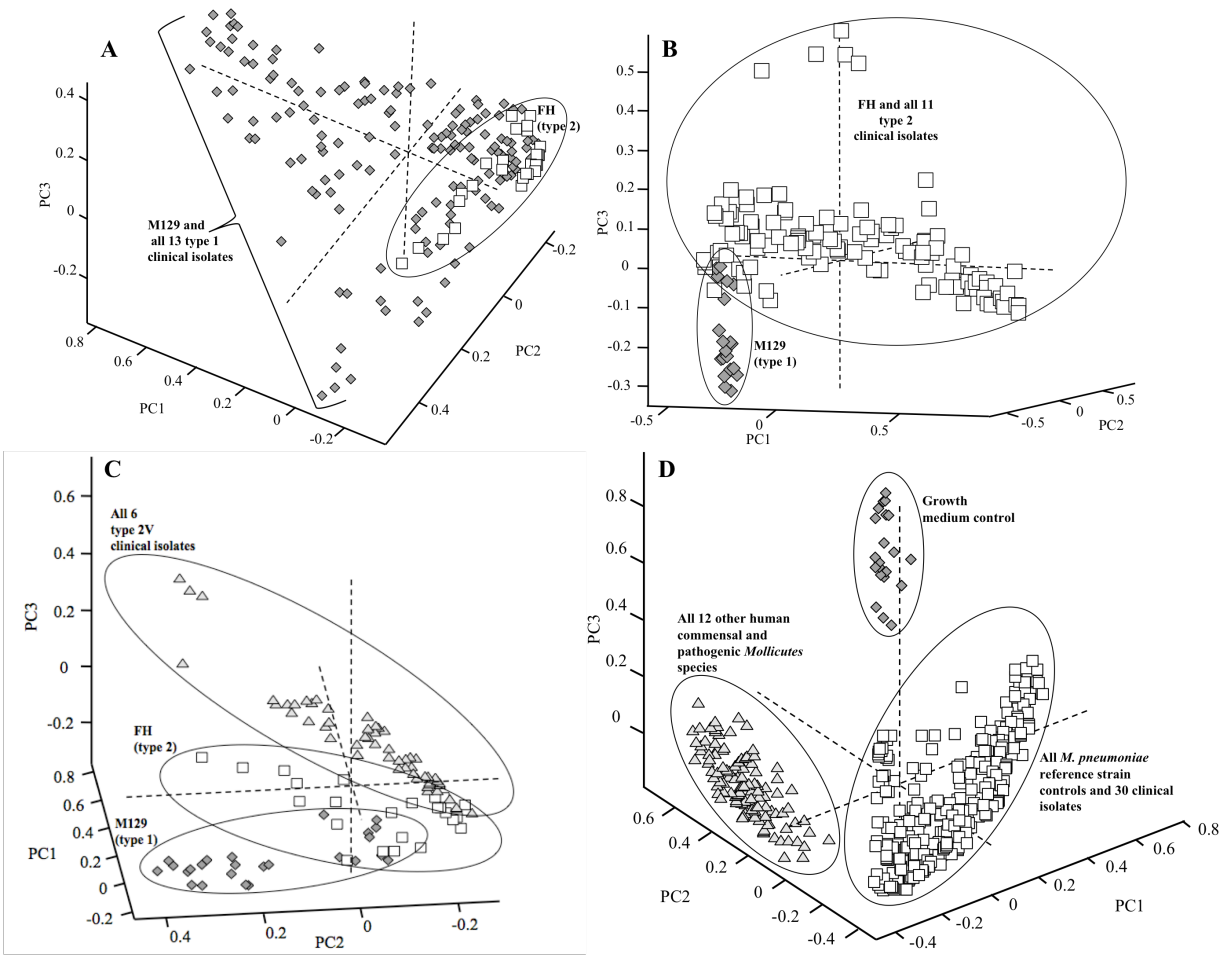
A
FH
(type 2)
M129 and
all 13 type 1
clinical isolates
PC3
PC1
PC2
B
FH and all 11
type 2
clinical isolates
M129
(type 1)
PC3
PC1
PC2
C
All 6
type 2V
clinical isolates
FH
(type 2)
M129
(type 1)
PC3
PC1
PC2
D
Growth
medium control
All 12 other human
commensal and
pathogenic Mollicutes
species
All M. pneumoniae
reference strain
controls and 30 clinical
isolates
PC3
PC2
PC1

CHAPTER 5

CONCLUSIONS

M. pneumoniae is a significant human respiratory tract pathogen in both incidence of infection and public health impact, but diagnostic strategies are complicated by the atypical and complex presentation of disease, non-descript symptoms, the requirement for separate tests for detection and genotyping, and the numerous challenges posed by direct culture. Serologic testing was historically the gold standard for diagnosis but suffers from severe limitations that make it both unreliable and impractical for rapid detection. Advances in qPCR technologies have overcome many issues with sensitivity and reliability, but the cost of reagents and requirement for technical expertise are still high, and independent tests must be done for detection and genotyping, limiting diagnosis by qPCR to hospital or advanced laboratory facilities and making it impractical for point-of-care use.

We previously established that the NA-SERS biosensing platform was capable of statistically significant detection of *M. pneumoniae* in true and simulated throat swabs, and here we have demonstrated that NA-SERS has a sensitivity that equals qPCR for *M. pneumoniae* detection. Additionally, our findings stress the significance of sample preparation when using NA-SERS technology. However, the question of whether cell lysis improves or hinders the detection capabilities of NA-SERS in the presence of a complex clinical background remains to be determined. Furthermore, we have shown that NA-SERS has statistically significant specificity for *M. pneumoniae* detection regardless of clinical isolate origin, year of isolation, macrolide susceptibility phenotype, or strain type, and found it was also able to distinguish 32 *M.*

pneumoniae clinical isolates and control strains from 12 other human commensal and pathogenic *Mollicutes* species. In addition, NA-SERS discriminated between the two major strain types of *M. pneumoniae* with a high degree of statistically significant accuracy and correctly identified variant strains as different from the two major genotypes. Most importantly, NA-SERS was capable of detecting and genotyping *M. pneumoniae* within the same dataset, although the effect of the presence of a clinical background on the platform's ability to genotype *M. pneumoniae* and distinguish it from other human commensal and pathogenic *Mollicutes* species remains to be determined. Nevertheless, NA-SERS is the first biosensing platform with the potential to simultaneously detect and genotype *M. pneumoniae* within a single test, which has significant implications and potential for the advancement of *M. pneumoniae* epidemiology. This capability would facilitate tracking epidemiological trends, such as type-switching and outbreak periodicity [12]. Additionally, from a point-of-care clinical standpoint, the ability to detect *M. pneumoniae* rapidly is critical to informing appropriate treatment regimens consistent with the responsible use of antimicrobials. This feature is underscored by the availability of handheld Raman instruments having the potential for point-of-care use [282-284]. In combination with the minimal sample preparation requirements and expedient detection, NA-SERS shows great promise for future application as a potential platform to apply for point-of-care *M. pneumoniae* diagnostics.

There are several immediate questions in need of evaluation for continuing the development of NA-SERS for point-of-care diagnostics in the short term. Most importantly, the endpoint of detection, genotyping capabilities, and specificity of NA-SERS needs to be evaluated in the presence of a clinical background. Establishing the appropriate PLS-DA modeling controls to incorporate the added complexity of a clinical background will be paramount in addressing these questions. Additionally, the ability of NA-SERS to correctly identify *M. pneumoniae* in the

presence of multiple commensal and/or pathogenic organisms within a single sample needs to be determined. The platform has shown success in the past (94% cross-validated accuracy) at correctly identifying lysed-cell *M. pneumoniae* in the presence of *Streptococcus pyogenes* and *Moraxella catarhalis* in laboratory strain and throat swab backgrounds [291]. However, further evaluation is needed to ensure that NA-SERS can still correctly identify intact-cell preparations of mixed samples with *M. pneumoniae* and combinations of other human commensal and pathogenic *Mollicutes* species, as well as of mixed samples of *M. pneumoniae* and the most commonly occurring respiratory pathogens present in co-infections, in both the presence and absence of a clinical background.

Once these questions have been answered, the next step will be to use all the previously collected spectra to build a calibration model of known class identities for predicting the identities of a true unknown, blinded sample set for external validation of NA-SERS for *M. pneumoniae* detection. Trial and error in calibration model building will likely be necessary to establish one that encompasses the representative heterogeneity of the sample population and, again, the importance of using appropriate controls to build the prediction model cannot be understated. Also, due to the increasing complexity of our sample content, factor analysis and spectral data mining could provide valuable information pertaining to the key variables (wavenumbers) within our data that drive *M. pneumoniae* detection and comprise the *M. pneumoniae* fingerprint or barcode. More so, comparing spectral band patterns of wild type 1 and 2 strains with cytadherence-deficient mutants could help identify key variables in distinguishing strain types, or even possibly provide insight on phenotypic differences that arise from the various genotypes.

In the long run, several steps must first occur for NA-SERS to be a viable next-generation platform for clinical diagnostics. While our method for nanorod array fabrication generates reproducible and consistent SERS substrates, the capabilities for mass production and distribution of these substrates is still limited and is in need of further development. In addition, quality control measures and substrate handling protocols require further investigation and need to be explicitly defined in order to meet the strict criteria required for clinical validation or eventual FDA approval. An example of one such unanswered question is which mode of packaging for distribution is most effective for optimized length of shelf-life in order to know how long a potential consumer could store a substrate before it is unfit for diagnostic or biosensing use. Another important consideration is whether or not to pre-load positive and negative control samples onto the substrates prior to distribution, and if so what would make the most appropriate controls for comparison to clinical samples in a point-of-care setting. To answer this question, a vast spectral database containing spectral fingerprints of *M. pneumoniae* in various clinical backgrounds needs to be acquired. Once it has been evaluated how patient age, sex, gender, naturally-occurring commensal flora, variation in immune responses, or secondary infections with other respiratory pathogens effects the ability of NA-SERS to detect *M. pneumoniae* in a clinical sample, it can be determined if substrate controls need to be catered and marketed towards independent demographic groups or if an average clinical background for all patients is sufficient for detection. This would allow for a physician to load a patient sample directly onto a substrate alongside the appropriate pre-loaded controls to make a direct comparison for diagnosis. An alternative option to pre-loading controls for point-of-care diagnostic applications would be to assimilate a vast spectral database in order to create a potential software program compatible with the handheld Raman instruments that could function

in a similar manner as the basic local alignment search tool (BLAST). In this example, the spectra obtained from scanning the patient's throat swab in the physician's office could be entered and compared algorithmically against the spectral database, in the same way the nucleotide sequence is the input compared against the BLAST sequence database in order to provide the user with a list of most probable matches. Furthermore, a step-wise algorithm could be developed into the software in which the spectra is first evaluated for the presence or absence of *M. pneumoniae*, where upon confirmation of the presence of the organism the software could proceed to determine which strain type is present, or even to subsequently inquire about additional epidemiological questions of interest one at a time. Having the algorithm ask one yes or no question at a time optimizes the use of PLS-DA-based classification, as the technique works best when the number of classes is minimized as much as possible. The ability to obtain that much information from a patient sample within the duration of an office visit would be invaluable. In either case the end goal of pre-loading controls or software and algorithm development is to simplify and minimize the input required on the physician's end to achieve the most rapid and accurate diagnosis possible.

REFERENCES

1. Daxboeck F, Krause R, Wenisch C (2003) Laboratory diagnosis of *Mycoplasma pneumoniae* infection. Clin Microbiol Infect 9: 263-273.

2. Kung CM, Wang HL (2007) Seroprevalence of *Mycoplasma pneumoniae* in healthy adolescents in Taiwan. Jpn J Infect Dis 60: 352-354.

3. Loens K, Goossens H, Ieven M (2010) Acute respiratory infection due to *Mycoplasma pneumoniae*: current status of diagnostic methods. Eur J Clin Microbiol Infect Dis 29: 1055-1069.

4. Thibodeau KP, Viera AJ (2004) Atypical pathogens and challenges in community-acquired pneumonia. Am Fam Physician 69: 1699-1706.

5. Waites KB, Balish MF, Atkinson TP (2008) New insights into the pathogenesis and detection of *Mycoplasma pneumoniae* infections. Future Microbiol 3: 635-648.

6. Chalker V, Stocki T, Litt D, Bermingham A, Watson J, et al. (2012) Increased detection of *Mycoplasma pneumoniae* infection in children in England and Wales, October 2011 to January 2012. Euro Surveill 17.

7. Zhao F, Cao B, Li J, Song S, Tao X, et al. (2011) Sequence analysis of the P1 adhesin gene of *Mycoplasma pneumoniae* in clinical isolates collected in Beijing in 2008 to 2009. J Clin Microbiol 49: 3000-3003.

8. Gerstenecker B, Jacobs E (1990) Topological mapping of the P1-adhesin of Mycoplasma pneumoniae with adherence-inhibiting monoclonal antibodies. J Gen Microbiol 136: 471-476.

9. Jacobs E, Pilatschek A, Gerstenecker B, Oberle K, Bredt W (1990) Immunodominant epitopes of the adhesin of *Mycoplasma pneumoniae*. J Clin Microbiol 28: 1194-1197.

10. Thurman KA, Walter ND, Schwartz SB, Mitchell SL, Dillon MT, et al. (2009) Comparison of laboratory diagnostic procedures for detection of *Mycoplasma pneumoniae* in community outbreaks. Clin Infect Dis 48: 1244-1249.

11. Krause DC (1998) *Mycoplasma pneumoniae* cytadherence: organization and assembly of the attachment organelle. Trends Microbiol 6: 15-18.

12. Jacobs E (2012) *Mycoplasma pneumoniae*: now in the focus of clinicians and epidemiologists. Euro Surveill 17.

13. Hennigan SL, Driskell JD, Dluhy RA, Zhao Y, Tripp RA, et al. (2010) Detection of *Mycoplasma pneumoniae* in simulated and true clinical throat swab specimens by nanorod array surface-enhanced Raman spectroscopy. PLoS One 5: e13633.

14. Winchell JM, Thurman KA, Mitchell SL, Thacker WL, Fields BS (2008) Evaluation of three real-time PCR assays for detection of *Mycoplasma pneumoniae* in an outbreak investigation. J Clin Microbiol 46: 3116-3118.

15. Dumke R, Luck PC, Noppen C, Schaefer C, von Baum H, et al. (2006) Culture-independent molecular subtyping of *Mycoplasma pneumoniae* in clinical samples. J Clin Microbiol 44: 2567-2570.

16. Kanack K, Amiott E, Nolte F, Saliminia H, Rogers B, et al. (2011) Analytical and Clnical Evaluation of the FilmArray Respiratory Panel. Idaho Technology, Inc.

17. Dumke R, Schurwanz N, Jacobs E (2008) Characterisation of subtype- and variant-specific antigen regions of the P1 adhesin of *Mycoplasma pneumoniae*. Int J Med Microbiol 298: 483-491.

18. Schwartz SB, Mitchell SL, Thurman KA, Wolff BJ, Winchell JM (2009) Identification of *P1* variants of *Mycoplasma pneumoniae* by use of high-resolution melt analysis. J Clin Microbiol 47: 4117-4120.

19. Schwartz SB, Thurman KA, Mitchell SL, Wolff BJ, Winchell JM (2009) Genotyping of *Mycoplasma pneumoniae* isolates using real-time PCR and high-resolution melt analysis. Clinical Microbiology and Infection 15: 756-762.

20. Abell JL, Driskell JD, Dluhy RA, Tripp RA, Zhao YP (2009) Fabrication and characterization of a multiwell array SERS chip with biological applications. Biosens Bioelectron 24: 3663-3670.

21. Driskell JD, Shanmukh S, Liu Y, Chaney SB, Tang XJ, et al. (2008) The use of silver nanorod arrays prepared by oblique angle deposition as surface-enhanced Raman scattering substrates. J Phys Chem C 112: 895-901.

22. Liu YJ, Zhang ZY, Zhao Q, Dluhy RA, Zhao YP (2009) Surface Enhanced Raman Scattering from an Ag Nanorod Array Substrate: The Site Dependent Enhancement and Layer Absorbance Effect. The Journal of Physical Chemistry C 113: 9664-9669.

23. Willemse-Erix DF, Scholtes-Timmerman MJ, Jachtenberg JW, van Leeuwen WB, Horst-Kreft D, et al. (2009) Optical fingerprinting in bacterial epidemiology: Raman spectroscopy as a real-time typing method. J Clin Microbiol 47: 652-659.

24. Harz M, Rösch P, Popp J (2009) Vibrational spectroscopy—A powerful tool for the rapid identification of microbial cells at the single-cell level. Cytometry Part A 75A: 104-113.

25. Otto A (2002) What is observed in single molecule SERS, and why? Journal of Raman Spectroscopy 33: 593-598.

26. Golightly RS, Doering WE, Natan MJ (2009) Surface-Enhanced Raman Spectroscopy and Homeland Security: A Perfect Match? ACS Nano 3: 2859-2869.

27. Shanmukh S, Jones L, Driskell JD, Zhao Y, Dluhy RA, et al. (2006) Rapid and Sensitive Detection of Respiratory Virus Molecular Signatures Using a Silver Nanorod Array SERS Substrate. Nano Letters 6: 2630-2636.

28. Chu H, Huang YJ, Zhao Y (2008) Silver Nanorod Arrays as a Surface-Enhanced Raman Scattering Substrate for Foodborne Pathogenic Bacteria Detection. Appl Spectrosc 62: 922-931.

29. Driskell JD, Zhu Y, Kirkwood CD, Zhao Y, Dluhy RA, et al. (2010) Rapid and sensitive detection of rotavirus molecular signatures using surface-enhanced Raman spectroscopy. PLoS One 5: e10222.

30. Granato PA, Poe L, Weiner LB (1983) New York City medium for enhanced recovery of *Mycoplasma pneumoniae* from clinical specimens. J Clin Microbiol 17: 1077-1080.

31. Page CA, Krause DC (2013) Protein kinase/phosphatase function correlates with gliding motility in *Mycoplasma pneumoniae*. J Bacteriol 195: 1750-1757.

32. Himmelreich R, Hilbert H, Plagens H, Pirkl E, Li BC, et al. (1996) Complete sequence analysis of the genome of the bacterium *Mycoplasma pneumoniae*. Nucleic Acids Res 24: 4420-4449.

33. Waites KB, Talkington DF (2004) *Mycoplasma pneumoniae* and its role as a human pathogen. Clinical Microbiology Reviews 17: 697-+.

34. Inamine JM, Ho KC, Loechel S, Hu PC (1990) Evidence that UGA is read as a tryptophan codon rather than as a stop codon by *Mycoplasma pneumoniae*, *Mycoplasma genitalium,* and *Mycoplasma gallisepticum*. J Bacteriol 172: 504-506.

35. Dandekar T, Snel B, Schmidt S, Lathe W, Suyama M, et al. (2002) Comparative genome analysis of the mollicutes. In: Razin S, Hermann R, editors. Molecular biology and pathogenesis of mycoplasmas. New York, N.Y.: Kluwer Academic/Plenum Publishers.

36. Pollack JD, Myers MA, Dandekar T, Hermann R (2002) Suspected utility of enzymes with multiple activities in the small genome Mycoplasma species: the replacement of the missing "household" nucleoside diphosphate kinase genes and activity by glycolytic kinases. OMICS 6: 247-258.

37. Simmons WL, Daubenspeck JM, Osborne JD, Balish MF, Waites KB, et al. (2013) Type 1 and type 2 strains of *Mycoplasma pneumoniae* form different biofilms. Microbiology 159: 737-747.

38. Großhennig S, Schmidl SR, Schmeisky G, Busse J, Stülke J (2013) Implication of glycerol and phospholipid transporters in *Mycoplasma pneumoniae* growth and virulence. Infect Immun 81: 896-904.

39. Halbedel S, Hames C, Stülke J (2007) Regulation of carbon metabolism in the mollicutes and its relation to virulence. J Mol Microbiol Biotechnol 12: 147-154.

40. Halbedel S, Hames C, Stülke J (2004) In vivo activity of enzymatic and regulatory components of the phosphoenolpyruvate:sugar phosphotransferase system in *Mycoplasma pneumoniae*. J Bacteriol 186: 7936-7943.

41. Hames C, Halbedel S, Hoppert M, Frey J, Stülke J (2009) Glycerol metabolism is important for cytotoxicity of *Mycoplasma pneumoniae.* J Bacteriol 191: 747-753.

42. Balish MF, Krause DC (2002) Cytadherence and the cytoskeleton. In: Razin S, Herrmann R, editors. Molecular Biology and Pathogenecity of the Mycoplasmas. New York: Kluwer Academic/Plenum Publishers. pp. 491-518.

43. Krause DC, Balish MF (2001) Structure, function, and assembly of the termina organelle of *Mycoplasma pneumoniae*. FEMS Microbiol Lett 198: 1-7.

44. Meng KE, Pfister RM (1980) Intracellular structures of *Mycoplasma pneumoniae* revealed after membrane removal. J Bacteriol 144: 390-399.

45. Gobel U, Speth V, Bredt W (1981) Filamentous structures in adherent *Mycoplasma pneumoniae* cells treated with nonionic detergents. J Cell Biol 91: 537-543.

46. Henderson GP, Jensen GJ (2006) Three-dimensional structure of *Mycoplasma pneumoniae's* attachment organelle and a model for its role in gliding motility. Mol Microbiol 60: 376-385.

47. Seybert A, Hermann R, Frangakis AS (2006) Structural analysis of *Mycoplasma pneumoniae* by cryoelectron tomography. J Struct Biol 156: 342-354.

48. Talkington DF, Waites KB, Schwartz SB, Besser RE (2001) Emerging from obscurity: understanding pulmonary and extrapulmonary syndromes, pathogenesis, and epidemiology of human *Mycoplasma pneumoniea* infections. In: Hughes JM, editor. Emerging Infections 5. Washington, D.C.: American Society or Microbiology.

49. Rottem S (2003) Interaction of mycoplasmas with host cells. Physiol Rev 83: 417-432.

50. Kasai T, Nakane D, Ishida H, Ando H, Kiso M, et al. (2013) Role of binding in *Mycoplasma mobile* and *Mycoplasma pneumoniae* gliding analyzed through inhibition of synthesized sialylated compounds. J Bacteriol 195: 429-435.

51. Baseman JB, Cole RM, Krause DC, Leith DK (1982) Molecular basis for cytadsorption of *Mycoplasma pneumoniae*. J Bacteriol 151: 1514-1522.

52. Baseman JB, Reddy SP, Dallo SF (1996) Interplay between mycoplasma surface proteins, airway Cells, and the protean manifestations of mycoplasma-mediated human infections. American Journal of Respiratory and Critical Care Medicine 154: S137-S144.

53. Bose SR, Balish MF, Krause DC (2009) *Mycoplasma pneumoniae* cytoskeletal protein HMW2 and the architecture of the terminal organelle. J Bacteriol 191: 6741-6748.

54. Hasselbring BM, Krause DC (2007) Proteins P24 and P41 function in the regulation of terminal-organelle development and gliding motility in *Mycoplasma pneumoniae*. J Bacteriol 189: 7442-7449.

55. Hasselbring BM, Sheppard ES, Krause DC (2012) P65 Truncation impacts P30 dynamics during *Mycoplasma pneumoniae* gliding. J Bacteriol 194: 3000-3007.

56. Nakane D, Adan-Kubo J, Kenri T, Miyata M (2011) Isolation and characterization of P1 adhesin, a leg protein of the gliding bacterium *Mycoplasma pneumoniae*. J Bacteriol 193: 715-722.

57. Hergermann J, Herrmann R, Mayer F (2002) Cytoskeletal elements in the bacterium *Mycoplasma pneumoniae*. Naturwissenschaften 89: 453-458.

58. Krause DC, Balish MF (2004) Cellular engineering in a minimal microbe: structure and assembly of the terminal organelle of *Mycoplasma pneumoniae*. Molecular Microbiology 51: 917-924.

59. Stevens MK, Krause DC (1992) *Mycoplasma pneumoniae* cytadherence phase-variable protein HMW3 is a component of the attachment organelle. J Bacteriol 174: 4265-4274.

60. Stevens MK, Krause DC (1991) Localization of the *Mycoplasma pneumoniae* cytadherence-accessory proteins HMW1 and HMW4 in the cytoskeltonlike triton shell. J Bacteriol 173: 1041-1050.

61. Waldo RH, 3rd, Krause DC (2006) Synthesis, stability, and function of cytadhesin P1 and accessory protein B/C complex of *Mycoplasma pneumoniae*. J Bacteriol 188: 569-575.

62. Dallo SF, Lazzell AL, Chavoya A, Reddy SP, Baseman JB (1996) Bifunctional domains of the *Mycoplasma pneumoniae* P30 adhesin. Infect Immun 64: 2595-2601.

63. Su CJ, Tyron VV, Baseman JB (1987) Cloning and sequence analysis of cytadhesin P1 gene from *Mycoplasma pneumoniae*. Infect Immun 55: 3023-3029.

64. Dallo SF, Su CJ, Horton JR, Baseman JB (1988) Identification of P1 gene domain containing epitope(s) mediating *Mycoplasma pneumoniae* cytadherence. The Journal of Experimental Medicine 167: 718-723.

65. Krause DC, Baseman JB (1983) Inhibition of *Mycoplasma pneumoniae* hemadsorption and adherence to respiratory epithelium by antibodies to a membrane protein. Infect Immun 39: 1180-1186.

66. Seto S, Layh-Schmit G, Kenri T, Miyata M (2001) Visualization of the attachment organelle and cytadherence proteins of *Mycoplasma pneumoniae* by immunofluorescence microscopy. J Bacteriol 183.

67. Seto S, Miyata M (2003) The attachment organelle formation represented by localization of cytadherence protein and formation of electron dense core in the wild-type and mutant strans of *Mycoplasma pneumoniae*. J Bacteriol 185: 1082-1091.

68. Inamine JM, Loechel S, Hu PC (1988) Analysis of the nucleotide sequence of the P1 operon of *Mycoplasma pneumoniae*. Gene 73: 175-183.

69. Layh-Schmit G, Potdtelejnikov A, Mann M (2000) Proteins complexed to the P1 adhesin of *Mycoplasma pneumoniae*. Microbiology 146: 741-747.

70. Dallo SF, Chavoya A, Baseman JB (1990) Characterization of the gene for a 30-kilodalton adhesin-related protein of *Mycoplasma pneumoniae*. Infect Immun 58: 4163-4165.

71. Chang H-Y, Jordan JL, Krause DC (2011) Domain analysis of protein P30 in *Mycoplasma pneumoniae* cytadherence and gliding motility. J Bacteriol 193: 1726-1733.

72. Romero-Arroyo CE, Jordan J, Peacock SJ, Willby MJ, Farmer MA, et al. (1999) *Mycoplasma pneumoniae* protein P30 is required for cytadherence and associated with proper cell development. J Bacteriol 181: 1079-1087.

73. Hasselbring BM, Jordan JL, Krause RW, Krause DC (2006) Terminal organelle development in the cell wall-less bacterium *Mycoplasma pneumoniae*. Proceedings of the National Academy of Sciences 103: 16478-16483.

74. Baseman JB, Morrison-Plummer J, Drouillard D, Puleo-Scheppke B, Tryon VV, et al. (1987) Identification of a 32-kilodalton protein of *Mycoplasma pneumoniae* associated with hemadsorption. J Med Sci 23: 474-479.

75. Morrison-Plummer J, Leith DK, Baseman JB (1986) Biological effects of anti-lipid and anti-protein monoclonal antibodies of *Mycoplasma pneumoniae*. Infect Immun 53: 398-403.

76. Krause DC, Proft T, Hedreyda CT, Hilbert H, Plagens H, et al. (1997) Transposon mutagenesis reinforces the correlation between *Mycoplasma pneumoniae* cytoskeletal protein HMW2 and cytadherence. J Bacteriol 179: 2668-2677.

77. Proft T, Hilbert H, Layh-Schmit G, Herrmann R (1995) The proline-rich P65 protein of *Mycoplasma pneumoniae* is a component of the Triton X-100 insoluble fraction and exhibits size polymorphism in the strins M129 and FH. J Bacteriol 177: 3370-3378.

78. Jordan JL, Berry KM, Balish MF, Krause DC (2001) Stability and sub-cellular localization of cytadherence-associated protein P65 in *Mycoplasma pneumoniae*. J Bacteriol 183: 7387-7391.

79. Willby MJ, Krause DC (2002) Characterization of a *Mycoplasma pneumoniae hmw3* mutant: implications for attachment organelle assembly. J Bacteriol 184: 3061-3068.

80. Balish MF, Hahn TW, Popham PL, Krause DC (2001) Stability of *Mycoplasma pneumoniae* cytadherence-accessory protein HMW1 correlates with its association with the triton shell. J Bacteriol 183: 3680-3688.

81. Balish MF, Santurri RA, Ricci AM, Lee KK, Krause DC (2003) Localization of *Mycoplasma pneumoniae* cytadherence-associated protein HMW2 by fusion with green fluorescent protein: implications for attachment and organlle structure. Mol Microbiol 47: 49-60.

82. Hahn TW, Wilby MJ, Krause DC (1998) HMW1 is required for cytadhesin P1 trafficking to the attachment organelle in *Mycoplasma pneumoniae*. J Bacteriol 180: 1270-1276.

83. Dirksen LB, Proft T, Hilbert H, Plagens H, Herrmann R, et al. (1996) Sequence analysis and characterization of the *hmw* gene cluster of *Mycoplasma pneumoniae*. Gene 171: 19-25.

84. Popham PL, Hahn TW, Krebes KA, Krause DC (1997) Loss of HMW1 and HMW2 in non-cytadhering mutants of *Mycoplasma pneumoniae* occurs posttranslationally. Proc Natl Acad Sci U S A 94: 13979-13984.

85. Ogle KF, Lee KK, Krause DC (1992) Nucleotide sequence analysis reveals novel features of the phase-variable cytadherence accessory protein HMW3 of *Mycoplasma pneumoniae*. Infect Immun 60: 1633-1641.

86. Krause DC (1996) *Mycoplasma pneumoniae* cytadherence: unraveling the tie that binds. Mol Microbiol 20: 247-253.

87. Hasselbring BM, Krause DC (2007) Cytoskeletal protein P41 is required to anchor the terminal organelle of the wall-less prokaryote *Mycoplasma pneumoniae*. Mol Microbiol 63: 44-53.

88. Kenri T, Seto S, Horino A, Sasaki Y, Sasaki T, et al. (2004) Use of fluorescent-protein tagging to determine the subcellular localization of *Mycoplasma pneumoniae* proteins encoded by the cytadherence regulatory locus. J Bacteriol 186: 6944-6955.

89. Bredt W (1968) Motility and multiplication of *Mycoplasma pneumoniae*. A phase contrast study. Pathol Microbiol 32: 321-326.

90. Kirchhoff H (1992) Motility. In *Mycoplasmas: Molecular Biology and Pathogenesis*; Maniloff JR, McElhaney RN, Finch LR, Baseman JB, editors. Washington, D. C.: ASM Press.

91. Miyata M (2007) Molecular mechanism of mycoplasma gliding - a novel cell motility system. In *Cell Motility*; Lenz P, editor. New York, New York: Springer.

92. Miyata M (2008) Centipede and inchworm models to explain *Mycoplasma* gliding. Trends Microbiol 16: 6-12.

93. Krivan HC, Olson LD, Barile MF, Ginsburg V, Roberts DD (1989) Adhesion of *Mycopalsma pneumoniae* to sulfated glycolipids and inhibition by dextran sulfate. J Biol Chem 264: 9283-9288.

94. Kurai D, Nakagaki K, Wada H, Saraya T, Kamiya S, et al. (2013) *Mycoplasma pneumoniae* extract induces an IL-17-associated inflammatory reaction in murine lung: implication for Mycoplasmal pneumonia. Inflammation 36: 285-293.

95. Loomes LM, Uemura K, Childs RA, Paulson JC, Rogers GN, et al. (1984) Erythrocyte receptors for *Mycoplasma pneumoniae* are sialylated oligosaccharides of Ii antigen type. Nature 307: 560-563.

96. Krause DC, Leith DK, Wilson RM, Baseman JB (1982) Identification of *Mycoplasma pneumoniae* proteins associated with hemadsorption and virulence. Infect Immun 35: 809-817.

97. Garcia-Sastre A (2010) Influenza virus receptor specificity: disease and transmission. Am J Pathol 176: 1584-1585.

98. Loveless RW, Griffiths S, Fryer PR, Blauth C, Feizi T (1992) Immunoelectron microscopic studies reveal differenecs in distribution of sialo-oligosaccharide receptors for *Mycoplasma pneumoniae* on the epithelium of human and hamster bronchi. Infect Immun 60: 4015-4023.

99. Halbedel S, Busse J, Schmidl ER, Stulke J (2006) Regulatory protein phosphorylation in *Mycoplasma pneumoniae.* A PP2C-type phosphatase serves to dephosphorylate HPr(Ser-P). J Biol Chem 281: 26253-26259.

100. Absalon C, Obuchowski M, Madec E, Delattre D, Holland IB, et al. (2009) CpgA, EF-Tu and the stressosome protein YezB are substrates of the Ser/Thr kinase/phosphatase couple, PrkC/PrpC, in *Bacillus subtillus*. Microbiology 155: 932-943.

101. Pereira SFF, Goss L, Dworkin J (2011) Eukaryote-like serine/threonine kinases and phosphatases in bacteria. Microbiol Mol Biol Rev 75: 195-212.

102. Shah IM, Laaberki MH, Popham DL, Dworkin J (2008) A eukaryotic-like Ser/Thr kinase signals bacteria to exit dormancy in response to peptidoglycan fragments. Cell 135: 486-496.

103. Schmidl SR, Gronau K, Hames C, Busse J, Becher D, et al. (2010) The stability of cytadherence proteins in *Mycoplasma pneumoniae* requires activity of the protein kinase PrkC. Infect Immun 78: 184-192.

104. Dirksen LB, Krebes KA, Krause DC (1994) Phosphorylation of cytadherence-accessory proteins in *Mycoplasma pneumoniae*. J Bacteriol 176: 7499-7505.

105. Krebes KA, Dirksen LB, Krause DC (1995) Phosphorylation of *Mycoplasma pneumoniae* cytadherence-accessory proteins in cell extracts. J Bacteriol 177: 4571-4574.

106. Eaton MD, Meikejohn G, Van Herick W (1944) Studies on the etiology of primary atypical pneumonia: a filterable agent transmissible to cotton rats, hamsters, and chick embryos. J Exp Med 79: 649-667.

107. Chanock RM, Hayflick L, Barile MF (1962) Growth on artificial medium of an agent associated with atypical pneumonia and its identification as a PPLO. Proc Natl Acad Sci U S A 48: 41-49.

108. Chanock RM, Rifkind DM, Kravetz HM, Knight V, Johnson KM (1961) Respiratory disease in volunteers infected with Eaton agent: a preliminary report. Proc Natl Acad Sci U S A 47: 887-890.

109. Razin S, Yogev D, Naot Y (1998) Molecular biology and pathogenicity of mycoplasmas. Microbiol Mol Biol Rev 62: 1094-1156.

110. Talkington DF, Waites KB, Schwartz SB, Besser RE (2001) Emerging from obscurity: understanding pulmonary and extrapulmonary syndromes, pathogenesis, and epidemiology of human *Mycoplasma pneumoniae* infections, In *Emerging Infections 5*; Scheld WM, Craig WA, Hughes JM, editors. Washington, D. C.: American Society for Microbiology.

111. Baseman JB, Tully JG (1997) Mycoplasmas: sophisticated, re-emerging, and burdened by their notoriety. Emerging Infect Dis 3: 21-32.

112. Dallo SF, Baseman JB (2000) Intracellular DNA replication and long-term survival of pathogenic mycoplasmas. Microbiol Pathog 29: 301-309.

113. Rottem S (2002) Invasion of mycoplasmas into and fusion with host cells. In *Molecular biology and pathogenicity of mycoplasmas*. ; Razin S, Herrmann R, editors. New York, NY: Kluwer Academic/Plenum Publishers.

114. Dallo SF, Kannan TR, Blaylock MW, Baseman JB (2002) Elongation factor Tu and E1beta subunit of pyruvate dehydrogenase complex act as fibronectin binding proteins in *Mycoplasma pneumoniae*. Mol Microbiol 46: 1041-1051.

115. Krause DC, Leith DK, Baseman JB (1983) Reacquisition of specific proteins confers virulence in *Mycoplasma pneumoniae*. Infect Immun 39: 830-836.

116. Jacobs E, Bartl A, Oberle K, Schiltz E (1995) Molecular mimicry by *Mycoplasma pneumoniae* to evade the induction of adherence inhibiting antibodies. Journal of Medical Microbiology 43: 422-429.

117. Jacobs E, Stuhlert A, Drews M, Pumpe K, Schaefer HE, et al. (1988) Host reactions to *Mycoplasma pneumoniae* infections in guinea-pigs preimmunized systemically with the adhesion of this pathogen. Microb Pathog 5: 259-265.

118. Lind K, Hoier-Madsen M, Wiik A, Clyde WA (1992) Antibodies to the mitotic spindle apparatus in patients with *Mycoplasma pneumoniae* infection. Immunol Infect Dis 2: 249-255.

119. Barile MF (1979) Mycoplasma-tissue cell interactions. In, *Molecular biology and pathogenicity of mycoplasmas*; Razin S, Herrmann R, editors. New York, NY: Academic Press.

120. Mizutani H (1983) Immunologic responses in patients with *Mycoplasma pneumoniae* infections. Am Rev Respir Dis 127: 175-179.

121. Jacobs E, Drews M, Stuhlert A, Buttner C, Klein PJ, et al. (1988) Immunological reaction of guinea-pigs following intranasal infection among hospital personnel studied by a nucleic acid hybridization test. J Hosp Infect 21: 213-221.

122. Hardy RD, Jafri HS, Olsen K, Hatfield J, Iglehart J, et al. (2002) *Mycoplasma pneumoniae* induces chronic respiratory infection, airway hyperreactivity, and pulmonary inflammation: a murine model of infection-associated chronic reactive airway disease. Infect Immun 70: 649-654.

123. Hardy RD, Jafri HS, Olsen K, Wordemann M, Hatfield J, et al. (2001) Elevated cytokine and chemokine levels and prolonged pulmonary airflow resistance in a murine *Mycoplasma pneumoniae* pneumonia model: a microbiologic, histologic, immunologic, and respiratory plethysmographic profile. Infect Immun 69: 3869-3876.

124. Almagor M, Kahane I, Yatziv S (1984) Role of superoxide anion in host cell injury induced by *Mycoplasma pneumoniae* infection: A study in normal and trisomy 21 cells. J Clin Invest 73: 842-847.

125. Tryon VV, Baseman JB (1987) The acquisition of human lactoferrin by *Mycoplasma pneumoniae*. Microb Pathog 3: 437-443.

126. Somerson NL, Walls BE, Chanock RM (1965) Hemolysin of *Mycoplasma pneumoniae*: tentative identification as a peroxide. Science 150: 226-228.

127. Tryon VV, Razin S (1996) Pathogenic determinants and mechanisms. In *Molecular diagnostic procedures in mycoplasmology, vol. 2. Diagnostic procedures*; Maniloff J, editor. New York, NY: Academic Press.

128. Medina JL, Coalson JJ, Brooks EG, Winter VT, Chaparro A, et al. (2012) *Mycoplasma pneumoniae* CARDS Toxin Induces Pulmonary Eosinophilic and Lymphocytic Inflammation. American Journal of Respiratory Cell and Molecular Biology.

129. Kannan TR, Provenzano D, Wright JR, Baseman JB (2005) Identification and characterization of human surfactant protein A-binding protein of *Mycoplasma pneumoniae*. Infect Immun 73: 2828-2834.

130. Hames C, Halbedel S, Hoppert M, Frey J, Stulke J (2009) Glycerol metabolism is important for the cytotoxicity of *Mycoplasma pneumoniae*. J Bacteriol 191: 747-753.

131. Schmidl SR, Otto A, Lluch-Senar M, Pinol J, Busse J, et al. (2011) A trigger enzyme in *Mycoplasma pneumoniae*: Impact of the glycerophosphodiesterase GlpQ on virulence and gene expression. PLOS Pathogens 7.

132. Clyde WA (1979) *Mycoplasma pneumoniae* infections of man. In *The mycoplasmas, II. Human and animal mycoplasmas, vol II.*; Tully JG, Whitcomb RF, editors. New York, NY: Academic Press.

133. Collier AM (1983) Organ culture techniques with mycoplasmas. Ann N Y Acad Sci 225: 277-289.

134. Waites KB, Simecka JW, Talkington DF, Atkinson TP (2007) Pathogenesis of *Mycoplasma pneumoniae* infections: adaptive immunity, innate immunity, cell biology and virulence factors. In: *Community acquired pneumonia*; Suttorp N, Welte T, Marre R, editors. Basel, Switzerland: Burkhauser Verlag.

135. Maniloff JR, McElhaney RN, Finch LR, Baseman JB (1992) Mycoplasmas: molecular biology and pathogenesis. Washington, D.C.: American Society of Microbiology.

136. Chan ED, Welsh CH (1995) Fulminant *Mycoplasma pneumoniae* pneumonia. West J Med 162: 133-142.

137. Opitz O, Pietsch K, Ehlers S, Jacobs E (1996) Cytokine gene expression in immune mice reinfected with *Mycoplasma pneumoniae*: the role of T cell subsets in aggravating the inflammatory response. Immunobiology 196: 575-587.

138. Hoek KL, Cassel GH, Duffy LB, Atkinson TP (2002) *Mycoplasma pneumoniae*-induced activation and cytokine production in rodent mast cells. J Allergy Clin Immunol 109: 470-476.

139. Hsieh CC, Tang RB, Tsai CH, Chen W (2001) Serum interleukin-6 and tumor necrosis factor-alpha concentrations in children with *Mycoplasma pneumoniae*. J Microbiol Immunol Infect 34: 109-112.

140. Lieberman DS, Livnat S, Schlaeffer A, Porath A, Horowitz S, et al. (1997) IL-1 beta and IL-6 in community-acquired pneumonia: bacteremic pneumococcal pneumonia versus *Mycoplasma pneumoniae* pneumonia. Infection 25: 90-94.

141. Narita M, Tanaka H, Abe S, Yamada S, Kubota M, et al. (2000) Close association between pulmonary disease manifestation in *Mycoplasma pneumoniae* infection and enhanced local production of interleukin-18 in the lung, independent of gamma interferon. Clin Diagn Lab Immunol 7: 909-914.

142. Narita M, Tanaka H, Yamada S, Abe S, Ariga T, et al. (2001) Significant role of interleukin-8 in pathogenesis of pulmonary disease due to *Mycoplasma pneumoniae* infection. Clin Diagn Lab Immunol 8: 1028-1030.

143. Tanaka H, Narita M, Teramoto S, Saikai T, Oashi K, et al. (2002) Role of interleukin-18 and T-helper type 1 cytokines in the development of *Mycoplasma pneumoniae* pneumonia in adults. Chest 121: 1493-1497.

144. Yang JW, Hooper WC, Phillips DJ, Talkington DF (2003) Interleukin-1beta responses to *Mycoplasma pneumoniae* infection are cell-type specific. Microb Pathog 34.

145. Yang JW, Hooper WC, Phillips DJ, Talkington DF (2002) Regulation of proinflammatory cytokines in human lung epithelial cells infected with *Mycoplasma pneumoniae*. Infect Immun 70: 3649-3655.

146. Hong SJ (2012) The Role of *Mycoplasma pneumoniae* Infection in Asthma. Allergy Asthma Immunol Res 4: 59-61.

147. Smith GN, Weir WRC (1980) Cold agglutinins accompanying *Mycoplasma pneumoniae* infection. Br Med J 281: 1391-1392.

148. Yang W, Hooper WC, Phillips DJ, Talkington DF (2002) Regulation of proinflammatory cytokines in human lung epithelial cells infected with *Mycoplasma pneumoniae*. Infect Immun 70: 3649-3655.

149. Cimolai N, Wensley D, Seear M, Thomas ET (1995) *Mycoplasma pneumoniae* as a cofactor in severe respiratory infections. Clin Infect Dis 21: 1182-1185.

150. Ito S, Abe Y, Kinomoto K, Saitoh T, Kato T, et al. (1995) Fulminant *Mycoplasma pneumoniae* pneumonia with marked elevation of serum soluble interleukin-2 receptor. Intern Med 34: 430-435.

151. Narita M (2000) Detection of *Mycoplasma pneumoniae* DNA in cerebrospinal fluid and local immune response. Clin Infect Dis 30: 405-406.

152. Radisic MA, Torn P, Gutierrez P, Defranchi HA, Pardo P (2000) Severe acute lung injury caused by *Mycoplasma pneumoniae*: potential role for steroid pulses in treatment. Clin Infect Dis 31: 1507-1511.

153. Tanaka G, Nagatomo Y, Kai Y, Matsuyama M, Kuroki M, et al. (2002) *Mycoplasma pneumoniae* of identical twin sisters with different clinical courses depending on the treatment. Kansenshogaku Zasshi 76: 1040-1044.

154. Tanaka H, Koba H, Honma S, Sugaya F, Abe S (1996) Relationships between radiological pattern and cell-mediated immune response in *Mycoplasma pneumoniae* pneumonia. Eur Respir J 9: 669-672.

155. Berkovich S, Millian SJ, Snyder RD (1970) The association of viral and mycoplasma infections with recurrence of wheezing in the asthmatic child. Ann Allergy 28: 43-49.

156. Huhti E, Mokka T, Nikoskelainen J, Halonen P (1974) Association of viral and mycoplasma infections with exacerbations of asthma. Ann Allergy: 145-149.

157. Biscardi S, Lorrot M, Marc E, Moulin F, Boutonnat-Faucher B, et al. (2004) *Mycoplasma pneumoniae* and asthma in children. Clin Infect Dis 38: 1341-1346.

158. Kraft M, Cassel GH, Henson JE, Watson H, Williamson J, et al. (1998) Detection of *Mycoplasma pneumoniae* in the airways of adults with chronic asthma. Am J Respir Crit Care Med 158: 998-1001.

159. Martin RJ, Kraft M, Chu HW, Berns EA, Cassel GH (2001) A link between chronic asthma and chronic infection. J Allergy Clin Immunol 107: 595-601.

160. Esposito S, Blasi F, Arosio C, Floravanti L, Fagetti L, et al. (2000) Importance of acute *Mycoplasma pneumoniae* and *Chlamydia pneumoniae* infections in children with wheezing. Eur Respir J 16: 1142-1146.

161. Kraft M, Cassel GH, Pak J, Martin RJ (2002) *Mycoplasma pneumoniae* and *Chlamydia pneumoniae* in asthma: effect of clarithromycin. Chest 121: 1782-1788.

162. Koh YY, Park Y, Lee HJ, Kim CK (2001) Levels of interleukin-2, interferon gamma, and interleukin-4 in bronchoalveolar lavage fluid from patients with *Mycoplasma pneumoniae*: implication of tendency toward increased immunoglobulin E production. Pediatrics 107.

163. Jeong YC, Yeo MS, Kim JH, Lee HB, Oh JW (2012) *Mycoplasma pneumoniae* infection affects the serum levels of vascular endothelial growth factor and interleukin-5 in atopic children. Allergy Asthma Immunol Res 4: 92-97.

164. Wark PA, Johnston SL, Moric I, Simpson JL, Hensley MJ, et al. (2002) Neutrophil degranulation and cell lysis is associated with clinical severity in virus-induced asthma. Eur Respir J 19: 68-75.

165. Barr Meir E, Amital H, Levy Y, Kneller A, Bar-Dayan Y, et al. (2000) *Mycoplasma pneumoniae*-induced thrombotic thrombocytopenic pupura. Acta Haematol 103: 112-115.

166. Kasahara I, Otsubo Y, Yanase T, Oshima H, Ichimaru H, et al. (1985) Isolation and characterization of *Mycoplasma pneumoniae* from cerebrospinal fluid of a patient with pneumonia and meningoencephalitis. J Infect Dis 152: 823-825.

167. Koletsky RJ, Weinstein AJ (1980) Fulminant *Mycoplasma pneumoniae* infection. Report of a fatal case, and a review of the literature. Am Rev Respir Dis 122: 491-496.

168. Narita M, Matsuzono Y, Itakura O, Togashi T, Kikuta H (1996) Survey of mycoplasmal bacteremia detected in children by polymerase chain reaction. Clin Infect Dis 23: 522-525.

169. Said MH, Layani MP, Colon S, Faraj G, Glastre C, et al. (1999) *Mycoplasma pneumoniae*-associated nephritis in children. Pediatr Nephrol 13: 39-44.

170. Smith R, Eviatar L (2000) Neurologic manifestations of *Mycoplasma pneumoniae* infections: diverse spectrum of diseases. A report of six cases and review of the literature. Clin Pediatr 39: 195-201.

171. Campbell TA, Strong PS, Grier GS (1943) Primary atypical pneumonia: two hundred cases at Ft. Eustin, Virginia. JAMA 122: 723-729.

172. Behan PO, Feldman RG, Segerra JM, Draper IT (1986) Neurological aspects of mycoplasmal infection. Acta Neurol Scand 74: 314-322.

173. Decaux GM, Szyper M, Ectors M, Cornhil A, Franken L (1980) Central nervous system complications of *Mycoplasma pneumoniae*. J Neurol Neurosurg Psychiatry 43: 883-887.

174. Gillberg C (1980) Schizophreniform psychosis in a case of *Mycoplasma pneumoniae* encephalitis. J Autism Dev Disord 10: 153-158.

175. Kikuchi M, Tagawa Y, Iwamoto H, Hoshino H, Yuki N (1997) Bickerstaff's brainstem encephalitis associated with IgG anti-GQ1b antibody subsequent to *Mycoplasma pneumoniae* infection: favorable response to immunoadsorption therapy. J Child Neurol 12: 403-405.

176. Lin WC, Lee PI, Lu CY, Hsieh YC, Lai HP, et al. (2002) *Mycoplasma pneumoniae* encephalitis in childhood. J Microbiol Immunol Infect 35: 173-178.

177. Ponka A (1978) Clinical and laboratory manifestations in patients with serological evidence of *Mycoplasma pneumoniae* infection. Scand J Infect Dis 10: 271-275.

178. Squadrini F, Lami G, Pellegrino F, Pinelli G, Bavieri M, et al. (1988) Acute hepatitis complicating *Mycoplasma pneumoniae* infection. J Infect 16: 201-202.

179. Stevens D, Swift PG, Johnston PG, Kearney PJ, Corner BD, et al. (1978) *Mycoplasma pneumoniae* infections in children. Arch Dis Child 53: 38-42.

180. Ponka A (1979) The occurrence and clinical picture of serologically verified *Mycoplasma pneumoniae* infections with emphasis on central nervous system, cardiac, and joint manifestations. Ann Clin Res 11: 1-60.

181. Thomas NH, Collins JE, Robb SA, Robinson RO (1993) *Mycoplasma pneumoniae* infection and neurological disease. Arch Dis Child 69: 573-576.

182. Feder RS, McCully RB, Oh JK, Smith TF (1981) Severe meningoencephalitis: complicating *Mycoplasma pneumoniae* infection in a child. Arch Pathol Lab Med 105: 619-621.

183. Fisher RS, Clark AW, Wolinsky JS, Parhad M, Moses H, et al. (1983) Postinfectious leukoencephalitis complicating *Mycoplasma pneumoniae* infection. Arch Neurol 40: 109-113.

184. Kleemola M, Kayhty H (1982) Increase in titers of antibodies to *Mycoplasma pneumoniae* in patients with purulent meningitis. J Infect Dis 146: 284-288.

185. Abramovitz PP, Schvartzman P, Harel D, Lis I, Naot Y (1987) Direct invasion of the central nervous system by *Mycoplasma pneumoniae*: a report of two cases. J Infect Dis 155: 482-487.

186. Dionisio D, Valassina M, Mata S, Rossetti R, Vivarelli A, et al. (1999) Encephalitis caused directly by *Mycoplasma pneumoniae*. Scand J Infect Dis 31: 506-509.

187. Ieven M, Demey H, Ursi D, Van Goethem G, Cras P, et al. (1998) Fatal encephalitis caused by *Mycoplasma pneumoniae* diagnosed by the polymerase chain reaction. Clin Infect Dis 27: 1552-1553.

188. Launes J, Paetau A, Linnavuori K, Iivanaineu M (1997) Direct invasion of the brain parenchyma by *Mycoplasma pneumoniae*. Acta Neurol Scand 95: 374.

189. Narita M, Matsuzono Y, Togashi T, Kajii N (1992) DNA diagnosis of central nervous system infection by *Mycoplasma pneumoniae*. Pediatrics 90: 250-253.

190. Dorigo-Zetsma JW, Wilbrink B, van der Nat H, Bartelds AI, Heijnen ML, et al. (2001) Results of molecular detection of *Mycoplasma pneumoniae* among patients with acute respiratory infection and in their household contacts reveals children as human reservoirs. J Infect Dis 183: 675-678.

191. Ferwerda A, Moll HA, de Groot R (2001) Respiratory tract infections by *Mycoplasma pneumoniae* in children: a review of diagnostic and therapeutic measures. Eur J Pediatr 163: 483-491.

192. Foy HM, Grayston JT, Kenny GE, Alexander ER, McMahan R (1966) Epidemiology of *Mycoplasma pneumoniae* infection in families. JAMA 197: 859-866.

193. Block S, Hedrick J, Hammerschlag MR, Cassel GH, Craft JC (1995) *Mycoplasma pneumoniae* and *Chlamydia pneumoniae* in pediatric community-acquired pneumonia: comparative efficacy and safety of clarithromycin vs. erythromycin ethylsuccinate. Pediatr Infect Dis J 14: 471-477.

194. Foy HM (1993) Infections caused by *Mycoplasma pneumoniae* and possible carrier state in different populations of patients. Clin Infect Dis 17: S37-S46.

195. Ieven M, Ursi D, Van Bever H, Quint W, Niesters HG, et al. (1996) Detection of *Mycoplasma pneumoniae* by two polymerase chain reactions and role of *M. pneumoniae* in acute respiratory tract infections in pediatric patients. J Infect Dis 173: 1445-1452.

196. Feizi T, Maclean H, Sommerville RG, Selwyn JG (1967) Studies on an epidemic of respiratory disease caused by *Mycoplasma pneumoniae*.

197. Luby JP (1991) Pneumonia caused by *Mycoplasma pneumoniae* infection. Clin Chest Med 12: 237-244.

198. Cassel GH, Clyde WA, Davis JK (1985) Mycoplasma respiratory infections. *In: The mycopalsmas, vol 4*; Razin S, Barile MF, editors. New York, NY: Academic Press.

199. Marston BJ, Plouffe JF, File TM, Hackman BA, Salstrom SJ, et al. (1997) Incidence of community-acquired pneumonia requiring hospitalization. Results of a population-based active surveillance study in Ohio. Arch Intern Med 157: 1709-1718.

200. Foy HM, Kenny GE, Cooney MK, Allan ID, van Belle G (1983) Naturally acquired immunity to pneumonia due to *Mycoplasma pneumoniae*. J Infect Dis 147: 967-973.

201. Zhao F, Lv M, Tao X, Huang H, Zhang B, et al. (2012) Antibiotic sensitivity of 40 Mycoplasma pneumoniae isolates and molecular analysis of macrolide rsistant isolates from Beijing, China. Antimicrob Agents Chemother 56: 1108-1109.

202. Pereyre S, Charron A, Renaudin H, Bebear C, Bebear CM (2007) First report of macrolide-resistant strains and description of a novel nucleotide sequence variation in the P1 adhesin gene in Mycoplasma pneumoniae clinical strains isolated in France over 12 years. J Clin Microbiol 45: 3534-3539.

203. Dumke R, von Baum H, Luck PC, Jacobs E (2010) Occurrence of macrolide-resistant *Mycoplasma pneumoniae* strains in Germany. Clin Microbiol Infect 16: 613-616.

204. Cardinale F, Chironna M, Dumke R, Binetti A, Daleno C, et al. (2011) Macrolide resistant *Mycoplasma pneumoniae* in paediatric pneumonia. Eur Respir J 37: 1522-1524.

205. Averbuch D, Hidalgo-Grass C, Moses AE, Engelhard D, Nir-Paz R (2011) Macrolide resistance in *Mycoplasma pneumoniae*, Israel. Emerg Infect Dis 17: 1079-1082.

206. Bebear C, Pereyre S, Peuchant O (2011) *Mycoplasma pneumoniae*: susceptibility and resistance to antibiotics. Future Microbiol 6: 423-431.

207. Kenny GE, Cartwright FD (2001) Susceptibilities of *Mycoplasma hominis, Mycoplasma pneumoniae* and *Ureaplasma urealyticum* to GAR-936, dalfopristin, dirithromycin, evernimicin, gatifloxacin, linezolid, moxifloxacin, quinupristin-dalfopristin, and telithromycin compared to their susceptibilities to reference macrolides, tetracyclines, and quinolones. Antimicrob Agents Chemother 45: 2604-2608.

208. Waites KB, Crabb DM, Bing X, Duffy LB (2003) In vitro susceptibilities to and bactericidal activities of garenoxacin (BMS-284756) and other antimicrobial agents against human mycoplasmas and ureaplasmas. Antimicrob Agents Chemother 47: 161-165.

209. Waites KB, Crabb DM, Duffy LB (2003) In vitro activities of ABT-773 and other antimicrobials against human mycoplasmas. Antimicrob Agents Chemother 47: 39-42.

210. Bebear CM, Renaudin H, Schaeverbeke T, LeBlanc F, Bebear C (2000) Comparative activities of telithromycin (HMR 3647), levofloxacin and other antimicrobial agents against human mycoplasmas. Antimicrob Agents Chemother 47: 1980-1982.

211. Duffy LB, Crabb DM, Bing X, Waites KB (2003) Bactericidal activity of levofloxacin against *Mycoplasma pneumoniae*. J Antimicrob Chemother 52: 527-528.

212. Waites KB, Crabb DM, Duffy LB (2003) Inhibitory and bactericidal activities of gemifloxacin and other antimicrobials against *Mycoplasma pneumoniae*. Int J Antimicrob Agents 21: 574-577.

213. Lucier TS, Heitzman K, Liu SK, Hu PC (1995) Transition mutations in the 23S rRNA of erythromycin-resistant isolates of *Mycoplasma pneumoniae*. Antimicrob Agents Chemother 39: 2770-2773.

214. Matsuoka M, Narita M, Okazaki N, Ohya H, Yamazaki T, et al. (2004) Characterization and molecular analysis of macrolide-resistant *Mycoplasma pneumoniae* clinical isolates obtained in Japan. Antimicrob Agents Chemother 48: 4624-4630.

215. Jacobs E, Vonski M, Oberle K, Opitz O, Pietsch K (1996) Are outbreaks and sporadic respiratory infections by *Mycoplasma pneumoniae* due to two distinct subtypes? Eur J Clin Microbiol Infect Dis 15: 38-44.

216. Ovyn C, van Strijp D, Ieven M, Ursi D, van Gemen B, et al. (1996) Typing of *Mycoplasma pneumoniae* by nucleic acid sequence-based amplification, NASBA. Mol Cell Probes 10: 319-324.

217. Sasaki T, Kenri T, Okazaki N, Iseki R, Yamashita R, et al. (1996) Epidemiological study of *Mycoplasma pneumoniae* infections in Japan based on PCR-restriction fragment length polymorphism of the P1 cytadhesin gene. J Clin Microbiol 34: 447-449.

218. Kenri T, Okazaki N, Yamazaki T, Narita M, Izumikawa K, et al. (2008) Genotyping analysis of *Mycoplasma pneumoniae* clinical strains in Japan between 1995 and 2005: type shift phenomenon of *M. pneumoniae* clinical strains. J Med Microbiol 57.

219. Nilsson AC, Bjorkman P, Welinder-Olsson C, Widell A, Persson K (2010) Clinical severity of *Mycoplasma pneumoniae* infection is associated with bacterial load in oropharyngeal secretions but not with MP genotype. BMC Infect Dis 10:39.

220. Su CJ, Dallo SF, Chavoya A, Baseman JB (1993) Possible origin of sequence divergence in the P1 cytadhesin gene of *Mycoplasma pneumoniae*. Infect Immun 61: 816-822.

221. Mra´zek J (2006) Analysis of distribution indicates diverse functions of simple sequence repeats in Mycoplasma genomes. Mol Biol Evol 23: 1370-1385.

222. Flores SC, Lu LJ, Yang J, Carriero N, Gerstein MB (2007) Hinge Atlas: relating protein sequence to sites of structural flexibility. BMC Bioinformatics 8: 167.

223. Thacker WL, Talkington DF (2000) Analysis of complement fixation and commercial enzyme immunoassays for detection of antibodies to *Mycoplasma pneumoniae* in human serum. Clin Diagn Lab Immunol 7: 778-780.

224. Beersma MF, Dirven K, can Dam AP, Templeton KE, Claas EC, et al. (2005) Evaluation of 12 commercial tests and the complement fixation test for *Mycoplasma pneumoniae*-specific immunoglobulin G (IgG) and IgM antibodies, with PCR used for the "gold standard". J Clin Microbiol 43: 2277-2285.

225. Aubert G, Pozzeto B, Gaudin OG, Hafid J, Mbida AD, et al. (1992) Evaluation of five commercia tests: complement fixation, microparticle agglutination, indirect immunofluorescence, enzyme-linked immunosorbent assay and latex agglutination, in comparison to immunoblotting for *Mycoplasma pneumoniae* serology. Ann Biol Clin 50: 593-597.

226. Kenny GE, Newton RM (1973) Close serological relationship between glycolipids of *Mycoplasma pneumoniae* and glycolipids of spinach. Ann N Y Acad Sci 225: 54-61.

227. Feldner J, Gobel U, Bredt W (1982) *Mycoplasma pneumoniae* adhesin liocalized to tip structure by monoclonal antibody. Nature (London) 298: 765-767.

228. Hu PC, Cole RM, Huang YS, Graham JA, Gardner DE, et al. (1982) *Mycoplasma pneumoniae* infection: role of surface protein in the attachment organelle. Science 216: 313-315.

229. Jacobs E, Buchholz A, Kleinmann B, Bredt W (1987) Use of adherence protein of *Mycoplasma pneumoniae* as antigen for enzyme linked immunosorbent assay (ELISA). Isr J Med Sci 23: 709-712.

230. Jacobs E, Fuchte K, Bredt W (1986) A 168 kDa protein of *Mycoplasma pneumoniae* used as antigen in a dot enzyme linked immunosorbent assay. Eur J Clin Microbiol 5: 435-440.

231. Barker CE, Sillis M, Wreghitt TG (1990) Evaluation of Serodia Mcyo II particle agglutination test for detecting *Mycoplasma pneumoniae* antibodyL comparison of mu-capture ELISA and indrect immunofluorescence. J Clin Pathol 43: 163-165.

232. Thurman KA, Warner AK, Cowart KC, Benitez AJ, Winchell JM (2011) Detection of *Mycoplasma pneumoniae*, *Chlamydia pneumoniae*, and *Legionella* spp. in clinical specimens using a single-tube multiplex real-time PCR assay. Diagn Microbiol Infect Dis 70: 1-9.

233. Yogev D, Browning GF, Wise KS (2002) Genetic mechanisms of surface variation. *In: Molecular biology and pathogenecity of mycoplasmas*; Razin S, Herrmann R, editors. New York, NY: Kluwer Academic/Plenum Publishers.

234. Maquelin K, Hoogenboezem T, Jachtenberg JW, Dumke R, Jacobs E, et al. (2009) Raman spectroscopic typing reveals the presence of carotenoids in *Mycoplasma pneumoniae*. Microbiology 155: 2068-2077.

235. Wolff BJ, Thacker WL, Schwartz SB, Winchell JM (2008) Detection of macrolide resistance in *Mycoplamsa pneumoniae* by real-time PCR and high-resolution melt analysis. Antimicrob Agents Chemother 52: 3542-3549.

236. Raman CV, Krishnan KS (1928) A new type of secondary radiation. Nature 121: 501-502.

237. Kerker M (1991) Founding fathers of light scattering and suface-enhanced Raman scattering. Appl Opt 30: 4699-4705.

238. Norris KP (1959) Infrared spectroscopy and its application to microbiology. J Hygiene 57: 326-345.

239. Naumann D, Helm D, Labischinski H (1991) Microbiological characterizations by FT-IR spectroscopy. Nature 351: 81-82.

240. Ling JY, Yang QZ, Luo SS, Li Y, Zhang CK (2005) Preliminary study on cordycepin-DNA interaction by Raman spectroscopy. Chin Chem Lett 16: 71-74.

241. Mrozek MF, Weaver MJ (2002) Detection and identification of aqueous saccharides by using surface-enhanced Raman spectroscopy. Anal Chem 74: 4069-4075.

242. Podstawka E, Ozaki Y, Proniewicz LM (2004) Adsorption of S-S containing proteins on a colloidal silver surface studied by Surface-enhanced Raman spectroscopy. Appl Spectrosc 58: 1147-1156.

243. Stewart S, Fredericks PM (1998) Surface-enhanced Raman spectroscopy of peptides and proteins adsorbed on an electrochemically prepared silver surface. Spectrochimica Acta Part A 55: 1615-1640.

244. Stewart S, Fredericks PM (1998) Surface-enhanced Raman spectroscopy of amino acids adsorbed on an electrochemically prepared silver surface. Spectrochimica Acta Part A 55: 1641-1660.

245. Kudelski A (2008) Analytical applications of Raman spectroscopy. Talanta 76: 1-8.

246. Vo Dinh T, Houck K, Stokes DL (1994) Surface-enhanced Raman gene probes. Anal Chem 66: 3379-3383.

247. Lombardi JR, al. e (1986) Charge-transfer theory of surface enhanced Raman spectroscopy: Herzberg-Teller contributions. J Chem Phys 84: 4174.

248. Lombardi JR, Birke RL (2009) A unified view of surface enhanced Raman scattering. Acct of Chem Res 42: 732-742.

249. Wiley BJ, al. e (2006) Maneuvering the surface Plasmon resonance of silver nanostrcutures through shape-controlled synthesis. J Phys Chem B 110: 15666-15675.

250. Schatz GC, Young M, Van Dyne RP (1986) Electromagnetic mechanism of SERS. Surface-enhanced Raman scattering - Physics and Applications.; Kneipp K, Moskovits M, Kneipp H, editors: Springer-Verlag Heidelberg.

251. Willets KA, Van Duyne RP (2007) Localized surface Plasmon resonance spectroscopy and sensing. Ann Rev Phys Chem 58: 267-297.

252. Kneipp K, Wang Y, Kneipp H, Pereleman LT, Itzkan I, et al. (1997) Single molecule detection using surface enhanced Raman scattering (SERS). Phys Rev Lett 78: 1667-1670.

253. Nie S, Emory SR (1997) Probing single molecules and single nanoparticles by surface-ehanced Raman scattering. Science 275: 1102-1106.

254. Shirtcliffe N, Nickel U, Schneider S (1999) Reproducible preparation of silver sols with small particle size using borohydride reduction: for use as nuclei preparation of larger particles. J Colloid Interface Sci 211: 122-129.

255. Chaney SB, Shanmukh S, Dluhy RA, Zhao YP (2005) Aligned silver nanorod arrays produce high sensitivity surface-enhanced Raman spectroscopy substrates. Appl Phys Lett 87: 031908.

256. Zhao YP, Chaney SB, Shanmukh S, Dluhy RA (2006) Polarized surface enhanced Raman and absobance spectra of aligned silver nanorod arrays. J Phys Chem B 110: 3153-3157.

257. Adams MJ, Barnett NW Chemometrics in Analytical Spectroscopy. - X001.

258. Ebensen KH (2004) Multivariate data analysis - In practice. 5th ed. Olso, Norway: CAMO Process.

259. Wold S (1976) Pattern recognition by means of disjoint principle components models. Pattern Recognition 8: 127-139.

260. Alfassi Z (2004) On the normalization of a mass spectrum for comparison of two spectra. Journal of The American Society for Mass Spectrometry 15: 385-387.

261. Andersen CM, Bro R (2010) Variable selection in regression - a tutorial. wilelyonlinelibrary.com: John Wiley & Sons, Ltd.

262. Patel IS, Premasiri WR, Moir DT, Ziegler LD (2008) Barcoding bacterial cells: A SERS based methodology for pathogen identification. J Raman Spectrosc 39: 1660-1672.

263. Savitzky A, Golay MJE (1964) Smoothing and Differentiation of Data by Simplified Least Squares Procedures. Anal Chem 36: 1627-1639.

264. Shelns J (2005) A tutorial of principle component analysis.

265. Sharaf MA, Illman DL, Kowalski BR (1986) Chemometrics. New York, NY: John Wiley & Sons.

266. Barker M, Rayens W (2003) Partial least squares for discrimination. J Chemom 17: 166-173.

267. Musumarra G, Barresi V, Condorelli DF, Fortuna CG, Scire S (2004) Potentialities of multivariate approaches in genome-based cancer research: identification of candidate genes for new diagnostics by PLS discriminate analysis. J Chemom 18: 125-132.

268. Chevallier S, al. e (2006) Application of PLS-DA in multivariate image analysis. J Chemom 20: 221-229.

269. Wold S (1978) Cross-validatory estimation of the number of components in factor and principal components models. Technometrics 20: 397-405.

270. Maniloff JR (1992) Phylogeny of mycoplasmas *In* Mycoplasmas: molecular biology and pathogenesis. Washington, D.C.: American Society for Microbiology.

271. Lipman RP, Clyde WA, Jr., Denny FW (1969) Characteristics of virulent, attenuated, and avirulent *Mycoplasma pneumoniae* strains. J Bacteriol 100: 1037-1043.

272. Smith PK, Krohn RI, Hermanson GT, Mallia AK, Gartner FH, et al. (1987) Measurement of protein using bicinchoninic acid. Anal Biochem 150: 76-85.

273. Diaz MH, Winchell JM (2012) Detection of *Mycoplasma pneumoniae* and *Chlamydophila pneumoniae* directly from respiratory clinical specimens using a rapid real-time polymerase chain reaction assay. Diagn Microbiol Infect Dis 73: 278-280.

274. Logan J, Edwards K, Saunders NA (2009) Real-time PCR: Current Technology and Applications. Norfolk, UK: Caister Academic Press.

275. Leverette CL, Jacobs SA, Shanmukh S, Chaney SB, Dluhy RA (2006) Aligned silver nanorod arrays as substrates for surface-enhanced infrared absorption spectroscopy. Appl Spectrosc 60: 906-913.

276. Negri P, Marotta NE, Bottomly LA, Dluhy RA (2011) Removal of surface contamination and self-assembled monolayers (SAMs) from silver (Ag) nanorod substrates by plasma cleaning with argon. Appl Spectrosc 65: 66-74.

277. Hatchel JM, Balish MF (2007) Attachment organelle ultrastructure correlates with phylogeny, not gliding motility properties in *Mycoplasma pneumoniae* relatives. Microbiology 154: 286-295.

278. Culha M, Adigüzel A, Yazici MM, Kahraman M, Sahin F, et al. (2008) Characterization of thermophilic bacteria using Surface-Enhanced Raman scattering. Appl Spectrosc 62: 1226-1232.

279. Jarvis RM, Blanch EW, Golovanov AP, Screen J, Goodacre R (2007) Quantification of casein phosphorylation with conformational interpretation using Raman spectroscopy. Analyst 132: 1053-1060.

280. Smith PF (1971) The Biology of Mycoplasmas. New York, New York: Academic Press, Inc.

281. Zubkov MV, Fuchs BM, Eilers H, Burkill PH, Amann R (1999) Determination of total protein content of bacterial cells by SYPRO staining and flow cytometry. Appl Environ Microbiol 65: 3251-3257.

282. Cullum BM, Mobley J, Chi Z, Stokes DL, Miller GH, et al. (2000) Development of a compact, handheld Raman instrument with no moving parts for use in field analysis. Rev Sci Instrum 71: 1602-1608.

283. Moore DS, Scharff RJ (2009) Portable Raman explosives detection. Anal Bioanal Chem 393: 1571-1578.

284. Jehlička J, Culka A, Vandenabeele P, Edwards HGM (2011) Critical evaluation of a handheld Raman spectrometer with near infrared (785 nm) excitation for field identification of minerals. Spectrochimica Acta Part A: Molecular and Biomolecular Spectroscopy 80: 36-40.

285. Yang X, Gu C, Qian F, Li Y, Zhang JZ (2011) Highly sensitive detection of proteins and bacteria in aqueous solution using surface-enhanced Raman scattering and optical fibers. Anal Chem 83: 5888-5894.

286. Maquelin K, Kirschner C, Choo-Smith LP, van den Braak N, Endtz HP, et al. (2002) Identification of medically relevant microorganisms by vibrational spectroscopy. J Microbiol Methods 51: 255-271.

287. Alexander TA (2008) Development of methodology based on commercialized SERS-active substrates for rapid discrimination of poxviridae virions. Anal Chem 80: 2817-2825.

288. Henderson KC, Sheppard ES, Rivera-Betancourt OE, Dluhy RA, Thurman KA, et al. (2014) Comparison of the endpoints for detection of *Mycoplasma pneumoniae* by nanorod array-surface enhanced Raman spectroscopy and qPCR. Manuscript submitted for publication to The Analyst.

289. Kim K-S, Ko K-S, Chang M-W, Hahn TW, Hong SK, et al. (2003) Use of *rpoB* sequences for phylogentic study of *Mycoplasma* species. FEMS Microbiology Letters 226: 299-305.

290. Beebe KR, Pell RJ, Seasholtz MB (1998) Chemometrics: a Practical Guide. New York: John Wiley & Sons.

291. Hennigan SL (2011) Detection and differentiation of *Mycoplasma pneumoniae* and avian mycoplasmas with focus on *Mycoplasma gallisepticum* by surface-enhanced Raman spectroscopy. Athens, Georgia: University of Georgia. 141 p.